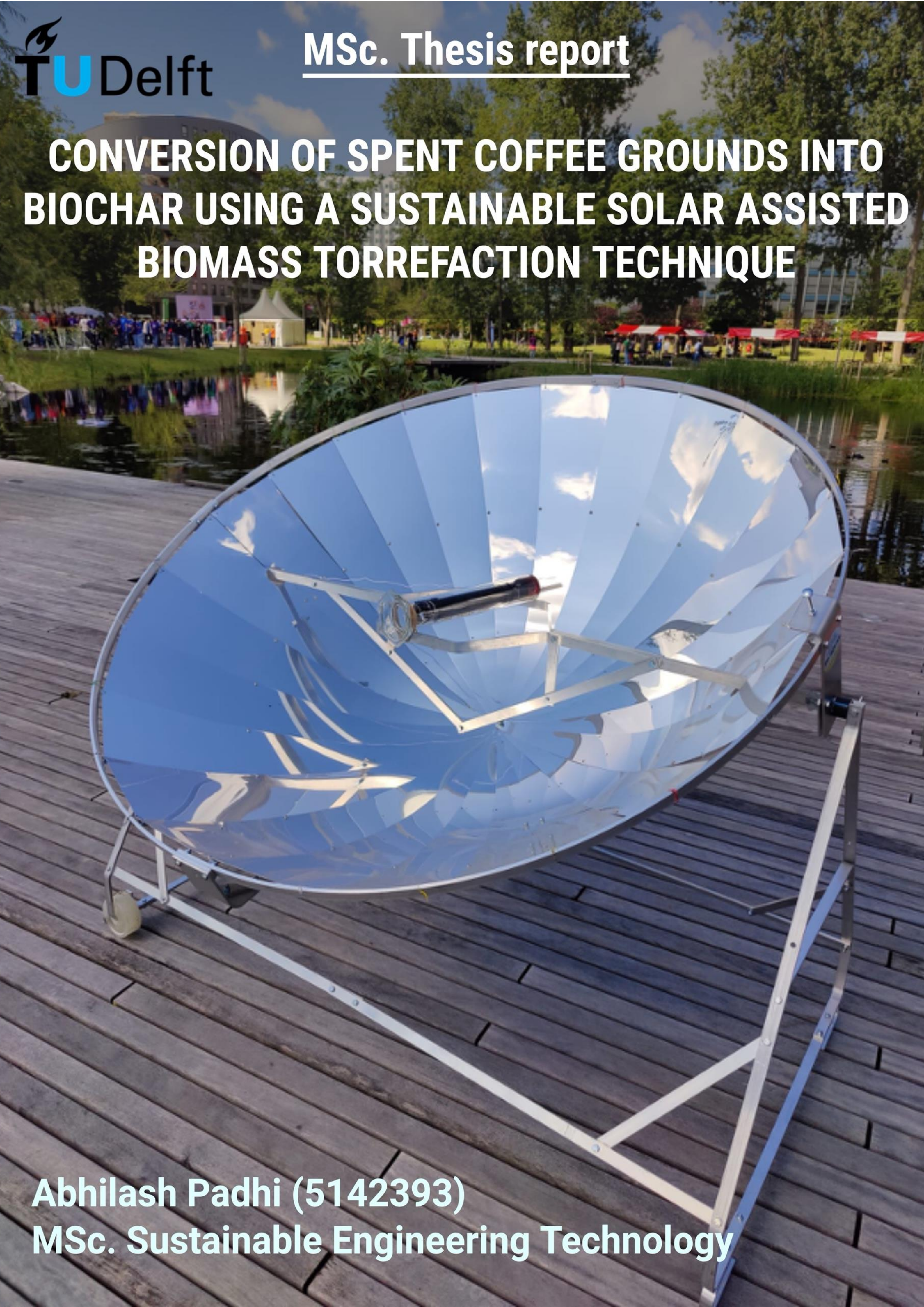

MSc. Thesis report

CONVERSION OF SPENT COFFEE GROUNDS INTO BIOCHAR USING A SUSTAINABLE SOLAR ASSISTED BIOMASS TORREFACTION TECHNIQUE

Abhilash Padhi (5142393)
MSc. Sustainable Engineering Technology

MSC THESIS REPORT

CONVERSION OF SPENT COFFEE GROUNDS INTO BIOCHAR USING A SUSTAINABLE SOLAR ASSISTED BIOMASS TORREFACTION TECHNIQUE

BY

ABHILASH PADHI

IN PARTIAL FULFILLMENT OF THE REQUIREMENTS FOR THE DEGREE OF

MASTER OF SCIENCE

IN SUSTAINABLE ENERGY TECHNOLOGY
AT THE DELFT UNIVERSITY OF TECHNOLOGY

AUTHOR: ABHILASH PADHI

STUDENT NUMBER: 5142393

GRADUATION COMMITTEE:

DR. IR. L. LORENZO BOTTO : CHAIR
PROF. DR. IR. W. DE JONG : CHAIR
DR. IR. RALPH LINDEBOOM : FIRST SUPERVISOR
DR. LUIS CUTZ : FIRST SUPERVISOR

ACKNOWLEDGEMENT

“A soul in tension that’s learning to fly; Condition grounded but determined to try” – Pink Floyd. Was it even worthwhile if it was easy? Is it even possible if you haven't tried enough? This thesis marks the end of a three-year journey as a masters student in Sustainable Energy Technology in TU Delft. And what a journey these three years have been, teaching me perseverance, grit while bringing me one step closer to my desire of making the world more sustainable. This would have been impossible without the consistent, unwavering support of those around me.

Firstly, I would like to thank my committee members for guiding me throughout the thesis. Thank you, Ralph, and thank you, Luis, for helping me put my ideas into perspective and inspiring me to be more practical than ever. Thank you, Ralph, for pushing me to go and conduct the experiment in Hyderabad and most importantly for providing me constructive criticism throughout, without which probably I would have just stopped at the simulation stage. And you Luis, for trusting in me to improve at conducting the experiments in the lab (“it is all a learning curve”) and constantly pushing me to innovate and clear my basics. Also, thank you for introducing me to Bart who gave me a hands-on experience on the functionality of an EVC. A shout-out to Hector, Sarvesh and Saqr for the extra-mile support during the experimental stages.

To my family, Maa and Papa, for being so patient and supportive for so long. And you, Nani, don’t know what I would do without you. Also, you bill, for that extra reason to strive away from home. I knew I loved you guys but had no idea how much you guys loved me. Thank you for putting up with my tantrums. And you Siri, for being a constant rock, and introducing the idea of COMSOL (we did it). And you Kunal and Shashank, for always pushing me, being positive and giving me that technological edge. A big shout out to my friends in Delft; Neeraj (GG bro), Lucas, R-Wade, Ruru, Surbhi, Shriya, Aishu, Ritz, Kavya, Shehab, Akarsh, Shef and Joseph. You guys were like family away from home and always will be (you guys know that). And those back at home; Srikar and Sesha the hangover group (Dhaara, Jai, Pratham, Sudhi, Gautham), Krishna and you Nisha (Finally!). There were many more involved in this wholesome, tough but worthwhile journey. A big-shout out to you guys too.

Finally, I would dedicate what I am, and what I have produced to “Shashank”. He was not only an amazing friend, but also taught everyone involved with him a very important life lesson. You would have been proud Broski.

Thank you all for getting through the good and bad times, make memories and share knowledge for which I will always be grateful. I am very excited to move forward and apply whatever I have learned in these years into productive use. Hope it’s all uphill from here.
I consider all of this **“our”** success.

Cheers,
Abhilash Padhi,
Delft, August 2022.

ABSTRACT

Coffee farmers and producers in Kerala (India) face a serious obstacle in their pursuit of a self-sustaining coffee processing technology and fuel deficiency. Research indicates that coffee, as one of the largest industries, generates a huge amount of waste, namely Spent Coffee Grounds (SCGs). This study aims to evaluate the feasibility and efficiency of converting SCG into biochar using a solar-assisted biomass torrefying technique, while keeping frugal or "jugaad" innovation in mind. To torrefy the feedstock, it was intended to use the available SK14 solar cooker in conjunction with a prototype reactor unit. Based on previous research on torrefying coffee waste, this study asks: Can the biomass torrefied using the SK 14 cooker be utilized as fuel? In this context: Solar biomass torrefaction is an endothermic process of converting the feedstock in an inert environment at low temperatures of 200-300 °C provided by concentrated solar energy in order to produce a high yield of solid biochar.

Based on the literature research, it was important to characterize the SK14 cooker, the feedstock, and to understand the operating principles of the chosen reactor, namely Evacuated Tube Vacuum Collectors (EVCs). Since the design of the reactor and cooker were interdependent, COMSOL was used to simulate the heat distribution profile and temperature profile of the reactor model. Literature and simulation results were used to construct a prototype reactor, and torrefaction tests were conducted in Hyderabad (India). SCG was effectively torrefied to generate biochar at 240 °C and 260 °C, as evidenced by high heating values of 26 MJ/kg (21% increase) and 26.3 MJ/kg (22.50% increase), respectively compared to the raw material. The results show that the current system can be utilized as a small-scale solar biomass torrefier, creating biochar that can be used as a fuel. However, the reactor's non-homogeneous heating rate and poor heat retention severely hampered its applicability. Further study is required to find other features and aspects that might not only improve the design and efficacy of the torrefier, but also facilitate its implementation for coffee producers in Kerala.

Keywords: jugaad, torrefier, EVCs, high heating value, small-scale, biochar.

LIST OF FIGURES

LIST OF TABLES

LIST OF ABBREVIATIONS

GHG	Greenhouse Gases
IEA	International Energy Agency
SDG	Sustainable Development Goals
EAI	Energy Alternatives India
SECI	Solar Energy Corporation of India
SCG	Spent Coffee Ground
HHV	High Heating Value
LPG	Liquid Petroleum Gas
MNRE	Ministry of New and Renewable Energy
CCRI	Central Coffee Research Institute
CFI	Carbon Farming Initiative
UNFCCC	United Nations Framework Convention on Climate Change
BET	Brunauer Emmett and Teller
VM	Volatile Matter
FC	Fixed Carbon
CEC	Cation Exchange Capacity
CH_4	Methane
OH	Hydroxyl group
C_2H_6	Ethane
XRD	X-Ray Diffraction
FPC	Flat Plate Collectors
CPC	Compound Parabolic Concentrators
EVC	Evacuate Vacuum tube Collectors
Co_3O_4	Black Cobalt Oxide

HTF	Heat Transfer Fluid
CSP	Concentrated Solar Power
PTC	Parabolic Trough Collector
HFC	Heliostat Field Collector
LFC	Linear Fresnel Collector
PDC	Parabolic Dish Collector
NGO	Non-Governmental Organization
GHI	Global Horizontal Irradiance
DNI	Direct Normal Irradiance
SPV	Solar Photovoltaics
SOMR	Solid Olive Mill Residue
PDE	Partial Differential Equation
BCR	Braided Composite Rod
FP	Focal Point
HDPE	High Density Polyethylene
PVC	Poly Vinyl Cushion
SS	Stainless Steel
GC	Gas Chromatography
FTIR	Fourier Transform Infrared
C	Carbon
H	Hydrogen
N	Nitrogen
O	Oxygen
TGA	Thermogravimetric Analysis

LIST OF SYMBOLS

D_{ap}	Aperture Diameter (m)
A_s	Surface area of parabola (m^2)
f	Focal length (m)
h	Height of parabola (m)
A_{ap}	Aperture area (m^2)
A_r	Collector aperture area (m^2)
C_A	Concentration ratio
C_p	Specific heat capacity at constant pressure (kJ/kg.K)
Δt	time taken to reach boiling temperature (mins)
ΔT	Difference between starting and boiling water temperature (K)
m	Mass of water (kg)
G_{av}	Average solar irradiance (W/m^2)
P_f	Density of solar radiation at focal point (W)
η_{Al}	Efficiency of reflector plates
η_{avg}	Efficiency of solar cooker
Q_f	Density of solar radiation at focal point (W/m^2)
P_b	Actual solar radiation power at the receiver area (W/m^2)
P_{bf}	Actual wattage at focal point (W)
P_c	Instantaneous cooking power (W)
τ	Instantaneous time (mins)
T_{w2}	Boiling temperature (℃)
T_{w1}	Instantaneous starting temperature (℃)
u	Velocity vector

u_{trans}	Velocity vector of translation motion in solids (m/s)
q	Heat flux (W/m^3)
q_r	Heat flux by radiation (W/m^2)
ρ	Density (kg/m^3)
k	Thermal conductivity (W/ (m.K))
Q_b	Boundary heat flux (W/m^2)
Q_{ted}	Thermoelastic damping (W/m^3)
Q_p	Work done by pressure change in fluid (W/m^3)
Q_{vd}	Viscous dissipation (W/m^3)
G_m	Radiation from boundaries (W/m^2)
G_{ext}	External radiation sources (W/m^2)
G_{amb}	Ambient radiation (W/m^2)
F_{ext}	View factor of external heat source
F_{amb}	Ambient view factor
T_{amb}	Faraway temperature (K)
P_s	Source Power (External radiation source) (W)
J	Radiosity (W/m^2)
$e_b(T)$	Blackbody hemispherical total emissive power (W/m^2)
σ	Stefan-Boltzmann constant (W/ (m^2 K^4))
ε	Surface emissivity
ρ_r	Reflectivity
α	Absorptivity
T	Surface temperature (K)
θ_{crit}	Critical angle (radian)

Table of Contents

1. Introduction

An approximate emission of 1100 gigatons of CO_2, aided by the world energy consumption, has been recorded from the modern 19th century fossil fuel usage, which is, directly or indirectly linked to the world population explosion that could further increase to 9.3 billion people by 2050 (Morales et al., 2014; Ndukwu et al., 2020). This consumption could further plummet by 56% to about 820 quadrillion Btus in 2040, as proposed by the International Energy Outlook (Bhaskar & Pandey, 2015). Figure 1 shows the total world energy consumption.

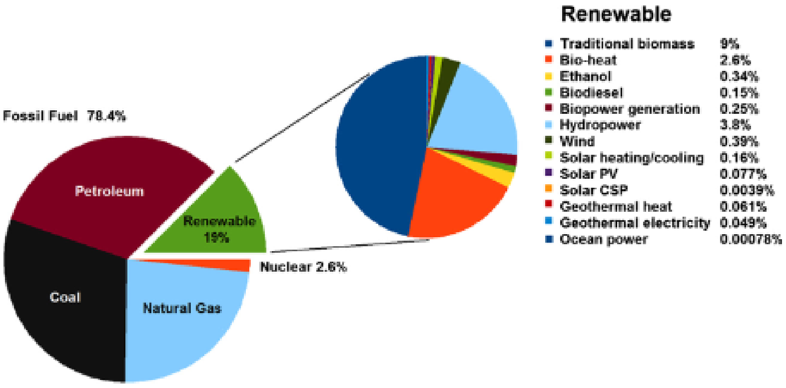

Figure 1: Overall world consumption with respect to renewable energy (Zeng, Gauthier, Soria, et al., 2017).

Owing to the majority consumption of non-renewable fossil fuels to meet the world energy demand, Chiari & Zecca (2011) demonstrate the models by different researchers projecting the fossil fuels to deplete between 2100 and 2200 with respect to the current reserves and emerging renewable technologies as shown in Figure 2. They also analyze the global CO_2 increase and its influence on global-mean temperature in Figure 2 and predict that by 2035, CO_2 levels might reach 450 ppm and the global temperature could rise by at least 1°C (Mukherjee et al., 2022), causing beyond-threshold anthropogenic climate intervention. Moreover, according to Bedi, (2021) energy-related greenhouse gas emissions accounted for two-thirds of the global emissions rise in 2018. This calls for severe steps to minimize fossil fuel consumption and replace it with more sustainable energy options to reduce GHG emissions.

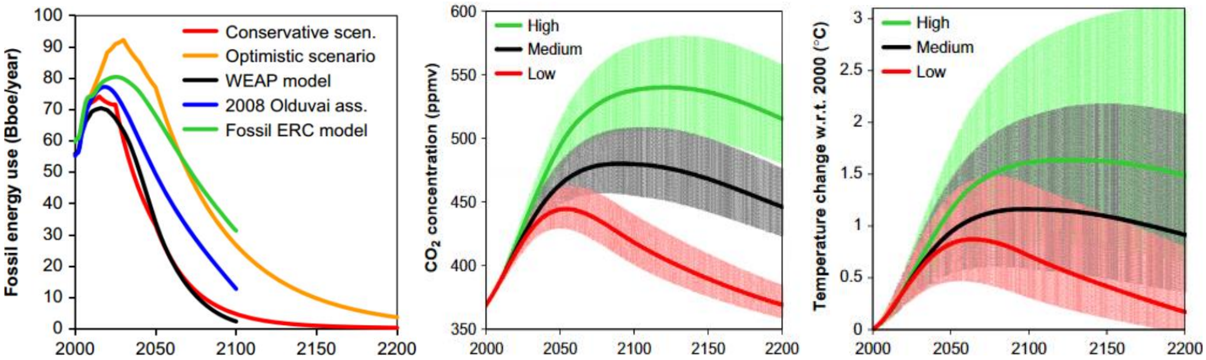

Figure 2: Projection of fossil fuels usage and temperature increase with respect to increasing global temperature for the 21st and 22nd century (Chiari & Zecca, 2011).

Concerns about greenhouse gas emissions, diminishing fossil fuel supplies, and rising energy demands have all increased interest in the use of clean, renewable energy. According to the International Energy Agency (IEA), the development of solar, wind, biomass, geothermal, hydropower, and ocean energy has increased by 1.7% annually (W. H. Chen et al., 2012). Also, according to Bedi, (2021), there has been a considerable reduction in emissions within the power and industrial sectors by switching from coal to natural gases, nuclear and renewable energy. The study by Colantoni et al. (2021) states that renewable energy production had also increased from 18.91% to 25.60% between 2008 and 2018. This data was supported by Zeng et al. (2017), who predict it to reach 47.7 % of the total energy consumption by 2040. However, present and future injustices from renewable energy lifecycles point to lost jobs, hazardous exposure, land dispossession, ecosystem destruction, etc., throwing a big question out as to who can afford cleaner renewable energy and who faces the consequences (Bedi, 2021).

As discussed, energy, when linked with waste management, is the most essential challenge for addressing climate change factors while balancing emerging national growth. That's where the tilt towards usage of biomass energy becomes significant, with it being the only carbon-neutral alternative source from which chemicals, materials, and fuels can be extracted, especially for the industrial, transport, and agricultural sectors (Kataki et al., 2015). Caputo & Mašek, (2021) state that over 50% of solid waste in low- and middle-income countries comes from agriculture and food, with rural areas producing the most. According to him, around 1.1 billion people still lack access to electricity, while 2.8 billion rely on traditional biomass combustion for cooking and warmth, mostly due to unsustainable forestry practices or usage. Therefore, both energy availability and electrification are linked to the Sustainable Development Goals (SDGs) to mitigate climate change in developing countries. India, for example, made 450–500 million metric tons of biomass every year, which made up 32% of its primary energy and, according to Energy Alternatives India (EAI) (Bhaskar & Pandey, 2015), has a power potential of 18,000–50,000 MW.

Table 1: Solar energy potential in India as approached by the Three Phase Approach (Suman & Ahamad, 2019)

Application Segment	**Phase I 2010-2013**	**Phase II 2013-17**	**Phase III 2017-22**
Utility Grid Power	1000-2000 MW	4000-10000 MW	20,000 MW
Off-Grid Application	200 MW	1000 MW	2000 MW
Solar Thermal Collectors Area	7 million sqm	15 million sqm	20 million sqm
Manufacturing Base	----	----	4000-5000 MW
Solar Lighting Systems	----	----	20 million
Solar RPO	0.25 %	----	3 %

Zeng et al. (2017) examined Figure 1 to forecast a 10% increase in solar energy consumption by 2040, indicating a significant shift toward solar energy utilization in the near future. With a 6 billion GW annual potential, an average of 250-300 sunny days with 2300-3200 sunny hours, India receives an annual radiation ranging from 1200-2300 kWh/sqm (Suman & Ahamad, 2019). With a three-phase approach, the grid-connected solar energy reached 2,766 MW in September 2014, 10,000 MW in 2017, and aimed for 20000 MW by 2022 (Bedi, 2021; Suman & Ahamad, 2019). Supporting this study, the Solar Energy Corporation of India (SECI) reported in April 2017 that India's solar grid has a cumulative capacity of 12.28 GW for solar energy, quadrupling in 3 years (Chintala et al., 2017). (Suman & Ahamad, 2019) also claim that India's electricity needs can be met with just 3000 km^2 (0.1 %) of the total land area, which is why more and more land have been designated also to solar thermal collectors as shown in Table 1.

Lately, a solution to combine renewable energy, principally solar and biomass, has been collectively used to create power and biofuel. Converting biomass or agricultural waste to biofuel lowers waste disposal (which poses health risks) and may not only provide cash for local producers and communities (rural and *Adivasi*) but may also pave the road for a zero-emission fuel (Ndukwu et al., 2020). Research has shown that concentrated solar-assisted thermal decomposition of biomass (pyrolysis, torrefaction, carbonization) can produce biofuel and biochar that can replace coal and other fossil fuels (D. Chen et al., 2020; Joardder et al., 2014; Morales et al., 2014; Zeng, Gauthier, Minh, et al., 2017).

Developing nations such as India are not vigorously pursuing energy development objectives, especially for small states like Kerala (South Indian State). According to Bedi, (2021), despite being the eighth richest state in India with a high literacy rate, solar energy dominated people's understanding of climate change, clean energy transition, and development challenges. Agricultural and coffee waste, on the other hand, is an uncommon but attractive source of biomass not only for Kerala but also for the vast majority of coffee-consuming and producing nations. In a society where nearly, everyone is aiming for a paradigm shift toward a more sustainable environment, some of the most obvious solutions are sometimes neglected. This is when the term "cheap innovation" or "jugaad" comes to the limelight. It is described as doing more with fewer resources via ingenuity and creativity in the face of resource constraint.

Coffee production is one of the biggest consumption and agricultural industries in the world, with over 10 million tonnes consumed in 2020 (Sermyagina et al., 2021). Among the vast variety of coffee wastes generated throughout the production and agricultural stages that can be directly used or converted into fuel, the treatment of spent coffee grounds appears to be undervalued. Y. C. Chen & Jhou, (2020) define SCG as a dark brown, moist solid leftover from brewing coffee (SCG) and instant coffee production, with one ton of unroasted coffee yielding over 650 kg of SCG. Kerala ranks second, producing 28 % of the country's overall coffee production not only because of its optimal temperature and weather conditions but also due to the availability of large communities of local farmers (Anil Kumar et al., 2019; Dr. Ambedkar Veedhi, 2021; Karunakaran, 2017). This, along with its high solar energy potential (D. Kumar, 2020; Parameshwaran et al., 2013), makes Kerala one of the optimum choices to investigate the adoption of solar-induced coffee-waste to fuel production while keeping local farmers in the loop. Moreover, the central government's subsidised schemes [1] have propelled the idea of innovating the already existing focus on solar cooking with fuel production in rural areas.

1.1 Problem Definition

Despite the immense potential for both biomass and solar energy, India's 11% growth in primary energy consumption accounted for 70% of the overall GHG emissions from the energy, industrial, agricultural, and waste sectors, totalling 2136.8 million tons of CO_2 equivalent (Bedi, 2021). However, the renewable energy sector accounted for only about 12% of the 200 GW of total electricity produced, leaving a huge gap to be filled by conventional fuels (Aggarwal RK, 2020). Conventional biomass produces low-quality energy relative to their economic and energy expenses, with their efficiency ranging from 5 to 20%, providing low-grade heat with little control. Due to poor material energy density, a huge amount of biomass is needed to meet daily demands, requiring women and children in rural areas to spend hours gathering biomass (Caputo & Mašek, 2021). Even though coffee cultivation is a labour-intensive activity, most small coffee growers in Kerala choose to sell the unprocessed yield indirectly, reducing farming jobs [2]. Thus, the scarcity of labor, the lack of assistance from the Coffee Board, and the growing cost of fertilizers have caused farmers to sell their coffee at a discount since they cannot store their crop for long. Difficult access to technical developments, both subsidized and non-subsidized, such as drying and pre-treatment processes for coffee, has made it even worse (Karunakaran, 2017).

The majority of coffee waste and by-products, such as SCG (6 million tons/year) and silver skin, are improperly dumped into the environment, especially by companies that produce more than 2 billion tons of by-products per year (Y. C. Chen & Jhou, 2020). Landfills or direct disposal can leach toxic components into the soil such as caffeine, tannin, and polyphenols, causing eutrophication when discharged into water and GHG pollution when combusted (Draper, 2018; Sermyagina et al., 2021).

Solar concentrators (such as solar cookers) can reach very high temperatures at the focal point (350 to 400 °C), but the temperature range decreases dramatically as the receiver area increases (Mekonnen et al., 2020). Solar cookers are functionally designed to only reach cooking and boiling temperatures (100 to 120 °C) (Mussard et al., 2013; Purohit, 2010). Moreover, as shown by Morales et al. (2014), direct heating solar concentrating reactor systems can have a few disadvantages, such as heat loss due to reflectivity of the biomass and an uneven distribution of heat. Since the primary goal was to use the available SK14 cooker as the concentrator, one of the biggest challenges was to innovate and propose a solution to reach the desirable torrefaction temperature. Moreover, a reactor had to be designed to not only retain but also elevate and evenly distribute the peak temperature.

1.1.1 Need for Research

Multiple technologies are currently in use to convert waste into usable fuel. Nevertheless, conventional non-renewable techniques contribute further to carbon emissions. Consequently, using agricultural waste (spent coffee) to produce fuel using available solar power can provide solutions for socio-economic and environmental issues by reducing carbon footprint and GHG emission levels at the grassroots level because it contains less sulphur and heavy metals than coal(W. Tsai, 2017).

The government of India is already subsidizing and educating farmers and the rural communities on the use of solar cooking equipment [1]. With easy access to coffee waste, production of fuel and biochar (soil enrichment) using the already existing solar cooking systems can help small producers and farmers in Kerala achieve self-sustainability.

SCG has very good potential to produce biofuel, biochar, and bio adsorbents using various thermochemical processes that are substantially underused. However, because of disadvantages such as very high moisture content, low calorific value, high biodegradability, heterogeneity, and poor capacity for long-term storage, its usage as a feedstock has not always been appealing (W. Tsai, 2017; Vakalis et al., 2019). According to the literature, raw SCG has a High Heating Value (HHV) of 20 to 25.5% and torrefied SCG has a HHV of 26.5 to 30%, with a torrefaction temperature ranging from 240 to 300 °C (Barbanera & Muguerza, 2020; W. H. Chen et al., 2012; Y. C. Chen & Jhou, 2020; W. T. Tsai & Liu, 2013). Due to its increased specific surface area, porosity, and absorption capacity, the torrefied biochar can be used not only as a fuel but also as a soil amendment (Draper, 2018; Lee et al., 2021; W. Tsai, 2017). Moreover, literature indicates that torrefied SCG has a very low moisture content and improved pelletability (W. Tsai, 2017), thus making it easier to store for a longer time and use as a precursor in other thermochemical processes.

1.1.2 Research Gap

1.1.2.1 *Methodological Gap:* Until now, numerous techniques have focused on the pyrolysis of various carbonaceous feedstocks using concentrated solar systems to produce bio-oil, biogas, and biochar (D. Chen et al., 2020; Weldekidan et al., 2018; Zeng, Gauthier, Soria, et al., 2017). These systems either use large reactors for large-scale pyrolysis reactions or aim to directly concentrate light at the focal point on the biomass in transparent reactors. This does not, however, provide a clear idea of how to apply the same principle to an SK14 solar cooker, which has a significantly larger receiver area. In addition, there were few studies supporting the use of an SK14 cooker to achieve the torrefaction temperature, but the reactor design was highly ambiguous (Cellatoglu & Ilkan, 2016; Swaminathan & Nandjembo, 2016). Although many studies support the benefits of torrefying SCG, little or no evidence points to the viability of small-scale solar torrefaction of coffee-waste to biochar. Moreover, linking "jugaad" to the resolution of technical and theoretical problems was a novel concept. **This research aims to bridge the gap between the numerous known approaches for solar-biomass pyrolysis principles and a small-scale SK14 cooker induced torrefier that can be used for both cooking and biochar production.**

1.1.2.2 *Knowledge Gap:* Due to a lack of clarity regarding the selection and characterization of the reactor to be paired with the cooker, a knowledge gap exists. The heat distribution profile in a reactor may play a significant role in regulating reaction parameters, temperature, heat distribution, and heat retention. Even after narrowing down the relevant literature, the complexity of the design process was increased by the numerous parameters and modifications. **Since no relevant literature was found investigating the specific reactor design to be used for this process, a simulation was used to analyse the heat distribution and temperature profile of the prototype reactor with realistic parameters to determine how well it corresponds to the principles stated in the literature.**

1.2 Research Agenda

This section explains the theoretical design of the research. Firstly, within subsection 1.2.1, the objective of the research is explained. Finally, subsection 1.2.2, presents the research questions tackled within the current research.

1.2.1 Research Objective

The research objective of the research is:

To check the feasibility and efficiency of converting Spent Coffee Grounds into biochar using a Solar assisted torrefying mechanism. "Frugal Innovation" is proposed to couple the available solar concentrator with a prototype reactor unit to enact the torrefaction of the feedstock.

1.2.2 Research Questions

In this subsection, the research topics that will be addressed by the current study are presented. Based on the overall study purpose, the primary research question is formulated. To address the primary research topic, a collection of sub-research questions is constructed.

Main RQ: Is it possible to attain the torrefaction temperature using a SK14 Cooker coupled with a Solar Collector unit? If yes, can raw SCG be torrefied in the reactor?

Sub RQ-1 aims at determining and demonstrating the need to focus on heat retention and distribution along the chosen model reactor using a physics-simulation software.

- **Sub RQ1: How is the heat distribution and retention along the simulated Solar Collector?**

Sub RQ-2 intends to address a hands-on experiment to understand the functionality and principles of the SK14 solar cooker, solar collector(s) and build a prototype reactor using 'frugal innovation' to conduct torrefaction (200-300 °C) of raw SCG.

- **Sub RQ2: Is it feasible to convert a SK14 solar cooker into a functioning solar torrefier? What function does the modified collector serve in the design of the torrefier?**

Sub RQ-3 aims at understanding the principles of torrefaction and to determine the feasibility of the produced biochar as a substantial fuel.

- **Sub RQ3: What are the test conditions required to effectively characterize the raw SCG and produced biochar? Can the biochar be used as a fuel?**

1.3 Research Approach

The research intends to address the technical complexities by applying jugaad innovation in a broad sense to answer the research questions. Figure 3 shows the research methodology followed for the study. It is separated into four general categories, including solar cooker characterization, COMSOL simulation, prototype reactor construction, and product characterization, to achieve results. These scenarios are interrelated, with each subsector linked to the review of the literature. The entire strategy was used to create a framework for constructing a Solar-Biomass torrefier and to analyze the product obtained after conducting trials in it.

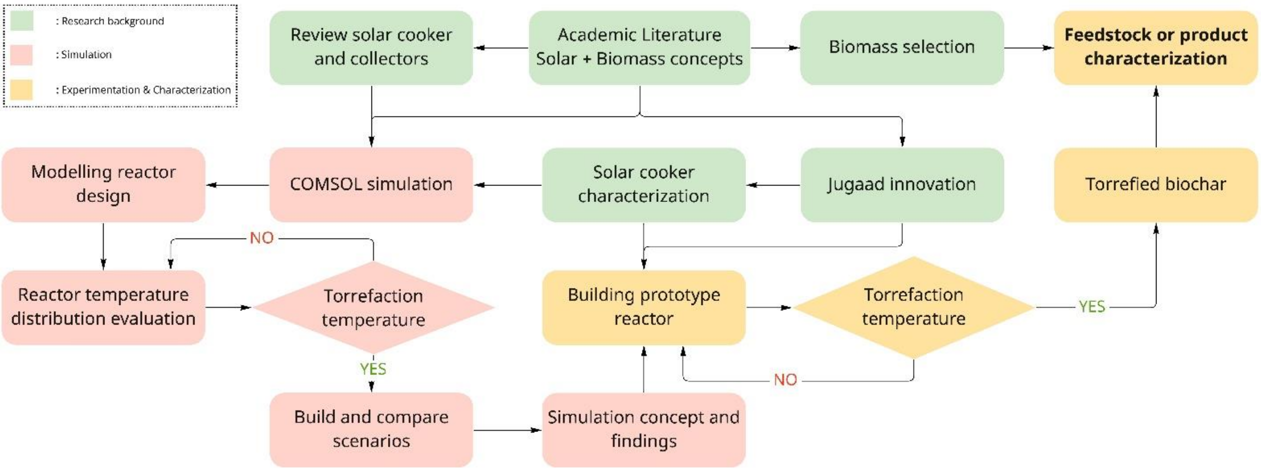

Figure 3:Research approach to tackle the research questions.

1.4 Research Outline

This section presents the overall narrative of the report. In all the required chapters, at the beginning of the chapter, a concise summary is provided. Similarly, at the end of the chapter, the relevant takeaway from the chapter is provided.

The thesis aims to explore in detail the several aspects of solar induced biomass torrefaction using Frugal or "Jugaad" innovation: including the process, potential, products, and technology.

Chapter 1: This chapter introduces the main objective of the research, research gaps, the research questions that need to be answered and the research approach that will be applied to do so.

Chapter 2: The main findings from the literature review is address here. Topics such as biomass, solar, torrefaction and potential of Kerala for biomass-solar torrefaction are addressed here.

Chapter 3: This chapter introduces the materials and methods involved in the research such as input parameters for simulation, designing the prototype reactor and SCG characterisation.

Chapter 4: The results while conducting the characterization, simulation and experiments are discussed in this chapter.

Chapter 5: Within this chapter, the answer to all the sub and main research question have been answered and collaborated to reach the conclusion of the research. This chapter also addresses the limitations faced through the research.

Chapter 6: Finally, the recommendations arising from this research have been listed.

2 Literature Review

In order to fully understand the principles and functions of each individual element involved in designing the thesis, it was important to conduct a literature review based on the research objective, questions, and gaps. It was divided into five major categories due to the involvement of various complicated elements in addressing the main questions.

The first half of the review dives into the application of Jugaad innovation, exploring the concepts and potential of biomass and solar energy in order to identify the thermochemical process required to torrefy SCGs into a possible fuel. As a result, the potential of SCG as a biomass for producing solid biochar for use as a fuel source was studied. Understanding the functionality of the SK14 cooker in stock required an understanding of solar collectors, concentrators, and their properties. This not only gave a notion of the projected prototype reactor unit, but it also laid the groundwork for future simulation.

The second half of the chapter focuses on Kerala's solar and biomass application potential based on its irradiation and biomass (coffee waste) availability. This sub-section would thus pave the way for a study of the fundamentals of combining solar and biomass and explore the possibilities of a solar-biomass torrefaction or pyrolysis unit. Finally, Section 2.7 summarizes the key points and brings together the fundamentals required to construct a robust framework for the experiments and simulations.

2.1 Implementation of Frugal Innovation in India

As the world's largest and most diverse democracy, with enormous demands and complexity, India may serve as the world's greatest living laboratory, operating as a fertile breeding ground for cost-effective solutions. With millennials increasingly favouring sustainable scenarios, manufacturing firms have shifted from "do more with less" to "do better with less" solutions [3]. This section includes examples of jugaad in small households as well as technical breakthroughs that are fundamentally a part of Indian culture. Some efforts based on solar and biomass (coffee) are emphasized to demonstrate the compatibility of large-scale modern technology with the simple and sustainable frugal revolution.

In 2017, “Brahma Kumari” constructed a 1 MW solar thermal plant with 70 × 60 m^2 large parabolic dishes and thermal storage technology to power nearly 25,000 people [4]. As mentioned by [5], their solar community kitchen uses 84 parabolic concentrators to prepare 35,000 meals for 17,500 people per day, saving around 184 kg of LPG, as seen in Figure 4. Aggarwal RK, (2020) demonstrated a comparable application of solar steam cooking and heating systems at the community level for approximately 1500 students. With a population of 1.4 billion, such technologies offer a way for India to use solar energy in a more sustainable and cost-effective manner, not just to generate electricity but also as a very efficient cooking medium.

The Indian government, in collaboration with the Ministry of New and Renewable Energy (MNRE), has launched the "Solar Cooker Programme" to encourage the decentralization of solar cookers [1]. Its objective was to promote off-grid cooking applications, raise awareness, and use non-governmental organizations to demonstrate effective use of the systems for individuals and communities. As illustrated in Figure 5, it is critical to convey the principles of sustainability and frugality, particularly among rural populations where jugaad is also a well-known concept.

Figure 4: Brahma Kumari solar community kitchen [5].

A Dutch team visited the Brahmagiri Development Society (Wayanad) in April as part of a global push to apply the concept of "climate-smart coffee" to understand their unique technique for cultivating coffee with very low carbon emissions and, as a result, to push Wayanad coffee into the global market [6]. Furthermore, the Central Coffee Research Institute (CCRI) has investigated the possibility of producing biochar from coffee stems and by-products such as coffee pulp, effluents, husk, and Spent Coffee Grounds (SCG) to be used not only for soil-entrenchment and fuel but also to manufacture cups, furniture, organic polymers, fabric, panels, and so on [7]. [8] exemplifies the concept of frugal sustainability by presenting the concept of sustainable coffee production or the Carbon Farming Initiative (CFI), which allows farmers, foresters, and landowners to earn and trade carbon credits for extra revenue.

Figure 5:MNRE subsidised solar cooker program [1].

Kerala has been evolving toward various decentralized waste management strategies through community engagement due to its high literacy rates. The best example is the “Haritha Karma Sena” (Green Task Force), which took on a complex waste management challenge and collected over 825 thousand euros, primarily from non-biodegradable solid waste, by 2021 [9]. The government has subsidized bio methanation, composting, and aerobic digestion units to process organic waste, and they have made a difference by enlisting women from Kerala's SPEM mission to facilitate the movement [10]. Figure 6 depicts the procedure. These surveys provided ideas for introducing frugality into solar and biomass literature studies in the future, as well as for addressing the main research objective.

Figure 6: Flowchart showing function of the Haritha Karma Sena [10].

2.2 Biomass Energy

Biomass ranks fourth, meeting 14% of world energy demands (Colantoni et al., 2021). This accounts for over 10% of global annual energy consumption, compared to natural gas, coal, and oil, which account for 21%, 27%, and 33%, respectively. Solid biomass, one of these emerging bioenergy systems, can be used directly or processed into liquid biofuels and gas fuels such as biogas or synthesis gas (syngas) and has been deemed a carbon-neutral fuel (W. H. Chen et al., 2012). According to Mekonnen et al. (2020), in rural and urban regions, around 90% of biomass is utilized for basic cooking and 14% to 0.4% for lighting, where an average household requires approximately 5-7 GJ of usable energy, or 3-5 tons per household.

Any organic substance (living organisms and their waste) produced by bacteria, plants (including algae), or animals is referred to as biomass. Agricultural wastes and by-products of food processing are also used as alternative fuels or valuable commodities to replace fossil fuels. However, these may pertain to economic (e.g., cost reduction), energy (e.g., biogas and biodiesel), agricultural, or environmental challenges (e.g., global warming) (W. Tsai, 2017).

Biomass energy not only diversifies fuel consumption but also reduces air pollution by emitting fewer sulfur, carbon, and heavy metals than traditional sources. The presence of a high concentration of lignocellulosic components or organic elements (i.e., carbon, hydrogen, oxygen, and nitrogen) indicates the presence of carbon-rich, low-ash compounds that encourage energy consumption and resource recycling (W. Tsai, 2017). As a result, environmentally acceptable methods of using agricultural wastes are being developed to alleviate environmental and energy issues by employing modern thermochemical energy conversion techniques such as combustion, gasification, and pyrolysis to smooth the path for climate change mitigation (Rafiq et al., 2016).

According to Kataki et al. (2015), biomass feedstocks include wood wastes, herbaceous species, agricultural wastes, coffee wastes, wood wastes, industrial residues, wastepaper, municipal solid waste, sawdust, food processing waste, aquatic plants, animal wastes, etc. They classify them into three basic categories: first generation (edible feedstock from agricultural waste), second generation (non-edible from lignocellulosic biomass and crop-waste residues), and third generation (photosynthetic and fermentative bacteria). Some of the characteristics that guarantee high-quality fuel and chemicals include high-quality, homogeneity, high biomass density, stability, repeatability, low moisture content, low ash, high productivity, and inexpensive cost (Kataki et al., 2015).

2.2.1 Compositional Analysis of Biomass Feedstock

According to the United Nations Framework Convention on Climate Change (UNFCCC), the above discussed lignocellulosic materials are a mixture of the following components, primarily consisting of carbon, nitrogen, hydrogen, oxygen, and sulfur (W. Tsai, 2017) . Their major components are shown in Figure 7:

- *Cellulose:* A long-chain linear high molecular weight polymer (with a molecular weight up to 10^6 or above), made of anhydro-D-glucose, makes up the structural element of biomass cell walls. It serves as the skeletal foundation for the majority of terrestrial biomass and decomposes at temperatures ranging from 240–350 °C (Kataki et al., 2015; W. Tsai, 2017; Tumuluru et al., 2011).
- *Hemicellulose:* A collection of heterogeneous polysaccharides branching polymers with 500–3000 sugar units per polymer, compared to cellulose's 7,000–15,000 and another component of plant cell walls that decomposes between 200 and 315 °C (W. H. Chen et al., 2012; W. Tsai, 2017). Depending on its chemical composition and connection with cell lignin, most of its weight loss occurs above 180°C, producing less tar and char than cellulose (Tumuluru et al., 2011).
- *Lignin:* It is the third most significant component of woody biomass cell walls. Lignin is a complex and highly branched polymer composed of phenylpropane units connected in a three-dimensional matrix that begins to degrade between 160 and 900 °C by breaking ether linkages and carbon-carbon bonds, resulting in the formation of phenols (W. H. Chen et al., 2012; W. Tsai, 2017; Tumuluru et al., 2011). It is covalently linked to hemicellulose and cross-links aromatic and hydrophobic plant polysaccharides. Lignin dehydrates more slowly than cellulose or hemicellulose and creates more char.
- *Others:* These include ash and extractives. Protein, oil (or fat), starch, and sugar may be extracted from the tissues of living organisms. The former refers to the inorganic components of the biomass (W. Tsai, 2017).

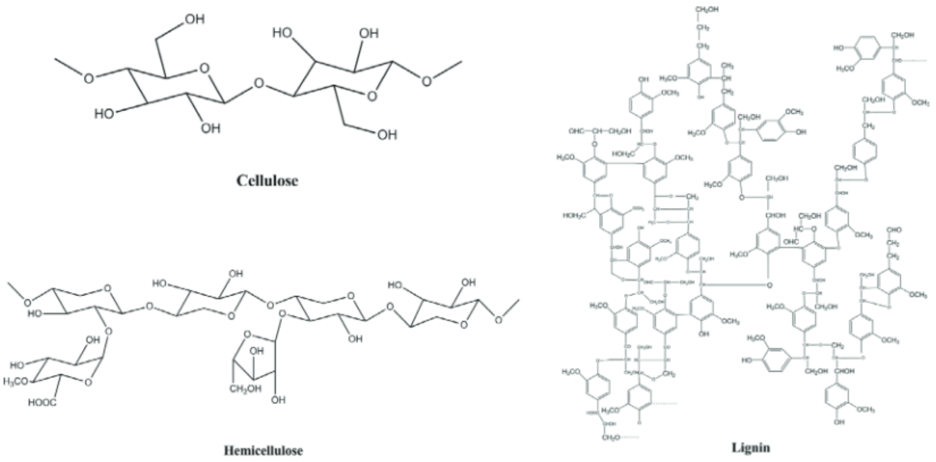

Cellulose

Hemicellulose

Lignin

Figure 7: Composition of cellulose, hemicellulose, and lignin (Kataki et al., 2015).

According to Kataki et al. (2015), cellulose composition is dominated by herbaceous and agricultural biomass, followed by woody and animal biomass. Hemicellulose content varies greatly, but generally follows a similar pattern. Lignin content, on the other hand, is higher in woody biomass than in agricultural products and, like hemicellulose, is highly variable. Agricultural wastes, in particular, are rich in lignocellulosic elements (i.e., cellulose, hemicellulose, and lignin) and thus have high heating values when dried (W. Tsai, 2017). However, untreated biomass inherently has a few disadvantages: high moisture content, low heating value, high hygroscopicity, and high heterogenicity (varying properties due to species, location, plantation, etc.), making it difficult to store, economically handle, or transport for conversion to fuel (W. H. Chen et al., 2012; W. Tsai, 2017).

2.2.2 Biomass Pre-treatment and Thermochemical Methods

Biomass is the only complex renewable energy source that can be transformed into liquid, solid, and gaseous fuels, in contrast to other renewable energy sources that provide heat and power (Kataki et al., 2015). Due to the heterogeneity and complexity of natural lignocellulosic biomass, as mentioned above in Section 2.2.1, it must be pre-treated to increase enzyme activity or greater hydrophobicity for easier combustion (W. Tsai, 2017). Among the two major types of treatment methods: biochemical and thermochemical, the latter is commonly adapted. According to Ronsse et al. (2015), thermochemical conversion of biomass is the use of heat to degrade or transform biomass into usable products. Pyrolysis, liquefaction, gasification and combustion are some of the thermochemical procedures to convert them to various fuels. These are shown in Table 2.

Table 2:Thermochemical conversion and their end products (Ronsse et al., 2015).

Thermochemical Conversion Process Type				
	Fast Pyrolysis	Carbonization	Gasification	Torrefaction
Temperature (°C)	~500	>400	600-1800	<300
Heating rate	Fast, up to 1000 °C/min	<80 °C/min	-	-
Residence Time	Few seconds	Hours ~ days	-	<2h
Pressure	Atmospheric (and Vacuum)	Atmospheric (or elevated up to 1 Mpa)	Atmospheric (or elevated up to 8 Mpa)	Atmospheric
Liquids (bio-oil)	75 %	30 %	5 %	5%
Non-condensable gases	13 %	35 %	85 %	15 %
Char/Solids	12 %	35 %	10 %	80 %
Medium	Oxygen-free	Oxygen-free or oxygen-limited	Oxygen-limited (air or steam/oxygen)	Oxygen-free

Among the aforementioned methods, pyrolysis is the most common where organic material is decomposed in oxygen-free or oxygen-limited circumstances. During pyrolysis, complex and polymeric biomass elements (lignin, cellulose, lipids, and starches) are thermally broken down into three fractions: bio-oil, char (solid fraction), and non-condensable gases.

Pyrolysis may be slow or fast, depending on the heating rate. The former is used to produce bio-coal, biochar, or charcoal at slower heating rates (less than 50 °C/min) (W. Tsai, 2017). Torrefaction, or mild pyrolysis, is the treatment process with the lowest reaction temperature and energy demand, with its products having a calorific value that is commercially viable (Lee et al., 2021). It subjects biomass feedstock to low temperatures of 200-300 °C in an oxygen-free atmosphere, where degradation of hemicellulose, depolymerization of cellulose, and thermal softening of lignin occur, altering the physical and chemical properties of the biomass (Kataki et al., 2015). He lauds torrefaction not only as a suitable pretreatment strategy for producing high biochar (80%) while treating biomass feedstocks with high moisture content and low grindability, but also as a pre-cursor for future pyrolysis/carbonization methods.

While cellulose and hemicellulose are the primary sources of resulting volatiles, lignin degrades much slower and over a wider temperature range (250-500 °C), making it the major contributor to char production (W. Tsai, 2017).

2.2.3 Biochar Characterization and Functionality

According to the International Biochar Initiative (IBI) [11], biochar is "a solid substance produced by thermochemically converting biomass in an oxygen-limited environment" [8]. (Rafiq et al., 2016) explains empirical mathematical links and biochar-relevant parameters including torrefaction/pyrolysis temperature and physio-chemical properties, which can be used to make biochar and analyze its quality, commercial value, applicability, stability, fuel ability, and effect on soil fertility. Biochar is one of the few compounds capable of actively removing CO_2 from the environment, as opposed to merely capturing or reducing it (Ronsse et al., 2015). Figure 8 represents biochar as an integrated carbon storage and bio renewable production system. In particular, owing to the variability and complexity of the feedstock, the biochar generated varies significantly, making it crucial to characterize and analyze it. There are a few common ways to describe biochar as a raw material and as a finished product:

2.2.3.1 *Physical Properties of Biochar*

- *Surface area and pore distribution*

  According to W. Tsai, (2017), the specific surface area is one of the most significant properties defining the pore volume and pore size distribution of biochar and can be studied using the Brunauer Emmett and Teller (BET) method. The porous structure of biochar results from the microstructure of the source biomass (xylem capillaries), shrinkage, physical cracking, and devolatilization. This not only promotes aeration and absorption but also the soil's capacity to retain water (Ronsse et al., 2015).

- *Densities*

  According to W. Tsai, (2017), two forms of density are often employed to define biochar: true density and bulk density. Bulk density is interlinked with the deformation of resultant pore collapse and thus decreases under increasing temperatures. Whereas true density increases with temperature and residence time (W. Tsai, 2017). Moreover, higher density biochar is frequently associated with better mechanical qualities due to its ordered structure and bigger concentrations of crystalline phases, which necessitates X-ray.

2.2.3.2 *Chemical Properties of Biochar*

- *Proximate Analysis*

Moisture, ash, volatile matter (VM), and fixed carbon (FC) are measured to proximate analyze biochar. Biomass feedstocks include various inorganic materials, including alkali, heavy metals, chlorine, phosphorus, and sulfur, collectively called "ash," which are affected by the feedstock type, growing conditions, fertilizers, and soil pollution (Ronsse et al., 2015).

Fixed carbon (FC) and volatile matter (VM) store the solid fuels' chemical energy. ASTM defines FC as organic (ash-free) material that remains after pyrolysis at 950°C [12]. VM measures the gaseous fuel content, and together they indicate the fuel's value by indicating its combustible fraction (Kataki et al., 2015). Higher VM in char reduces ignition and combustion temperatures but increases smoke, while low VM chars are difficult to ignite but burn cleanly (Ronsse et al., 2015).

- *Ultimate Analysis (elemental analysis)*

On a dry, ash-free basis, the concentration of carbon (C), hydrogen (H), oxygen (O), nitrogen (N), and sulfur (S) mass percentages are often determined using Ultimate Analysis (Kataki et al., 2015). These organic components also contribute to the volatile matter and fixed carbon compositions of biochar or biomass (W. Tsai, 2017).

- *High Heating Value (HHV)*

According to W. Tsai, (2017) , the HHV (also known as gross calorific value) of typical biomass ranges between 15 and 20 MJ/kg, which is comparatively lower than the range of **25–35 MJ/kg for coal**. This value represents the heat emitted by the sample's combustion in an adiabatic oxygen bomb calorimeter with the original and created water in a condensed condition.

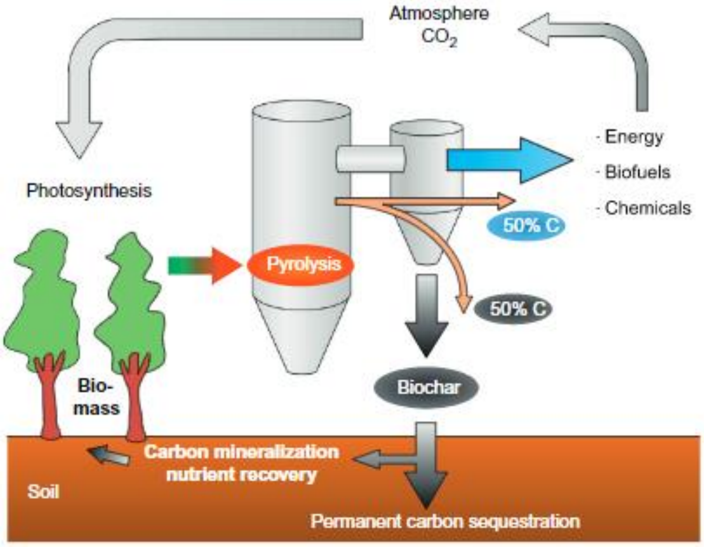

Figure 8: Biochar circular integrated production through mild / severe pyrolysis and it's uses (Ronsse et al., 2015).

- *pH and Cation Exchange Capacity (CEC)*

  (Ronsse et al. (2015); W. Tsai, (2017) state that pyrolyzed biochar mostly has an alkaline pH and can be used to mitigate acidic soils. The breaking down of acidic functional groups and soil exposure enable biochar's surface to get oxidized, thus producing oxygen-containing functionalities at its surface, such as carboxylic groups. Soil biochar enhances the CEC of soil, i.e., its ability to electrostatically adsorb or attract cations in soil water, which improves soil nutrient retention and reduces leaching (Ronsse et al., 2015; W. Tsai, 2017).

2.2.4 Potential of Spent Coffee Grounds as a Biomass

Spent coffee grounds (also termed ECRs) are formed from soluble coffee manufactured during the extraction (brewing) process, in which roasted, ground coffee is used to extract flavours in soluble or instant coffee-manufacturing factories and coffee shops. Finally, the screw-pressed insoluble residue (a slurry of SCGs) containing a high content of cellulose, hemicellulose, lignin, fatty acid, and other polysaccharides acts as a bioresource (W. Tsai, 2017). SCG has high carbon and hydrogen levels (>50% and >7.0 wt.%, respectively) and low ash content and can be estimated from Table 3.

Globally, around 8 MMT of SCG is produced each year [8]. According to Colantoni et al. (2021), coffee leftovers account for approximately 50% of coffee feedstock and contain a variety of potentially valuable chemical compounds. He states that 2 kilograms of wet SCG is produced for every kilogram of soluble coffee, and according to Vakalis et al. (2019), a 4 kg batch of SCG yields 500g of biodiesel. Interestingly, because coffee beans are already roasted, the biochar produced from the treatment of SCG is more than that of agricultural waste or woody biomass, as illustrated in Figure 9.

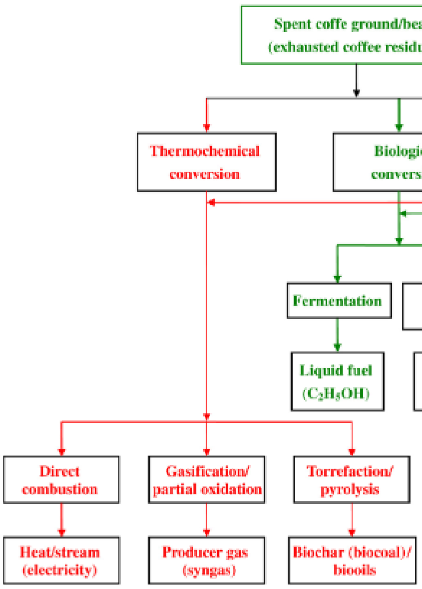

Figure 9: Conversion of SCG to alternative fuels (W. Tsai, 2017).

Due to its high carbon content, dried SCG can be used directly as a biomass fuel in mills, as a precursor for making activated carbon; as a bio-sorbent for removing pollutants from aqueous solutions; an agent for soil enrichment; and an avenue for GHG mitigation (primarily CO_2 and CH_4) (Lee et al., 2021; W. Tsai, 2017; W. T. Tsai & Liu, 2013). According to them, the high surface area and porosity of SCG biochar prevent hazardous components from leaching and runoff while also keeping soil pH stable,

making it highly advantageous for agricultural industries. Furthermore, Vakalis et al. (2019) show how treated SCG combined with granulated limestone acts as an effective absorbent for the removal of methylene blue and orange II. Research also compares the high heating value of torrefied SCG (26-32 MJ/kg) to that of fossil coal (28-32 MJ/kg); this can be compared by the Van-Krevelen diagram shown in Figure 10 (W. Tsai, 2017; W. T. Tsai & Liu, 2013). According to W. Tsai, (2017), this was also very similar to the industrial coal-based char in terms of carbon content on a dry basis (72.6–76.2 wt.%).
This section displayed the principles, composition, and definitions of biomass along with its thermal treatment processes to convert it into biofuel. The review not only provided substantial examples of the potential of using SCG as a biomass but also added the possibility of using torrefaction as a thermochemical method to produce biochar.

2.3 Torrefaction of Spent Coffee Grounds (SCG)

As shown in Table 2, torrefaction is mild-pyrolysis at lower temperatures (200-300°C) and shorter residence times than carbonization and pyrolysis. Torrefaction serves to pre-treat the biomass to produce superior fuel properties compared to its parent biomass, providing 70-80% solid yield and 90% of its energy in subsequent procedures such as pyrolysis, gasification, or combustion—which may be carried out in its pure form or in combination with fossil coal as feedstock (Ronsse et al., 2015).

2.3.1 Torrefaction Fundamentals

Torrefaction destroys stubborn fibers and increases energy density by dehydrating, devolatilizing, depolymerizing, and carbonizing biomass. According to Bhaskar and Pandey (2015), the primary cause of mass loss during torrefaction below 200 °C is bound water evaporation, which begins at 160 °C. The majority of the reduced mass yield during the torrefaction process, which yields volatile molecules such as H_2O, CO, CO_2, H, acetic acid, and other organics, is compensated by bound moisture removal and thermal degradation (Ronsse et al., 2015). The dehydration and devolatilization events are generally exothermic, but some endothermic condensation reactions can occur (Joshi, 2015). As shown in Figure 11, hemicellulose degrades at torrefaction temperatures as low as 230 °C, with devolatilization reactions beginning even lower than 200 °C (W. H. Chen et al., 2012; Joshi, 2015). Even at high torrefaction temperatures (240-320 °C), cellulose and lignin do not decompose, according to research (W. H. Chen et al., 2012; W. H. Chen & Kuo, 2011b, 2011a; Joshi, 2015).

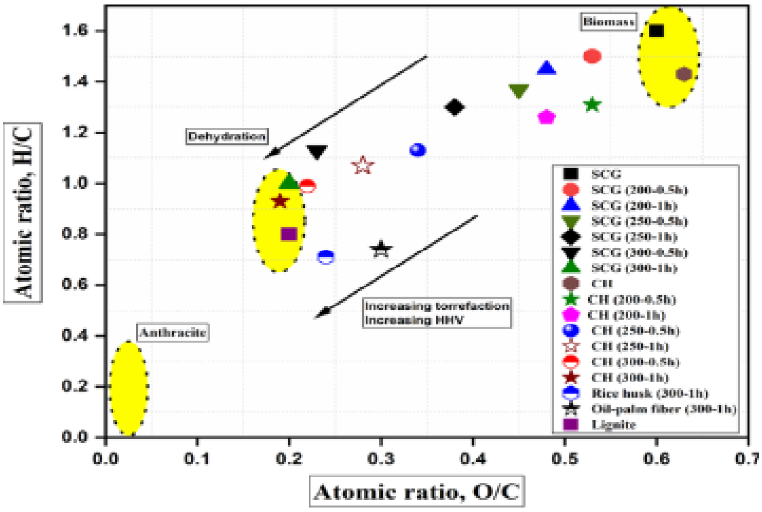

Figure 10: Van Krevelen diagram of raw and torrefied SCG (Mukherjee et al., 2022).

Ballesteros et al. (2014) showed a composition of hemicellulose (40%), cellulose (12.5%) and lignin (23.9%) in the raw SCG sample along with inorganic ash and moisture. Although there was a difference in composition, morphology, and decomposition behaviour, the thermal behaviour of the macromolecules stayed defined (Joshi, 2015). Torrefied SCG samples revealed decreased atomic ratios (H/Cand O/C) due to low H and O content and thus a movement left-downwards in the Van Krevelen diagram, approaching the atomic ratios of lignite coal as shown in Figure 10.

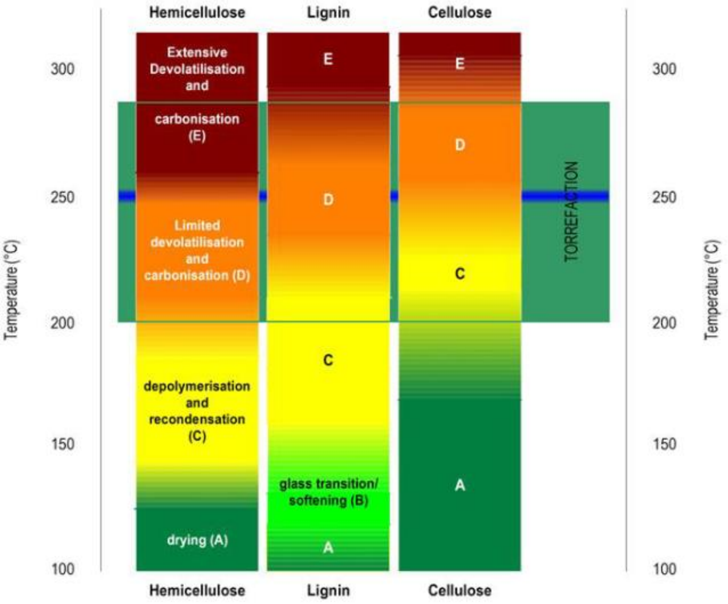

Figure 11: Various stages involved in Torrefaction (Tumuluru et al., 2011).

2.3.2 Physical properties and advantages of Torrefied SCG

According to Kosov et al. (2016), torrefaction alters the physical properties of biomass, such as moisture content, density, grindability, pelletability, hydrophobicity, and calorific value, as well as the storage behaviours of spontaneous combustion and self-heating. The fundamental advantage of torrefaction is that the pellets or chips created can be utilized to substitute coal as a non-renewable fuel in different energy units. Some of the advantages linked with the physical properties of torrefied SCG are listed below:

- *Reducing Moisture Content and biological activity*

  Raw biomass absorbs water well owing to hydroxyl groups (OH). Thus, to avoid degradation, initial raw SCG must be dried to 6.5 percent before pre-treatment (Nosek & Tun, 2020).Torrefaction destroys these OH groups and forces biomass to lose hydrogen bonding ability, resulting in a hydrophobic product (Tumuluru et al., 2011). He also states that torrefaction can reduce pre-dried biomass moisture from 10% to 6%. Torrefied biomass molecules are nonpolar and exothermic, so they don't break down or absorb moisture during storage and transportation thus maintaining the quality of the product.

- *Density*

  Torrefaction enhances energy density by eliminating moisture and decomposing cellulose polymers into CO_2 and H_2O while leaving carbon as char, conserving more energy-containing components, and losing more non-energy ones (W. H. Chen & Kuo, 2011b, 2011a; Dhungana et al., 2012). Mass loss of solids, liquids and gases result in increasing the porosity thus reducing volumetric density by around 180–300 kg/m^3 depending on biomass density and torrefaction conditions (Joshi, 2015; Tumuluru et al., 2011). Although torrefied material has a low bulk density, its heating value per volume is not necessarily increased.

- *Pelletability*

Unpelletized biomass leftovers are harder to transport and store. According to Tumuluru et al. (2011), torrefying biomass before pelletization creates a homogenous, high-quality feedstock and is affected by the amount of lignin as it improves binding and eases densification. Torrefaction breaks down the hemicellulose matrix and forms fatty unsaturated compounds, improving lignin binding. Moreover, W. Tsai, (2017) states that torrefied biomass can be readily ground and compressed into dense pellets without the use of binders.

- *Improvement in Heating Value*

A substantial increase in HHV is due to drying supported by the increased hydrophobicity, preventing water reabsorption during torrefaction. The calorific value of torrefied SCG can be substantially increased, depending on parameters such as residence time, temperature and moisture content.

- *Visual Observation*

Torrefaction produces a dark char-like product with a similar aesthetic effect as carbonization, although the output isn't as dark. Torrefaction converts only a small portion of hydrocarbons to char and Dhungana et al. (2012) found that as temperature and residence time increases, more biomass polymers are turned into char making torrefied biomass darker and more carbonized.

- *Improved Grindability*

Biomass fibres bind particles, making raw ground samples difficult to handle. Hemicellulose gives lignocellulose fibres their binding strength, and as it "melts," it becomes brittle, making its disintegration the principal step of torrefaction, followed by lignin (Dhungana et al., 2012). According to Tumuluru et al. (2011) , reduced particle length, but not diameter, improves grindability and handling, making solid biomass easier to crush and pulverize. He also claims that torrefying biomass reduces grinding mill power consumption by 70-90%.

- *Improved Specific area and Porosity*

Torrefied biochar can be further activated by chemical or physical activation to create more porous activated charcoal or activated carbon, which is more accessible for absorption (W. Tsai, 2017). In contrast to the bulk density, the total pore volume of SCG biochar rises with increasing temperature and residence time (Lee et al., 2021). Moreover, due to its brittle, coal-like structure, torrefied biomass yields smaller, more uniform particle sizes than untreated biomass (Kataki et al., 2015).

2.3.3 Torrefaction Characterization and of SCG

A literature study was done on the characterization of torrefied SCG samples. Proximate Analysis, Ultimate Analysis, Moisture Content, and the calorific value of the samples showed a significant improvement in the fuel characteristics of the SCG upon torrefaction.

SCG was torrefied in a comparative study in an inert (N_2) experimental setup by W. H. Chen et al. (2012), at two torrefaction temperatures of 240 and 270°C and residence times of 0.5 hr and 1 hr. The influence of torrefaction temperature and residence time on SCG, as shown in Figure 12, showed the high sensitivity of SCG to torrefaction temperature and residence time compared to other agricultural wastes due to the presence of higher volatile matter and hemicellulose content. A 16% and a 35 % weight loss were observed at 240° and 270°C at a residence time of 1 hour. Moreover, the HHV of the SCG sample increased with increasing residence time and temperature (12.74 % and 37.25 % at 240°C/1 hour and 270°C/1 hour, respectively). To infer from this increase, W. H. Chen et al. (2012) conclude that the more hemicellulose in biomass, the greater the torrefaction enhanced HHV.

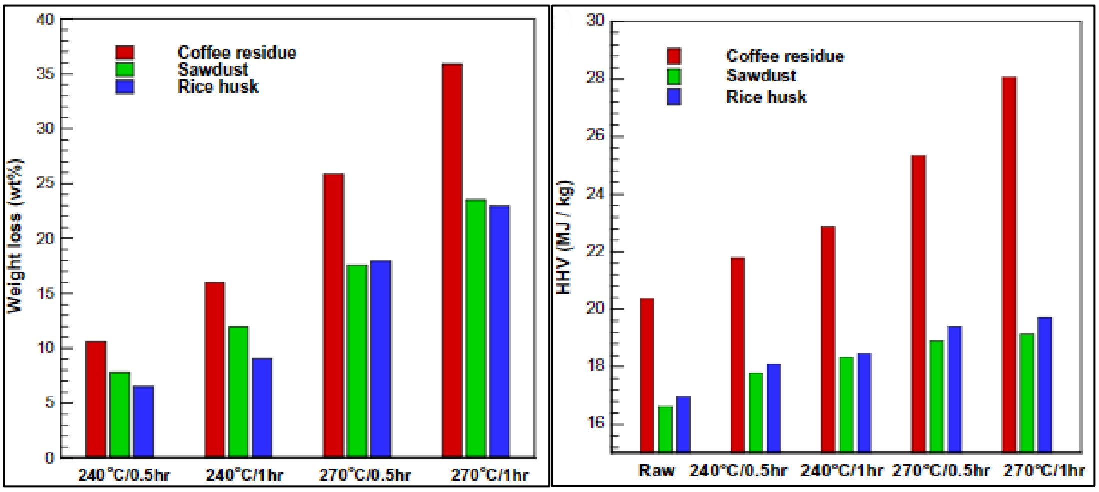

Figure 12: Weight loss and HHV of SCG with respect to increasing temperature and residence time (W. H. Chen et al., 2012).

Vakalis et al. (2019) also conducted pyrolysis experiments in a quartz pyrolysis reactor under inert environmental conditions (N2) at a heating rate of 50 °C/min and a residence time of 30 minutes. He stresses the importance of drying the sample, which is generally more than 62 percent. The volatiles were gradually vaporized with increasing temperature, causing the carbon content to increase with a decrease in recovered solid yield as shown in Figure 13. On the other hand, he mentioned a peculiarity between 240 and 250 °C where not only carbonization of the feedstock occurs but also the yield percentage is significantly high, and he uses this trade-off to aim for an optimal torrefaction temperature. At 240, 250, and 260 °C, mass loss was observed to be 15%, 25%, and 30%, respectively.

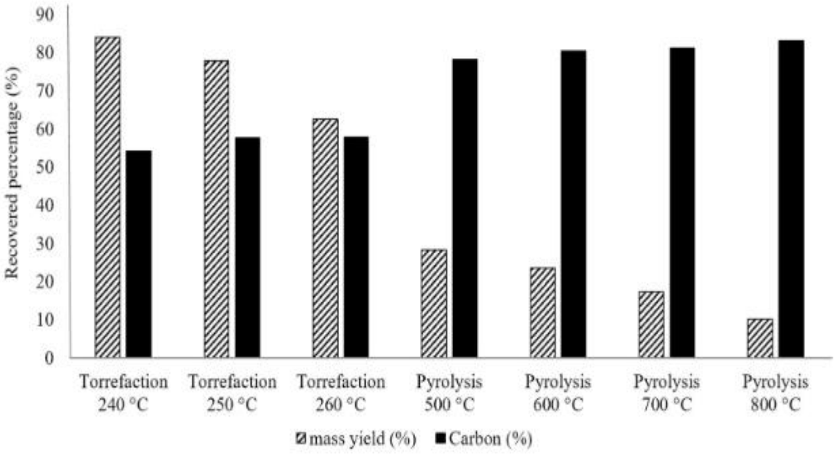

Figure 13: Solid recovery yields and carbon content variation of torrefied and pyrolyzed (Vakalis et al., 2019).

According to Barbanera & Muguerza, (2020), the solid yield decreases, and the liquid and gas yields increase with increasing temperature, as shown in Figure 14. The torrefied SCG was characterized by a mass loss of 20 %, 33%, and 47 % at 210 °C, 235 °C, and 260 °C, respectively, following a similar trend as other literature. It was mentioned by Y. C. Chen & Jhou, (2020) that a lower mass yield leads to a lower energy yield, and it decreased when temperature or oxygen concentration increased.

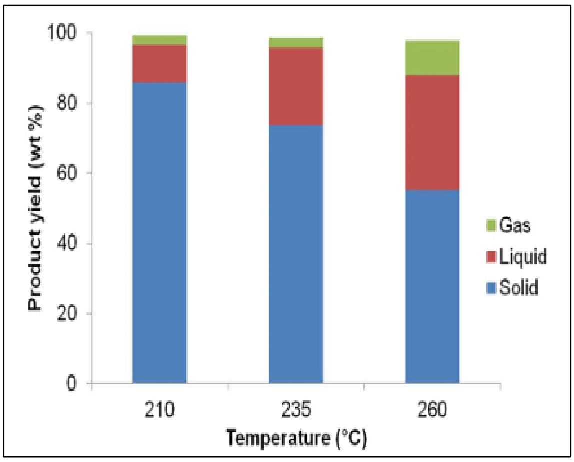

Figure 14:Relation of solid yield based on reaction temperature (Barbanera & Muguerza, 2020).

Lee et al., (2021) , show that the HHV of torrefied SCG increases with increasing temperature as shown in Figure 15(a), with the highest HHV of 30.32 MJ/kg obtained at 300 °C. This showed a 10% increase in calorific value at 200 °C, a 29 % increase at 250 °C, and a 45.6% increase at 300 °C. Work by W. T. Tsai & Liu (2013) seen in Figure 15(b), showed a similar behaviour. At 623 K (350 °C), the calorific value increased by about 24%, and the slope increased significantly at 565 K (290 °C). Additionally, the significant increase in carbon dioxide content as seen in Table 2 suggested 298–320 °C as the optimum temperature range for torrefaction (W. T. Tsai & Liu, 2013), which was a little different than other literature. A similar increase in calorific value for torrefied material with increasing temperature was shown by (Barbanera & Muguerza, 2020; W. H. Chen et al., 2012), as inferred from Table 3.

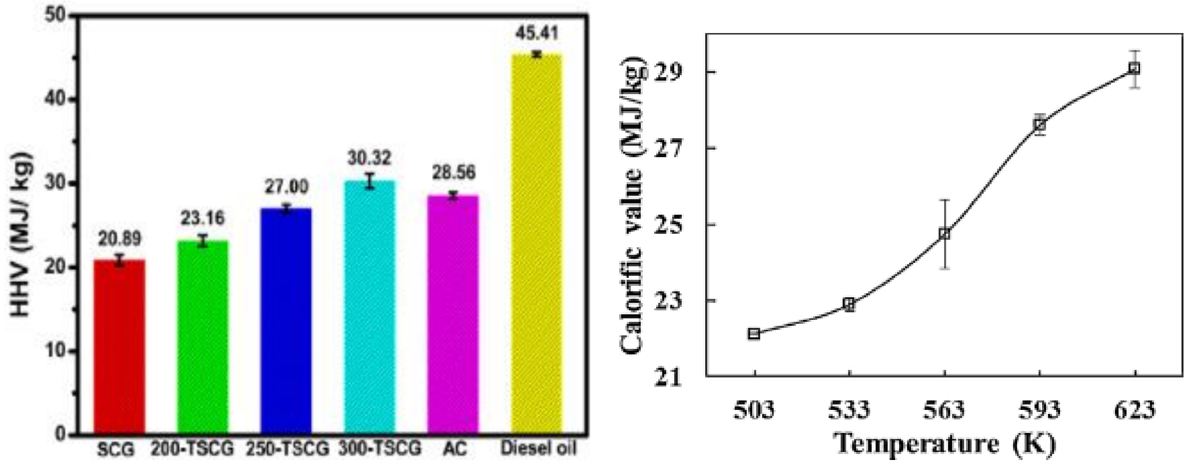

(a) *(b)*

Figure 15:HHV of raw SCG and that at different torrefaction temperatures ((a)Lee et al., 2021; (b) W. T. Tsai & Liu, 2013).

The experiment performed by Colantoni et al. (2021) showed very low ash remains compared to other common solid biomass, proving that SCGs could be used as a clean biomass resource. According to the correlation matrix shown by Colantoni et al., (2021) and Mukherjee et al., (2022), the heating values decrease with an increase in ash and nitrogen content due to the larger quantity of unburnt products, slagging, fouling, obstruction in combustion, and thus lower calorific value of the same. SCGs with a higher concentration of N atoms also lead to higher production of ash, a lower percentage of C, H, and O, and hence lower heating values. However, the torrefied SCG had an ash content still lower than that of lignite coal (8.5 % wt.) (Mukherjee et al., 2022).

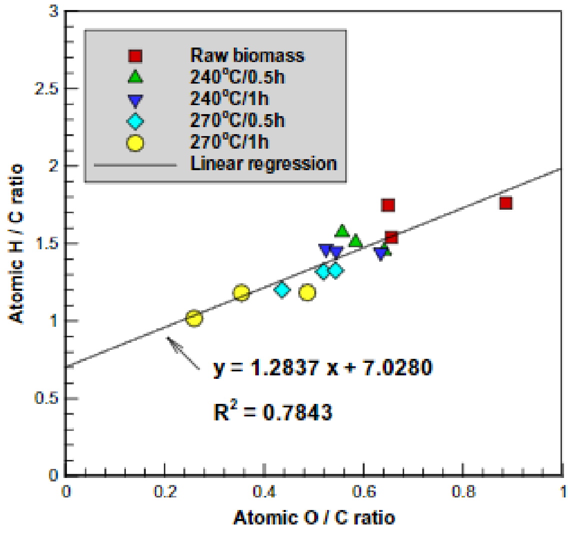

Figure 16: Distribution of atomic H/C and Atomic O/C ratio (W. H. Chen et al., 2012).

The studies performed by Y. C. Chen & Jhou, (2020) focused on finding the O/C and H/C ratios to prove the benefits of torrefaction, which resulted in decreasing atomic oxygen-to-carbon and hydrogen-to-carbon ratios. This decrease in O/C ratio resulted in lignocellulosic components devolatilizing and decomposing, reducing the oxygen content. The drop in hydrogen content with higher torrefaction temperatures was due to the emission of hydrocarbons (CH_4 and C_2H_6), thus increasing the HHV of the biomass (Mukherjee et al., 2022). Figure 16 shows the distribution of atomic H/C and atomic O/C ratios of torrefied SCG. The relationship between the elemental compositions of raw and torrefied SCG could be described by a linear equation with a slope, suggesting that the torrefaction treatment was more effective on the H/C ratio than on the O/C ratio by a factor of around 1.3 (Barbanera & Muguerza, 2020;

W. H. Chen et al., 2012). This increase in H/C and O/C as temperature rose from 240 to 270 °C was comparable to sub-bituminous coal values. The torrefied sample by Y. C. Chen & Jhou, (2020) also had a chemical composition like lignite.

The authors (Bangkha et al., 2020; Barbanera & Muguerza, 2020; W. H. Chen et al., 2012, 2019; Y. C. Chen & Jhou, 2020a; Colantoni et al., 2021; Mukherjee et al., 2022) use Equations 1, 2 and 3 to find out the co-dependency between the torrefaction temperature and energy properties (solid yield, energy yield, enhancement factor and HHV).

(1)

$$Enhancement\ Factor = \frac{HHV_{torrefied\ biomass}}{HHV_{raw\ biomass}}$$

(2)

$$Mass\ Yield = \frac{Mass\ of\ torrefied\ biomass}{Mass\ of\ dried\ initial\ biomass} \times 100$$

(3)

$$Energy\ yield\ (\%) = \frac{Total\ energy\ of\ torrefied\ biomass}{Total\ energy\ of\ raw\ biomass}\% = Enhancement\ Factor \times Mass\ Yield\ \%$$

The amount of energy retained by torrefied biomass after losing some energy components during the torrefaction process, resulting in a lower energy output, is referred to as energy yield (Bangkha et al., 2020). The energy yield decreases due to biomass degradation during the torrefaction process, i.e., increasing torrefaction temperatures and mass losses. Energy yield is directly related to the mass yield value and the HHV as per Equation (3). As a result, as demonstrated by studies, the former was more influential than the latter, and thus the percentage of energy yield decreased with increasing temperature (Barbanera & Muguerza, 2020; W. H. Chen et al., 2012; C. Zhang et al., 2019).

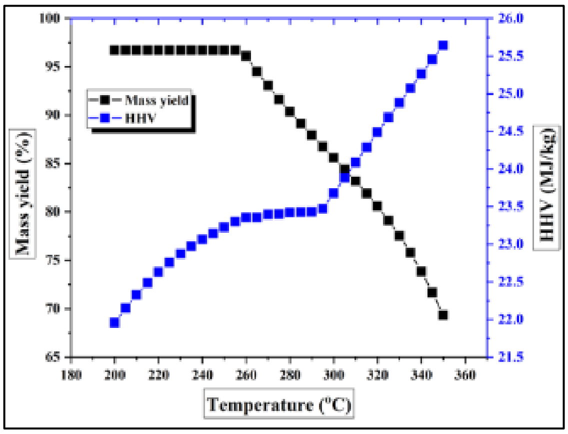

Figure 17: Torrefaction temperature affecting the mass yield % and HHV of SCG (Mukherjee et al., 2022).

Figure 17 shows how mass yield and HHV of torrefied SCG are linked to torrefaction temperature (Mukherjee et al., 2022). The solid mass yield is virtually constant between 200 and 250 °C but decreases above 250 °C. The HHV increased from 22 MJ/kg to 23.7 MJ/kg when heated from 200 to 300 °C. Compared to other research, the differences in mass yield and HHV increase in this experiment show that SCG feedstock is heterogeneous and may be subjective.

Table 3:Literature review: Proximate, Ultimate Analysis and Calorific value of different samples of SCG.

ANALYSIS	**(Barbanera & Muguerza, 2020)**				**(Y. C. Chen & Jhou, 2020b, 2020a)**				**(W. T. Tsai & Liu, 2013)**					**(W. H. Chen et al., 2012)**					**Lee et al., 2021**			
Proximate Analysis (% Dry Basis)	Raw SCG	SCG 210 °C	SCG 235 °C	SCG 260 °C	SCG A	Sample 1	SCG B	Sample 4	SCG Sample	SCG 230 °C	SCG 250 °C	SCG 270 °C	SCG 290 °C	Raw SCG	SCG 240°C (0.5 hrs)	SCG 240°C (1 hr)	SCG 270°C (0.5 hrs)	SCG 270°C (1 hr)	SCG	SCG 200 °C	SCG 250 °C	SCG 300 °C
Volatile Matter	82.5	77.4	75.6	70.8	81.58	60.59	82.37	64.15	79.5	--	--	--	--	68.8	---				72	73	66	49
Ash Content	0.41	0.53	0.58	0.86	1.36	3	1.4	3.38	0.7	--	--	--	--	1.76	1.97	2.45	3.21	3.86	2.87	1.24	3.04	2.09
Fixed Carbon	17.1	22.1	23.8	28.3	17.06	34.54	16.23	32.21	8.3	--	--	--	--	14.9	---				19.83	20.81	27.96	42.91
Moisture Content %	Dried at 105 °C for 24 hours 58% → 10%				Dried at 105 °C for 24 hours 55% →10%				Dried at 100 °C for 24 hours (11.5 %)					Dried at 105 °C for 24 hours To 14.5%					5.30	4.95	3	6
HHV (MJ/kg, Dry Basis)	25.3	26.6	27.3	29.5	22.12	27.28	21.81	26.55	23.5	22	23	25	27.8	20.4	21.8	23	25.8	28.2	22.63	22.74	26.45	30
C	59.7	62.2	63.7	66.6	--	71.15	--	67.83	52.2	55.10	56.63	58.82	66.77	47.45	50.83	52.10	55.93	65.10	50	51.14	59.49	68.61
H	7.8	7.7	7.7	7.5	--	4.55	--	4.47	7	6.36	6.22	6	5.46	6.91	6.66	6.36	5.6	5.52	7.89	7.52	7.01	3.19
N	2.2	2.2	2.3	2.7	--	0.31	--	0.28	2.5	2.25	2.45	2.64	3.04	2.55	2.74	2.57	2.67	2.94	2.44	2.65	3.18	3.56
S	0.1	0.1	0.1	0.1	--	0	--	0	0.1	--	--	--	--	0.24	0.06	0.09	0.07	0.08	0.33	0.35	0.28	0.26
O	30.2	27.8	26.2	23.1	--	23.99	--	27.42	34.8	36.29	34.70	32.53	24.73	41.09	37.74	36.43	32.52	22.50	39.35	38.34	29.57	20.56

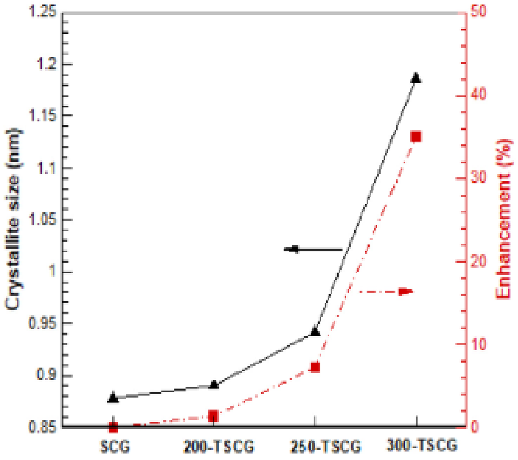

Figure 18: XRD and crystal size enhancement factor of SCG and torrefied SCG with respect to increasing torrefaction temperature (Lee et al., 2021).

Figure 18 shows a comparison of the crystalline structures of SCG and torrefied products using an X-ray diffractometer. According to the results, as intermolecular forces increase, crystallinity increases, improving the material's thermal stability. According to Ballesteros et al. (2014), hydrogen-strong microfibre interactions in crystalline regions give cellulose its high tensile strength and chemical resistance. XRD spectra can show its crystalline and amorphous structures, whereas hemicellulose and other SCG components are chemically amorphous. In addition, he claims that heat treatment of coffee beans may contribute to SCG crystallinity by eliminating certain water molecules.

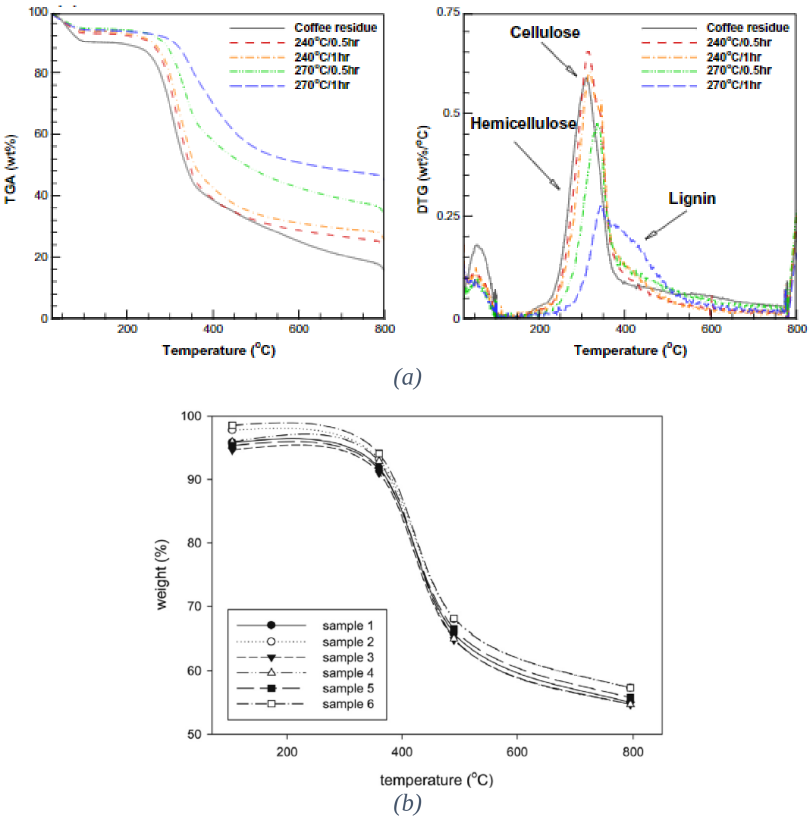

(a)

(b)

Figure 19: TGA and DTG of raw and torrefied SCG ((a)W. H. Chen et al., 2012; (b)Y. C. Chen & Jhou, 2020).

The research by the authors demonstrates the thermal decomposition characteristic as the TGA curve from 5 samples at 10% moisture in Figure 19 (Y. C. Chen & Jhou, 2020; W. H. Chen et al., 2012; W. T. Tsai & Liu, 2013). Raw waste lost more weight than torrefied waste when the thermogravimetry temperature was between 25 and 105 °C, demonstrating that torrefied waste is hydrophobic. *First Stage:* (105-350 °C) The emission of water and low-molecular-mass volatiles led to a five percent drop in mass. *Phase two:* (360-490 °C) Hemicellulose and cellulose decomposed at 220–315°C and 315–400°C, respectively, resulting in a weight loss of 35%. In the *third step*, more carbonaceous materials were produced, resulting in a 10% decrease in mass. A 30% biofuel residual was detected at 800 °C indicating a weight loss with increasing temperature until burnout (Y. C. Chen & Jhou, 2020). These results complemented the previously indicated rise in calorific value.

2.4 Solar Collectors and applications

The earth's surface receives an average horizontal irradiance of 170 to 300 W/m^2, which can only produce an ambient temperature of less than 50 °C; hence, Ndukwu et al. (2020) suggest the use of optical devices to boost the radiation density and storage system. As shown in Figure 20, there are two basic categories for converting solar energy into heat: stationary and tracking systems. These may include flat-plate collectors, evacuated water heating systems, and central concentrating receivers utilized in high-tech industrial applications. In this study, only stationary collectors are considered.

The thermal energy acquired by converting solar energy can be used to heat a functioning system and is frequently accompanied by a second collector if there is insufficiency. A concentrating collector features a parabolic reflecting surface to focus solar irradiation on a smaller aperture area than a stationary collector. Stationary collectors such as Flat-Plate Collectors (FPCs), Compound Parabolic concentrators (CPCs), and Evacuated Vacuum Collectors (EVCs) operate between 30 and 240 °C with a low concentration ratio (1 to 5), whereas tracking collectors operate at higher concentration ratios (10 to 1500) at significantly higher temperatures (60 to 2000 °C) (Cassidy, 1981; Ndukwu et al., 2020).

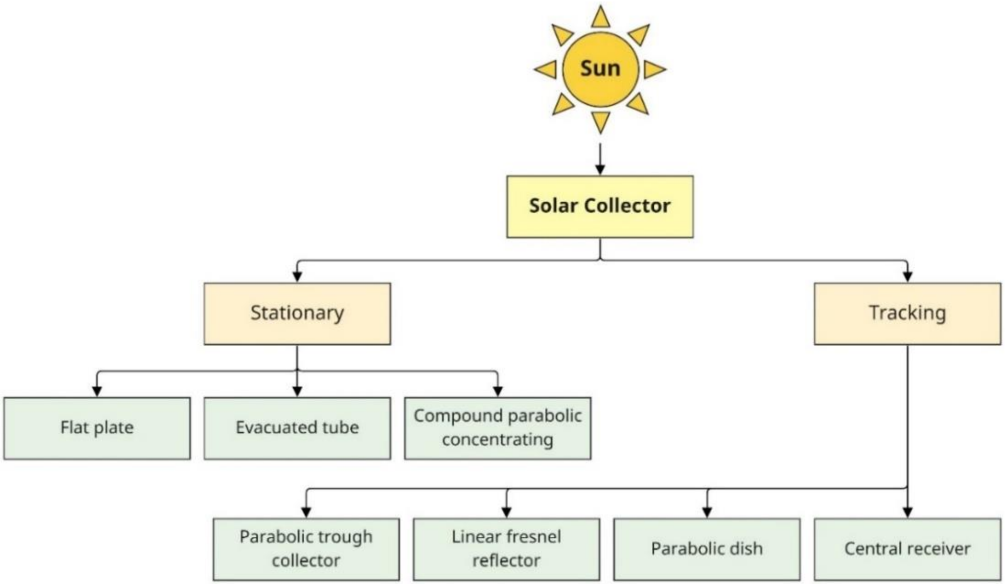

Figure 20: Classification of different Solar Collectors available in the market (A. Kumar et al., 2021).

2.4.1 Flat Plate Collectors

Flat Plate Collectors (FPCs) are intended for use in low- to medium-temperature (60-100 °C) environments. It is used to absorb solar energy, transform that energy into heat, and then transport that heat to a stream of liquids or gases. They utilize both direct and diffuse solar energy, do not require sun tracking, and little maintenance. FPC is often permanently positioned and does not require sun monitoring. Glass has been widely used to glaze FPCs due to its ability to transmit up to 90% of incoming shortwave solar radiation while transmitting very little of the absorber plate's longwave radiation. Antireflective coating and surface roughness can dramatically increase transmission (Cassidy, 1981).

2.4.2 Evacuated Tube Collectors

According to Arora et al. (2011), each evacuated tube is made up of two borosilicate glass tubes that are extremely durable and work on a complex thermos principle. Solar light passes through the external low-reflective and high-transmissive glass tube, and the selective absorbing coating absorbs it, heating the highly absorptive black painted aluminium or copper fin, and eventually, the inner fluid (Gao et al., 2014). The ends of the tubes connected to the copper header are welded together, generating a vacuum (Arora et al., 2011; Siva Kumar et al., 2017). As demonstrated in Figure 21, the vacuum is a perfect insulator that prevents short-wave radiation from escaping, acting as a greenhouse (Arora et al., 2011). Because of the insulation, the outer tube is substantially cooler than the inner tube, allowing it to be handled with bare hands (ALKE Heating Technology, 2005).

Glass evacuated tube collectors outperform flat plate collectors in terms of thermal insulation and performance, eliminating the need for sun tracking in a tube-shaped device (Sharma et al., 2018). The drawbacks, however, are its low-pressure resistance (often less than 0.1 Mpa) and cracking when exposed to cold and hot water (Gao et al., 2014), as well as heat extraction from the tube (Liang et al., 2012). To address this shortcoming, metal-in-glass absorbers and U-pipe-type tubes have been developed. The U-pipe clamped onto a copper plate produced the best beam, diffuse, and shade effects (Gao et al., 2014).

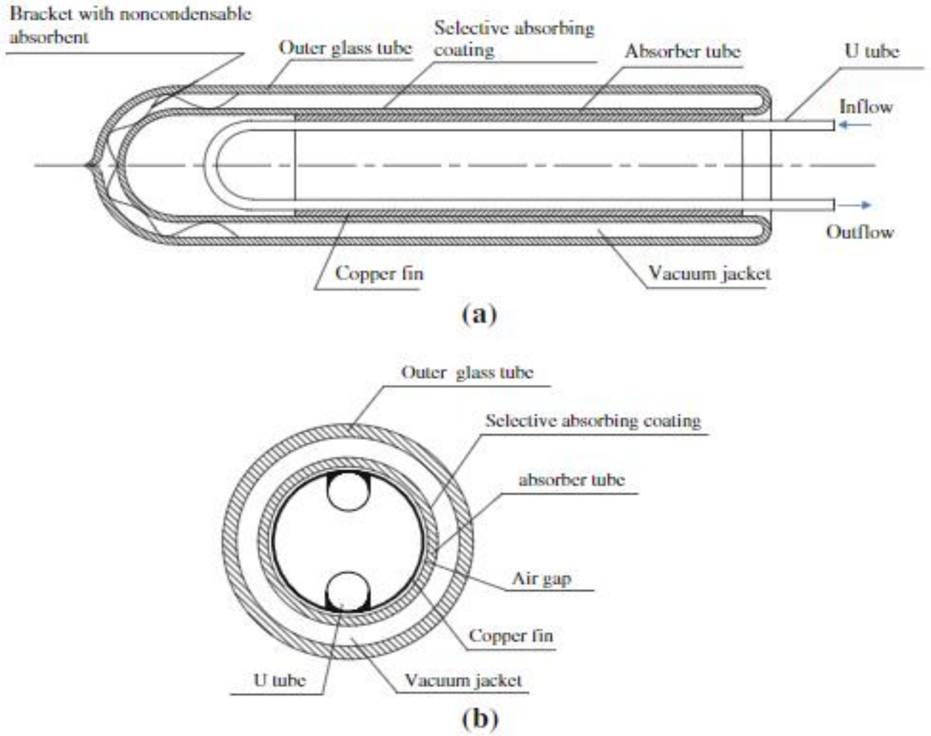

Figure 21: Glass EVC with U-tube (a) illustration of the glass evacuated tube; (b) cross-section (Liang et al., 2012).

Figure 22(a), depicts a U-pipe glass EVC made of two-layer glass tubes with a vacuum between them to reduce conduction and convection losses to the atmosphere. According to X. Chen & Yang, (2022), EVCs can deliver temperatures ranging from 50 to 150 °C on a stand-alone basis. His research also presents the idea of combining the EVC with a concentrated compound collector, as shown in Figure 22(b). He also recommends inserting a cylindrical aluminium fin within the absorber tube to transfer heat to the subsequent layers, but these fins cannot be securely mounted on the surface of the absorber tube, resulting in heat resistance. The emissivity of the fin surface in the original tube was 0.1, and air conduction dominates the air gap heat transfer, which thus suggested a layer of high emissive coating on the fin (X. Chen & Yang, 2022). Because the heat transfer coefficient of the air gap is essential in facilitating heat transfer, Liang et al. (2012) conducted a study using a filled-type evacuated tube with a heat transmission component instead of air gaps inside the inner tube. His research revealed that the filled-type evacuated tube had a 55% higher energy efficiency and a 12% higher heat efficiency than the metal fin-evacuated tube due to the absence of heat losses caused by air.

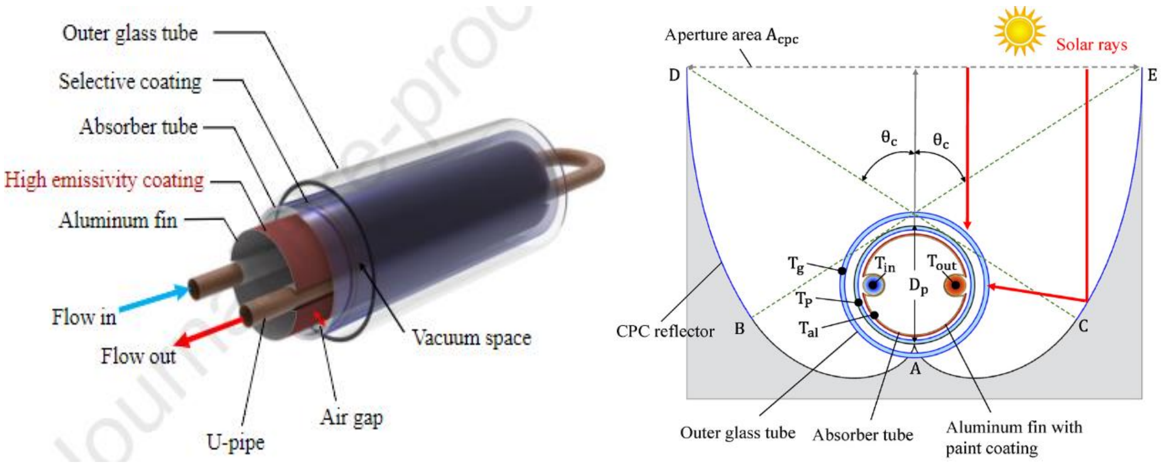

(a) *(b)*

Figure 22: (a) Structure of a U-pipe evacuated tube with high emissivity coating (b)U-tube EVC coupled with a CPC with concentration factor of 2 (X. Chen & Yang, 2022).

Experiments on the theory of heat distribution revealed that the inner glass tube had a significantly higher temperature than the outer glass tube and the aluminium fin had a lower temperature than the inner tube, indicating heat loss due to the air layer between the two existing heat conducting layers (Diwan & S. Soni, 2015; Gao et al., 2014; Hlaing & Soe, 2014; Mon et al., 2015). Allegrini et al. (2016) and Hlaing & Soe, (2014) used COMSOL Multiphysics to show that the temperature distribution through the evacuated glass tube and metal fin marginally increases on the inside surface compared to the outside, based on additional heat losses, as illustrated in

(b)

Figure 23(a). Gao et al., (2014) also modelled the collector's detailed thermal behaviour and the heat transfer between the U-pipe and the aluminium fins, including the temperature distribution on the fins, to produce a temperature profile similar to that displayed in

(b)

Figure 23(b).

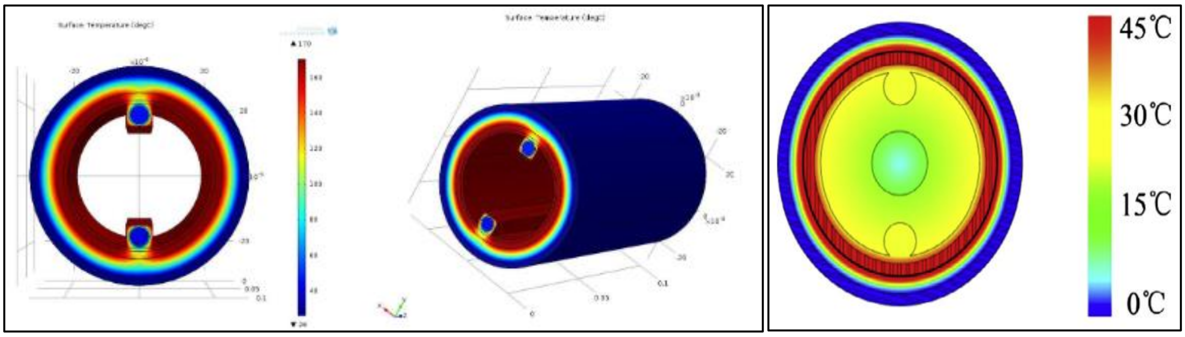

(a) (b)

Figure 23: Tube cross-section temperature profile as shown by (a)Allegrini et al., 2016;(b) Gao et al., 2014.

As discussed earlier, X. Chen & Yang (2022) studied the performance of U-tube pipe evacuated tubes with and without CPC integration. The use of a Compound Parabolic Concentrator (CPC) reflector increased the thermal efficiency of the collector by 24.3% to 29.2%, depending on the conditions. He also states that, with a higher concentration ratio, the CPC integrated EVC efficiency increased due to a larger heat flux concentrated on the absorber tube, resulting in a relatively higher absorber temperature and enhanced radiation heat transfer as shown in Figure 24. Moreover, by applying a high-emissivity fin coating, the CPC collector with a concentration ratio of 6.0 at a fluid temperature of 200 °C, increased its efficiency by 8.4%.

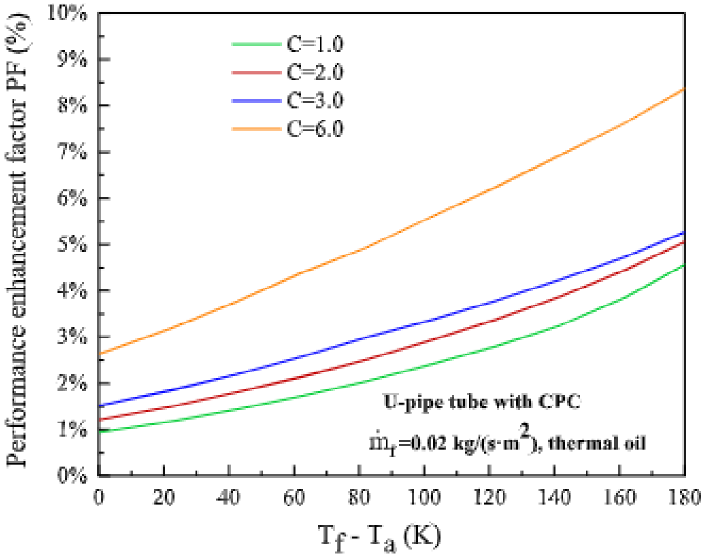

Figure 24: Increase in efficiency of a U-Tube EVC with increasing temperature and increasing concentration factor (Chen & Yang, 2022)

Several authors investigated the heat retention capabilities, stability, and efficiency of an evacuated vacuum tube collector system even when solar radiation was low and found promising results (Gao et al., 2014; Paradis et al., 2015; Sharma et al., 2018; Tong & Cho, 2015). Due to its strong thermodynamic performance (200 °C) even with limited solar irradiation, Sharma et al. (2018) mentioned the household and industrial usage of EVCs as water heaters and solar drying systems, respectively.

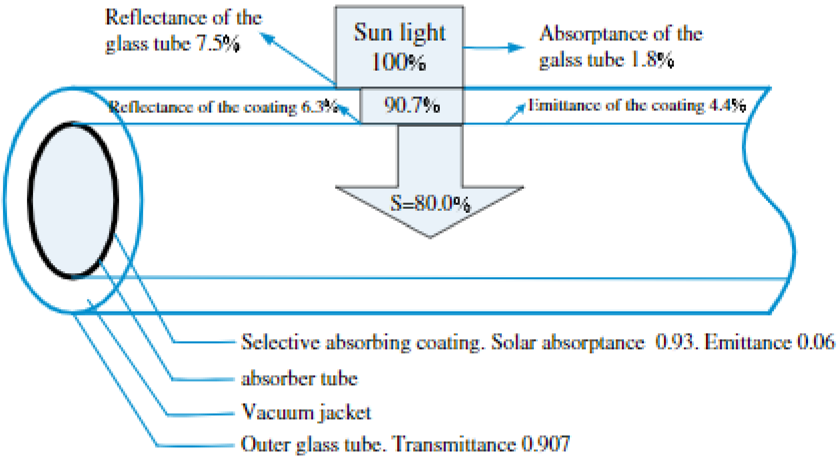

Figure 25: Optical losses involved in an evacuated tube collector (Ma et al., 2010)

A selective coating on the absorber surface is introduced to reduce thermal radiation losses. Black cobalt oxide (Co_3O_4) has an absorbance greater than 0.90 and eemittances of 0.20 (Mcdonald, 1980). Ti0.5Al0.5N has an absorbance of 0.945 and an emittance of 0.04 (Du et al., 2011). (Badar et al., 2011) suggested usage of Copper Titanium Nitroxide (Cu/TiNoX) as a surface coating with an emissivity of 0.5. According to A. Kumar et al. (2021), selective coatings should have higher absorbance compared to their emittance so that most of the received solar irradiance is absorbed and the transmission and reflection losses are minimised. It was studied by Nkwetta et al. (2012) that borosilicate glass tubes with 3.5 mm wall thickness had higher transmission losses than 1 mm thick glass layers due to additional optical losses as shown in Figure 25. This made 1.2 mm thick borosilicate glasses with an anti-reflective coating the preferred choice over thicker glasses.

2.4.3 Concentrating Parabolic Collectors

Using mirrors to reflect sunlight, focus it, and gather heat to run a power turbine or heat engine has been used to create energy on a small and large scale for the past decade. As a result, solar-to-electricity conversion efficiency increased while prices remained unchanged in comparison to fossil fuel usage. According to Barlev et al. (2011), using a heat transfer fluid (HTF), a solar concentrator transforms solar radiation into thermal energy for power generation by decreasing convective losses aided by an optical device that can boost light concentration to 10,000 suns, which can be done by lowering the receiver area. The reduced receiver size and material compared to stationary collectors allows adjustment of operation temperature, aiming for a more thermodynamically sustainable system by eliminating heat loss (Barlev et al., 2011).

This can be categorized into three methods of heat transfer: direct, indirect, and intermediate transfer fluid. According to Ndukwu et al. (2020), medium-range concentrators can achieve temperatures ranging from 100 to 500 °C, making them ideal for small-scale operations such as the one required in this experiment. Figure 26 shows the four primary CSPs: Parabolic Trough Collectors (PTCs), Heliostat field collectors (HFCs), Linear Fresnel Collectors (LFCs), and Parabolic Dish Collectors (PDCs). Barlev et al. (2011) say that the output power efficiency is mostly determined by the CSP material, the rate of absorption, the storage of heat transfer, and the number of power conversion cycles.

PTCs use curved reflectors to focus incident solar rays onto an absorber tube located in the parabola's focal length. The absorber tube is comprised of a metal tube and a glass envelope element to minimise conventional losses (H. L. Zhang et al., 2013) and can reach 50 to 400 °C temperatures (Barlev et al., 2011). HFCs use sun-tracking reflectors to focus insolation on a central tower-mounted receiver and can operate at 1500 °C in big systems (Barlev et al., 2011). LFCs, like PTCs, focus irradiance on a tower's central receiver with flat or slightly curved lenses. LFCs are versatile yet less efficient than PTCs and HFCs (H. L. Zhang et al., 2013). PDCs can achieve a concentration ratio up to 1000 suns and a temperature of about 1500 °C. Figure 26 shows a construction similar to a solar cooker but with larger parabolic mirrors. According to Barlev et al. (2011), PDCs are expensive and require near-perfect concavity to concentrate solar light. Furthermore, PDCs are the only direct technologies that can focus irradiance on pyrolytic feedstock.

Table 4:Comparison between the variable CSP Technologies (H. L. Zhang et al., 2013).

Technology	Relative Cost	Land Occupancy	Thermo-dynamic efficiency	Operating Temperature (°C)	Solar Concentration
PTC	Low	Large	Low	20-400	15-45
LFR	Very Low	Medium	Low	50-300	10-40
SPT	High	Medium	High	300-565	150-1500
PDC	Very High	Small	High	120-1500	100-1000

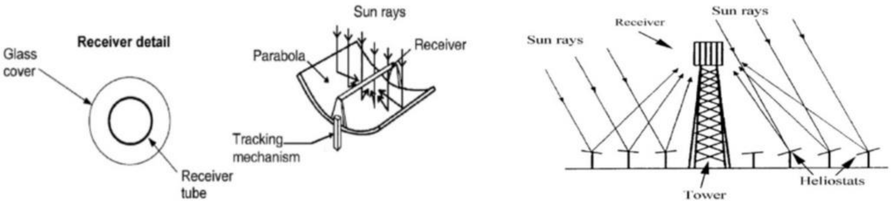

a. Parabolic trough collectors (PTC)   b. Heliostat field collectors (HFC)

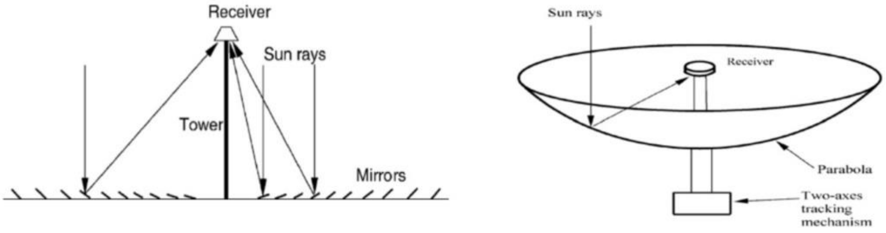

c. Linear Fresnel collectors (LFC)   d. Parabolic dish collectors (PDC)

Figure 26: Schematic diagrams of Concentrated solar collectors (Barlev et al., 2011).

Table 4 compares the leading CSP technologies. As mentioned later in Section 2.5, Kerala gets about 5.59 kWh/m^2/day of solar insolation every year, making it a good place for solar-assisted pyrolysis, torrefaction, or carbonization, which need a lot of solar insolation (Hegde & Ramachandra, 2012). High Direct Normal Irradiance (DNI) in this region makes it suitable for installing CSPs.

2.4.4 SK14 Solar Cooker

In a large portion of the developing world, solar cooking has the potential to replace the use of wood in food preparation. Solar cookers of the box and parabolic types are commercially available in India (Purohit, 2010). Instead of non-renewable energy sources (charcoal, wood from local forests, and kerosene), these solar cookers utilize the vast quantity of energy available straight from the sun (Mussard et al., 2013). According to Purohit (2010), individual families in urban and semi-urban regions use box and parabolic solar cookers, and in India, more than six million box-type solar cookers have been propagated, mostly via various schemes of the MNRE. India's solar cooking factory is the largest, and the Brahma Kumari kitchen, as mentioned in Section 2.4.3, is a live example. A SK14 solar cooker falls under the Parabolic Dish Collectors (PDC) category.

In a solar cooker, the cooking utensil is supported so that most of the reflected radiation hits the bottom at the focal point, which can reach 150 to 400 °C depending on sun irradiation and load (Purohit, 2010). He also suggests that the cooker requires periodic two-axis tracking every 10-15 minutes so that the focus of concentrated radiation is maintained on the cooking utensil. Depending on the material of the dish and the manufacturer's features, a parabolic concentrator solar cooker may cost between Rs. 4500 and Rs. 6000 (48–72 €) and have a lifespan of over 20 years (Purohit, 2010).

Mussard et al. (2013) suggest using an external heat storage unit or a quick heating technology such as evacuated tubes to decrease intermittency such that cooking at night or on a foggy day is potentially possible. In bright sunlight, the concentrator can generate 600–700 watts with a stagnation temperature of 300 °C at an ambient temperature of 28 °C and 660 W/m^2 of solar beam radiation (Mussard et al., 2013). Heat delivery is proportional to aperture size, such that on a sunny day, two litres of water boil in 15 minutes. Solar EG, a German non-profit, developed the SK-14 solar concentrator as a residential solar dish cooker. This 1400 mm dish has a parabolic reflecting surface that concentrates solar radiation on the cooking pot, holding 24 to 36 reflector sheets that are polished, anodized, hardened aluminium [13]. The schematic diagram is shown in Figure 27. According to Mekonnen et al. (2020), it can deliver up to 600 W and the vessel's bottom can reach 350 °C–400 °C. He also claims that the SK14 cooker can reach around 50 % thermal efficiency and feed 10 to 15 people. He also claims that the cooker may be used from 1 hour after dawn to 1 hour before sunset on clear days, saving small businesses up to 10 LPG cylinders per year. According to Chandak et al. (2011), these cookers are suitable for low-wind countries like India, where NGOs are popularizing these cookers and teaching rural women about cooking and fuel production.

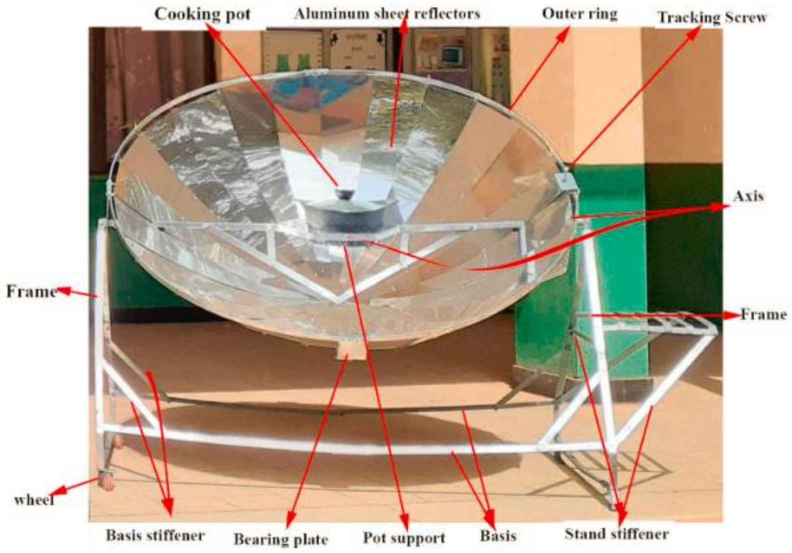

Figure 27: Components and diagram of the SK14 solar cooker obtained from EG Solar (Mekonnen et al., 2020).

Solar cooking system benefits include job development for unemployed youngsters through technology and small business ownership in India. The tried-and-true system will make up for the lack of energy in rural homes and create opportunities for fuel mixing in the country's energy strategy.

2.4.5 Characterization of a Solar Collector

The design of a parabolic dish torrefier is based on a parabolic dish solar collector. A collector's geometric, optical, and thermal properties are all unique to it. Detailed descriptions of parabolic dish collector geometries, optical analyses, and thermal analyses are provided in this section.

The focal length and surface area of the parabola are given by the equations (Ahmed et al., 2020):

$$f = \frac{D_{ap}^2}{16h} \tag{4}$$

$$A_s = \frac{8\pi}{3} f^2 \left[\left[\left(1 + \left(\frac{D_{ap}}{4f} \right)^2 \right) \right]^{3/2} - 1 \right] \tag{5}$$

The aperture area (A_{ap}) of the parabola can be calculated using Equation (6) and the collector aperture area (A_r) can be calculated considering the aperture as a circle.

$$A_{ap} = \frac{\pi D_{ap}^2}{4} \tag{6}$$

$$A_r = \frac{\pi D_r^2}{4} \tag{7}$$

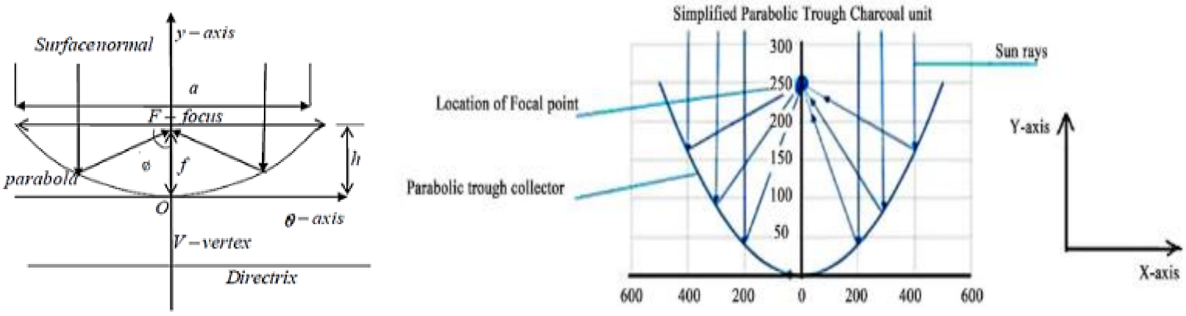

Figure 28: Geometry and dimension of a Solar collector parabolic dish (Aljabair et al., 2019; Swaminathan & Nandjembo, 2016).

The basis parameters of a concentrating collector are the concentration ratios. The geometric concentration ratio C_A is the ratio of the aperture are to the receiver area shown in Equation 8.

$$C_A = A_{ap}/A_r \tag{8}$$

The concentration ratio is the factor by which the incident energy flux is optically or geometrically enhanced on the receiving surface. So, by confining the available energy coming through a chosen aperture to a smaller area on the receiver, the flux can be increased. Since the areas of the devices are known, it is adequate to use if the radiation flux falls uniformly over the aperture and the receiver area [14]. The typical concentration factor of a solar cooker can range from 20 to 25 and is highly dependent on the aperture and receiver diameter (Ahmed et al., 2020; Cuce & Cuce, 2013; Mekonnen et al., 2020).

According to Coccia et al., (2017) and Mekonnen et al., (2020), the first and simplest parameter to characterize a cooker is to note its time required to reach the fluid boiling temperature, referred to as Δt. This can be used to calculate the average overall solar cooker thermal efficiency using Equation 9.

$$\eta_{av} = \frac{mC_p\Delta T}{G_{av}A_{ap}\Delta t} \tag{9}$$

where C_p is the specific heat capacity of the fluid and ΔT is the temperature difference between the maximum boiling temperature and the starting temperature of the fluid. G_{av} is the average solar irradiation during the time interval Δt. The thermal efficiency of the solar cookers was found to be 47%, 28% and 46.4 % as stated by Chandak et al. (2011); Cuce & Cuce, (2013) and Mekonnen et al., (2020) respectively. According to Ahmed et al., (2020) the efficiency can range from 20 to 50 %. He suggested that the density of the solar radiation at the focal point (Q_f) can be calculated by Equations 10.

$$Q_f = C_A \times G_{av} \times \eta_{Al}\ (W/m^2) \tag{10}$$

where η_{Al} is the efficiency of the reflector plates in the parabolic dish. Further, the actual solar radiation at the receiver area (P_b) and actual wattage at the focal point (P_{bf}) can be calculated by Equation 11 and 12 respectively:

$$P_b = P_f \times A_r\ \ [W] \tag{11}$$

$$P_{bf} = P_b\ \times \eta_{av}\ \ [W] \tag{12}$$

Cooking power is defined as the usable energy available while heating. Equation 13 determines the sensible heat change of the water in the cooking utensil. It's a function of the change in water temperature at each interval and the water's mass and specific heat capacity. Dividing a product by a periodic interval gives cooking power in Watts (Cuce & Cuce, 2013; Mekonnen et al., 2020; Purohit, 2010).

$$P_c = mC_p\left[\frac{T_{w2} - T_{w1}}{\tau}\right]\ [W] \tag{13}$$

where T_{w1} and T_{w2} signifies the initial and final instantaneous water temperatures respectively and τ is the instantaneous time difference in which water temperature rises between the intervals.

2.5 Solar - Biomass (Coffee) Potential in Kerala

Solar energy is one of the first solutions to India's energy crisis. According to Kuthanazhi et al. (2014), the "Solar India" mission has entered its second phase thanks to 578 MW of grid-connected solar electricity. India experiences 250-300 sunny days per year and 6,000 million GW of solar energy potential, making it the greenest option (Bedi, 2021). According to Suman & Ahamad, (2019) , in a growing country like India, although energy imbalance is the biggest concern, decentralizing energy transmission makes grassroots sanctions simpler. He claims that India's solar energy potential is between 4 and 8 kWh per square meter per day, or 1200 to 2300 kWh per square meter per year, and that merely 0.1% (3000 km^2) of the country's land could meet India's energy needs.

According to Bedi, (2021), Kerala (a southern state) is a prime example of an affluent, educated, and developed state that is not fulfilling its full potential. Although there was no solar output during this time period, as of September 30, 2016, Kerala was producing 13.05 MW of solar energy compared to 0.03 MW on March 31, 2015, indicating a significant increase in the small state's solar energy production (Suman & Ahamad, 2019). Figure 29 shows a grid-wise (100 km × 100 km) variation in GHI and DNI ranging from 3.71 kWh/m^2 to 5.55 kWh/m^2 and 4.82 kWh/m^2 to 5.93 kWh/m^2, respectively. From this analysis, the minimum and maximum solar energy potential values for Kerala were determined to be GHI (4.82 kWh/m^2 - 5.93 kWh/m^2) and DNI (3.71 kWh/m^2 - 5.55 kWh/m^2), respectively (D. Kumar, 2020).

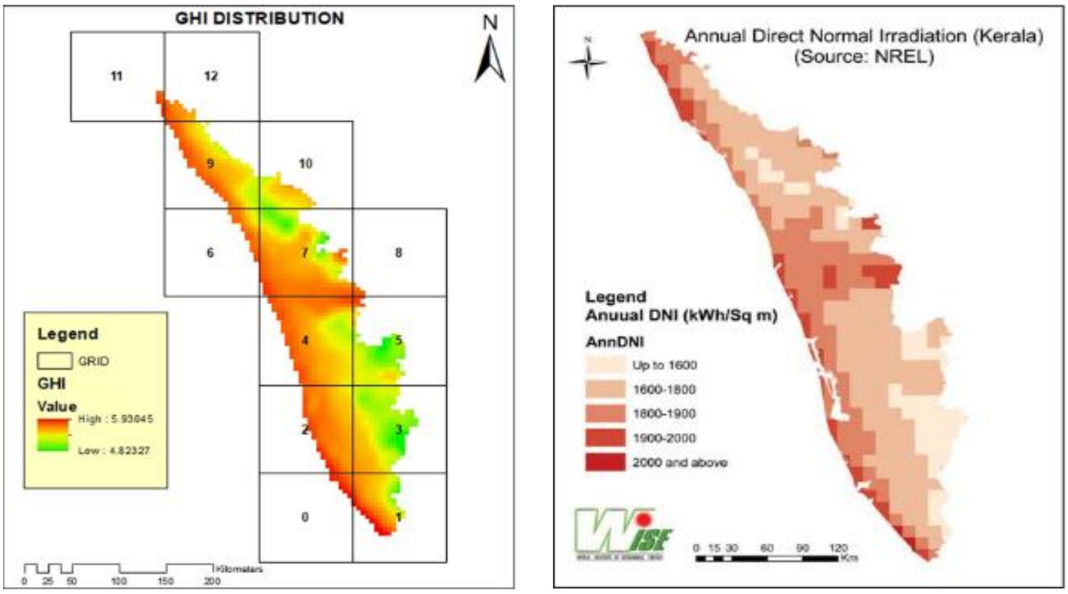

Figure 29: Solar Insolation Variability and Annual DNI Kerala conducted by WISE study (D. Kumar, 2020; Parameshwaran et al., 2013).

In addition, a study by Parameshwaran et al. (2013) reveals that the overall annual DNI in Kerala is between 1800 and 2100 kWh/m^2 relative to the total land area, as indicated in Figure 29. The average land usage factor for Concentrated Solar Power (CSP) and Solar Photovoltaic (SPV) was estimated to be 35 MW/km^2 and 50 MW/km^2, respectively, based on the WISE study conducted by the National Renewable Energy Laboratory. From the evaluation, he determined that Palakkad and Thrissur had a combined SPV potential of around 6,816 MW and a CSP potential of approximately 2,649 MW.

The MNRE claims that 70% of the Indian population relies on biomass, and thus, the central government has spent Rs. 4.6 billion on biomass power and waste-to-energy systems, which use agricultural wastes, bagasse, coconut shells, soya husks, de-oiled cakes, and coffee waste [15]. However, seasonal fuel availability limits the share of biomass targets compared to solar and wind. According to the Biomass Resource Atlas of India (Parameshwaran et al., 2013), the potential for biomass-based power generation in Kerala, as backed by the Energy Report 2011, is roughly 501 MW, and the state is expected to run out of non-renewable energy sources by 2050. According to Figure 30, biogas, biomass, and other biofuels, coupled with centralized and de-centralized PV, cover the majority of the energy supply scenarios.

According to Karunakaran, (2017), Kerala accounts for 85501 hectares (211.277 thousand acres) of India's coffee production. Kerala is India's second-largest coffee producer, producing 28% of the country's 8,200 tons, making a gross total of 0.5% and 19.2% of the country's Arabica and Robusta coffee (Dr. Ambedkar Veedhi, 2021; Karunakaran, 2017; Padmapriya et al., 2019). Kerala's environment is perfect for coffee cultivation, with temperatures ranging from 23 to 28 degrees Celsius and rainfall ranging from 60 to 80 inches, as well as a dry spell lasting 70 to 90 days. In Kerala, 76,000 smallholder plantations of 1.1 hectares support 100,000 households [2]. Wayanad, Kozhikode, Palakkad, and Idukki share most of the state's production ([2], (Dr. Ambedkar Veedhi, 2021)). Wayanad's terrain, hot and humid climate, and plentiful rainfall (2000-3000 mm/year) spread over 10 months make it a hotspot (80% production) for Robusta growth and Kerala's largest coffee producer (Anil Kumar et al., 2019).

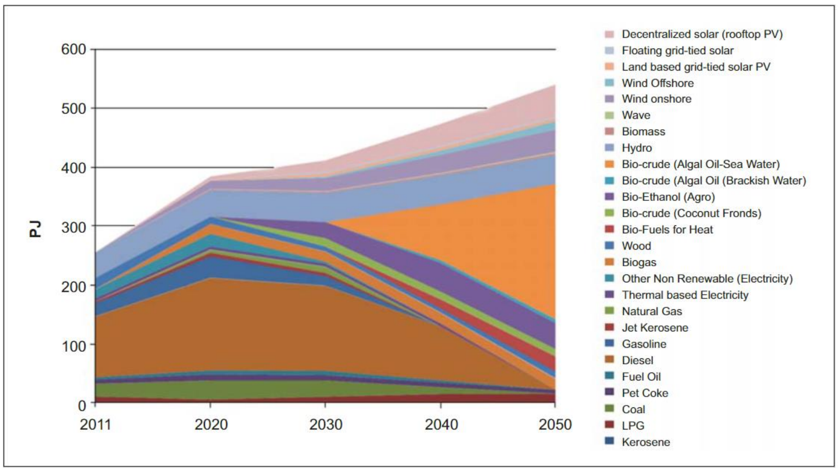

Figure 30: Biofuels energy potential for Kerala (Parameshwaran et al., 2013).

All of this coffee production generates residues, which are collected either directly from the fields (in-situ) or from the relevant processing industries, such as coffee pulp, husk, spent coffee grounds, stems and stocks, etc. (Padmapriya et al., 2019;[8]). According to [8], the SCG produced is directly used as a fuel and only a small number of coffee planters-processors transform cherry husk and SCG into briquettes for catering (or) tobacco curing equipment.

As stated by Parameshwaran et al. (2013), despite the fact that coffee feedstocks have a high conversion potential for combustion technologies, smaller and decentralized power generation prefers gasification, pyrolysis, or other thermo-chemical processes to reach out to families and individuals, particularly in rural areas, through government-subsidized operations. He also hinted at the state's emerging torrefaction and pyrolysis processes, which are at various stages of development. As a result, even in a tiny state like Kerala, the produced bio-resources, together with the high potential of concentrated sun, present a strong case for a solar-biomass biochar production method.

2.6 Solar Induced Torrefaction/Pyrolysis Technology

Solar biomass mild/severe pyrolysis is an endothermic process that converts biomass in an inert environment using concentrated solar energy, which is typically assisted by an optical system. These optical concentrating devices (with temperatures reaching 1000 °C) can concentrate solar energy into a tubular reactor or directly onto the feedstock. This can be achieved by concentrating solar radiation heat on a restricted location through the reactor's walls, or by directly irradiating the feedstock, which raises its temperature while the reactor remains relatively cool (Ndukwu et al., 2020). This not only eliminates the need for fossil fuels and improves the carbon footprint and economics of biochar, but it also achieves mild pyrolysis temperature faster than fossil fuel heating (Ndukwu et al., 2020). However, only regions with high DNI and a high agro-industrial waste production are possible (Morales et al., 2014).

Figure 31 shows a horizontally oriented continuous heated reactor where the feedstock is pyrolyzed inside a borosilicate glass tube reactor in an inert helium atmosphere (Morales et al., 2014; Ndukwu et al., 2020). At a concentration factor of 31.03, the system was designed to enable direct irradiation of the biomass, making the feedstock the hottest component (Morales et al., 2014). The design was improved so that the reactor received both direct and concentrated solar irradiation from the parabolic trough, with an average and peak temperatures of 290 °C and 450 °C, respectively. He also characterized the primary heat loss mechanism as biomass reflectivity (38%), and the reactor's poor heat retention (36%). (Weldekidan et al., 2018) used a similar setup to pyrolyze rice husk in an argon environment to get a maximum yield of 43 wt.% biochar at 500 °C.

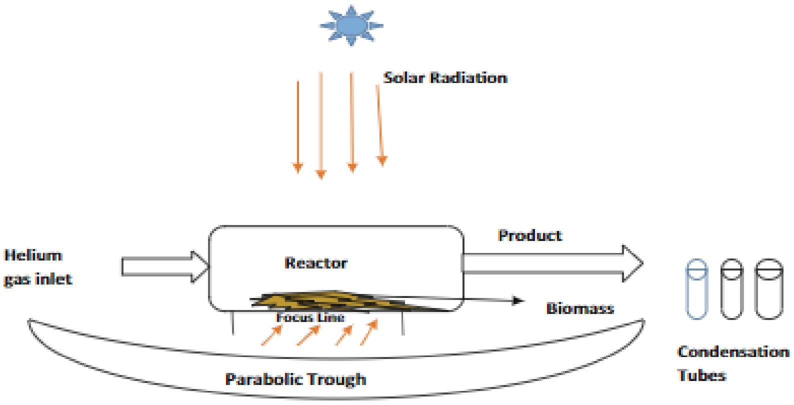

Figure 31: Fixed bed horizontal Solar biomass pyrolysis orientation (Ndukwu et al., 2020).

A vertically oriented continuous reactor was studied by A. Ayala-Cortés et al, (2019); Ndukwu et al. (2020), to allow easy collection of fuel aided by gravity. Horizontally placed heliostats were used to pyrolyze the feedstock with the furnace temperature ranging from 450-1550 °C in an inert Argon environment, producing a majority of biochar as shown in Figure 32.

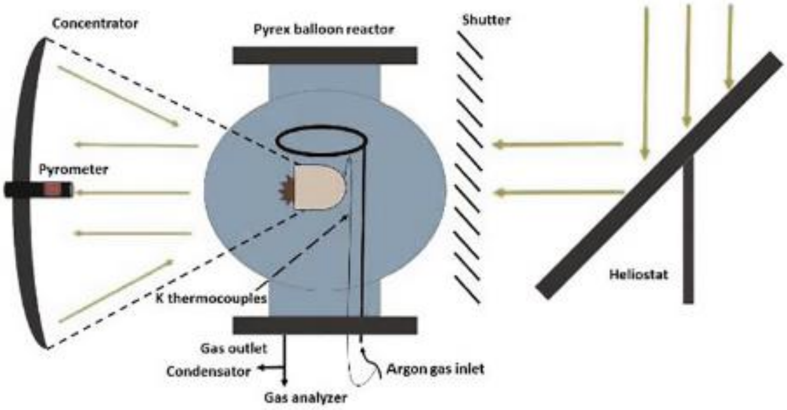

Figure 32: Solar biomass pyrolysis orientation (A. Ayala-Cortés, n.d.).

Cellatoglu & Ilkan (2016) used a parabolic dish solar torrefier to torrefy solid olive mill residue in a nitrogenated inert condition at a torrefaction temperature of 250 °C and a residence time of 10 minutes to produce a biochar with a carbon percentage increase of 7.65 %. The study not only showed an increase in the calorific value of the product but also obeyed the changes associated with the torrefaction process, making concentrated solar a viable option for torrefying biomass.
Figure 33 shows the design of the torrefier used to produce biochar from raw SOMR.

(D. Chen et al., 2020) used a solar vacuum tube as a reactor to dry and torrefy biomass at 100 °C and 250 °C, respectively, using a parabolic trough solar receiver system in an inert nitrogen environment. A shutter was used to control the drying and torrefaction temperatures for a residence time of 30 minutes to decompose the hemicellulose in the feedstock, thus improving the final pyrolytic product. This has been displayed in Figure 34.

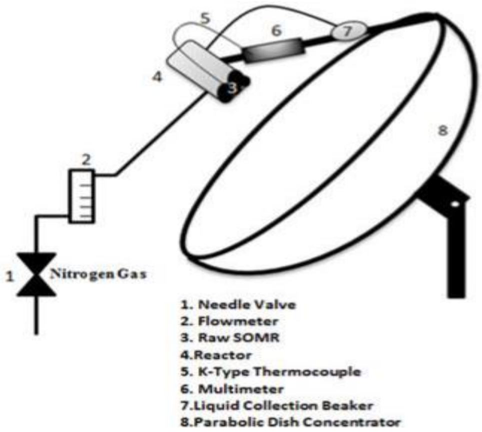

Figure 33: Parabolic dish SOMR torrefier (Cellatoglu & Ilkan, 2016).

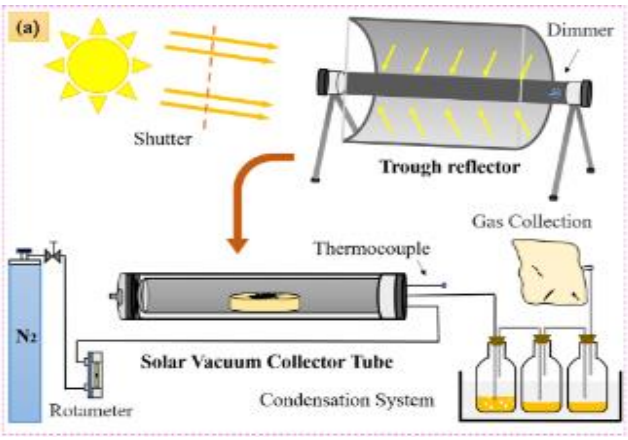

Figure 34: Biomass drying, and torrefying system coupled with a parabolic trough collector (D. Chen et al., 2020).

(Swaminathan & Nandjembo, 2016) uses a solar-biomass torrefying unit to produce charcoal (21–35 wt. % yield) in an all-borosilicate evacuated vacuum glass reactor heated with a solar concentrator. The inference was aimed towards finding the efficiency of the evacuated tube under intense sunlight, cloudy conditions, and diffused sunlight. Caputo & Mašek, (2021) developed a design approach for a solar slow pyrolysis energy access reactor using a concentrated parabolic dish system integrated with a manual tracking system and optimised with a Monte-Carlo ray tracking system. The biochar obtained was optimal for soil enrichment and energy measurements, with the design having the potential to produce 5 kg of biochar product every day.

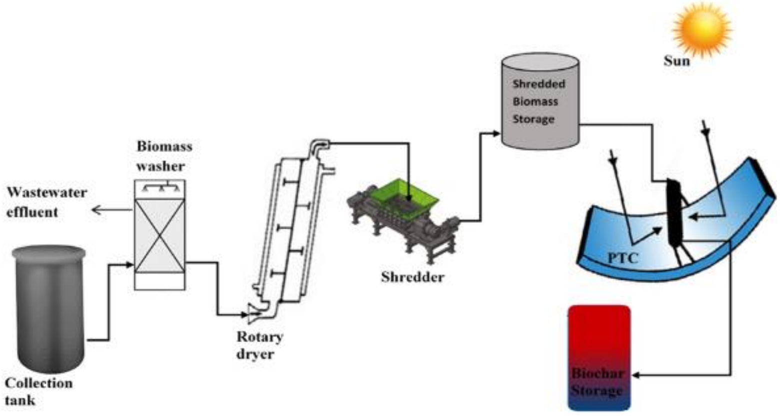

Figure 35: Biochar production schematic process (Giwa et al., 2019).

Giwa et al. (2019) developed and simulated a system for pyrolyzing date palm waste to charcoal using a concentrated solar thermal system to access the economic and environmental sustainability (electric heating-based pyrolysis) as shown in Figure 35. Payback time was stipulated as 4 years and 132 days, with a gross margin of 35.5%. Based on environmental impact assessments, concentrated solar energy pyrolysis emitted 38% less CO_2 than traditional pyrolysis, making it more ecologically benign.

This section provided a few examples of combining concentrated solar and biomass feedstocks to produce biofuels, as well as an idea of how to develop such a design using the suggested experimental methods. The different setups seen also suggest that EVCs could be used as a reactor for torrefaction of the SCG feedstock and the SK14 cooker could be used instead of parabolic trough collectors, as shown in the diagrams above.

2.7 Takeaways and Insights

Section 2.1 presented numerous instances of how to use "Jugaad Innovation" as a strategy for resolving potential technical obstacles and breakthroughs for this research. Furthermore, it provided strong supporting assertions to link it to a sustainable technological future with diminishing resources. This approach can be a true lifesaver, especially in developing nations like India, where solar cooking is already subsidized by the central government and non-governmental organizations.

To choose SCG as a viable feedstock for the study, it was necessary to first understand the principle of biomass, its characteristics, and its potential for conversion into fuel using various thermochemical processes. As shown in Table 2, torrefaction can produce the highest solid yield while also increasing the calorific value. Furthermore, because of its high availability and potential as a biomass waste and solid fuel, it was an appropriate feedstock for the research. As a result, as described in Section 2.3, it was essential to investigate the torrefaction of SCGs from various literature. This review offered valuable insights about the characteristics of waste SCG upon thermolysis. According to many authors, torrefaction can not only raise the calorific value (HHV) of SCG but also provide a high output of solid biochar, thus supporting the research question (Sub RQ3).

It was also essential to investigate the current solar collectors and concentrators and their functionality in order to link SCG torrefaction to solar energy. According to the literature referenced in Section 2.4.2, Evacuated Vacuum Tube Collectors (EVCs) can be employed as a potential reactor for future studies. Because of its heat retention ability, minimal optical loss (Figure 25), and ability to integrate with solar concentrators (Figure 22 (b), the principle of a functional EVC could be implemented in future simulations. However, little changes to the EVC's design would be required, such as changing the heat transmission medium to air via conduction and mostly convection. The principles and properties of solar concentrators and cookers were studied to couple the EVC-inspired reactor to the accessible SK14 cooker. Several studies have revealed that the SK14 can reach extremely high temperatures (350 to 400 °C) at the focal point despite being designed to only reach cooking and boiling temperatures. As a result, before building the prototype, it was critical to identify the efficiency, focus point, and power of the SK14 cooker in order to emulate the modelled reactor. These studies gave some context for understanding Sub RQs 1 and 2.

Although the solar and biomass principles had been identified, it was important to figure out the solar and coffee potential in Kerala. Section 2.5 contains a discussion of Kerala's high solar energy potential and coffee production. It was evident that the majority of the focus was on harnessing its solar energy.

Despite the fact that Kerala produces 28% of India's coffee, the associated coffee waste has received little attention. This provides an excellent chance to dive deep into the concept of solar-induced fuel production from coffee waste, especially for coffee farmers.

Finally, after laying out the skeleton of the literature review, the technical application of solar-biomass torrefaction was introduced. Section 2.6 contains a few examples of existent technologies. Despite the fact that the majority of the work has focused on pyrolyzing carbonaceous feedstock, the same concept can be used to solar-torrefy SCG. The ideal scenario of combining the reactor and the concentrator was shown in Figure 31. Figure 34 also provided another vision for converting the previously chosen EVC into a torrefying unit. While the majority of the research concentrated on pyrolyzing the feedstock, some background for solar torrefaction was obtained from the work shown in
Figure 33 by Cellatoglu & Ilkan (2016). The most difficult takeaway from the literature was the requirement to create an inert environment in the reactor for torrefaction, which would require a constant supply of nitrogen or argon. Furthermore, as previously noted, another significant problem they faced was retaining heat inside the single-layered transparent reactor. This problem could be solved by first simulating the scenarios for a model reactor and then using the results of the study simulations to create a prototype. Because no research on solar-torrefying SCG or coffee waste was available, this proved to be a novel and sustainable approach. This research provided further background for understanding RQs 1 and 2.

3 Materials and Methods

Given the intermittency of solar energy in the Netherlands, it was very difficult to implement solar torrefaction. Therefore, it was proposed to link the modern torrefaction of biomass using an SK14 Solar Cooker, simulation, and SCG characterisation with frugal innovation. In addition, a prototype reactor was designed and tested in Hyderabad (India) to validate the primary study question "whether the solar cooker may be utilized as a solar-biomass torrefier. Figure 36 shows a flowchart dividing the research method into five basic areas. This was followed by a combination of experimental and simulation-based methodologies, each of which complemented a fully applied practical approach.

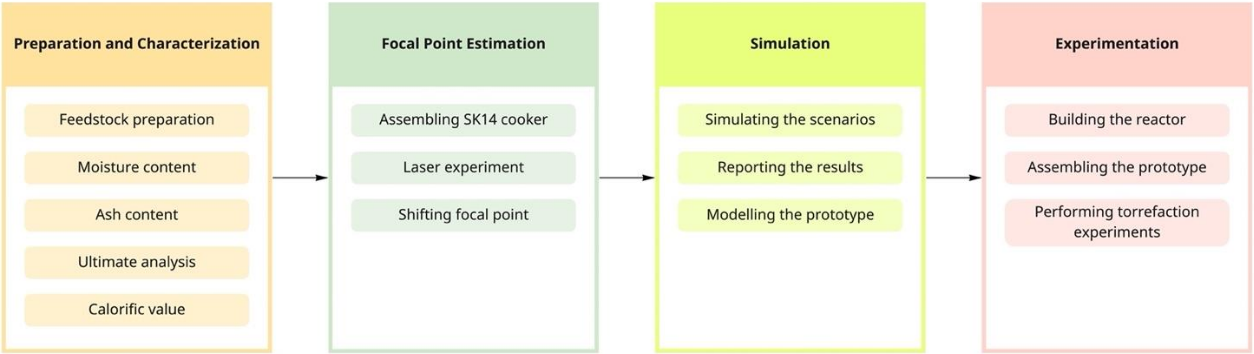

Figure 36: Methodology flowchart

3.1 Preparation of feedstock and characterization

Raw ground coffee was obtained from Kerala to ensure accuracy [16]. The manufacturer labeled it as a Robusta, but characterization of the coffee was critical because coffee attributes can vary based on location, soil, harvest temperature, and so on.

3.1.1 Moisture Content

Fresh coffee was brewed, and SCGs were collected and dried overnight, which had a very high moisture content. Therefore, the first step for characterization of the sample was to dry the content to a dry basis weight percentage. The moisture content was calculated using a standardized *NREL/TP-510-42621*. This was performed by drying 2 g of the raw SCG biomass at 105 °C in a Nabertherm drying oven for a minimum of four hours (Sluiter, Hames, Hyman, et al., 2008). Precautions were taken to keep the conditions dry to also achieve a further high precision. The experiment was replicated to improve precision to the nearest percentage.

3.1.2 Proximate Analysis

The volatile matter, ash content, and fixed carbon content were to be calculated to infer the effect of torrefaction on the characteristics of the SCG as a fuel. This was calculated on a dry-basis weight percentage.

Ash Content: The ash content was calculated by following the standard *NREL/TP-510-42622* (Sluiter, Hames, Ruiz, et al., 2008). 2 g of the sample was burned in a Nabertherm drying oven at 575 °C for at least 3 hours, or until all the carbon was eliminated. To avoid flaming of the sample, it was advised to initially heat the SCG sample to 250 °C at a rate of 10 °C/min and hold it for 30 minutes before heating it to 575 °C. Overnight ignition was advised if the proposed ash content was more than 5% by mass. The content that remains is the ash, and the ash percent can be calculated following the norm.

3.1.3 Ultimate Analysis

Ultimate analysis of the sample was carried out to standard *UNI EN ISO 16948:2015/EN 15104:2011* by the *vario Micro CHNS* analyser. A percentage of carbon, nitrogen, hydrogen, and sulphur were found on a dry basis. The leftover was the oxygen content in the SCG. This was done by the laboratory at Groningen University. An overnight dried SCG sample in the Nabertherm Oven was sent in duplicate for the analysis. Due to the limitation of biochar availability, only one sample from each of the 8 experiments conducted was sent. Duplication analysis of the biochar was not possible.

3.1.4 Calorific Value

The Higher Heating Value (HHV) of the raw and torrefied samples was conducted to determine the change in calorific value for different torrefaction temperatures. The HHV of the feedstock and biochar product was determined using the *ISO 18125* standard in an oxygen environment at 35 bars with a *Parr 6772 Bomb Calorimetric Thermometer*. The samples used for the experiments were pelletized and connected with a wick (for solid samples). Like Ultimate Analysis, only duplication of the raw biomass was possible due to limited biochar availability.

3.2 SK14 Focal point characterization

By estimating and analysing the focal point of the SK14 cooker, this experiment illustrated the principle of concentrated solar energy. A laser reflection method was devised to provide a precise approximation of the focus plane, a "jugaad" breakthrough. This was considered a prerequisite for achieving more realistic modelling and simulation for building the prototype as well as simulation.

The *'EG Solar'* cooker was put in a dark room to conduct the experiment. The *aperture* and *receiver* diameter were measured to be **1.4 m^2** and **0.3 m^2** respectively. The purpose was to focus two Class 1 lasers fixed perpendicular to the plane of the cooker and examine the resulting pattern on a graph sheet. As shown in Figure 37, a beam was installed above the solar cooker and a "leveller" was used to make it horizontal to the ground and in line with the solar cooker in order to make the necessary adjustments. To imitate mid-noon sun rays falling on the collector, the cooker was positioned perpendicular to the plane, and the laser pointers were aligned along the y-axis with the ground.

It was ensured that there was sufficient distance between the two laser pointers for the possible intersection of the two beams to be observed. On the potential focus plane (the pot stand), a graph paper sheet was set out with the support of a hollow cardboard sheet to visualize laser beams travelling through the sheet in the dark. The carboard was then attached to an external moveable support and lowered along the plane in seven steps, as shown in Figure 37. Each step was 1 cm away from the focal point. This was performed to study the nature of the reflected rays on the graph sheet when the focal length of the cooker was decreased. During the experiment, an average of six steps were done while simultaneously recording the shift in focal point on video. The values were extracted and analyzed from the recording.

Figure 37: Arrangement of the 'EG Solar' cooker for the laser experiment to estimate the focal point.

3.3 Modelling and Simulating the Reactor configuration

COMSOL Multiphysics® 5.6 was used to model the reactor to test the SCG using an SK14 solar concentrator. Using parallel geographic settings, the program simulated various parameters. This was inspired to support the solar torrefier idea and create a prototype. The goal was to explore the thermal behavior of an evacuated solar tube collector converted into a reactor inspired by Section 2.6 by utilizing a time variable and heat transfer module to solve the relevant PDEs. The simulation approach followed a logical tree-like sequence to build the model. Before starting, the problem's spatial dimension and the physics were mentioned (1D, 2D, 2D axisymmetric, or 3D). Then, a stationary or time-dependent study type was selected and various options such as global parameters, variables, and functions were selected to sketch or set the simulation settings (e.g., heat source, physics involved, boundary conditions). Importing files or drawing methods were used to build the geometry (COMSOL Multiphysics, 2015).

The Heat Transfer module's internal material database is comprised of a variety of fluids, gases, and solid properties. Pre-existing properties such as thermal conductivity, heat capacity, density, etc. were included. To solve the related Partial Differential Equations (PDEs) defining the unique occurrence, the mesh was created from extra-fine to extra-coarse alternatives, resulting in separate and accurate solutions. The EVC's heat transmission process involves conduction, convection, and thermal radiation. The COMSOL Multiphysics package's Conjugate Heat Transport interface covers heat transfer in solids and fluids, and the Surface-to-Surface Radiation contact accounts for radiation contributed to the physics (Allegrini et al., 2016; COMSOL Multiphysics, 2015).

To investigate the impact of temperature and heat distribution on the suggested reactor architecture, the model was simulated, reflecting on Section 3.4.1. This was done to comprehend the evacuated vacuum chamber's internal heat retention principle and the potential for using it as a reactor. A boundary heat flux as estimated from the experiment in Section 3.2 was added to the simulation geometry to replicate the concentrated solar light from the SK14 cooker on the reactor. The temperature profile in the reactor and the prototype's development could be potentially verified by this simulation. Figure 38 shows the overall methodology and steps followed for the simulation.

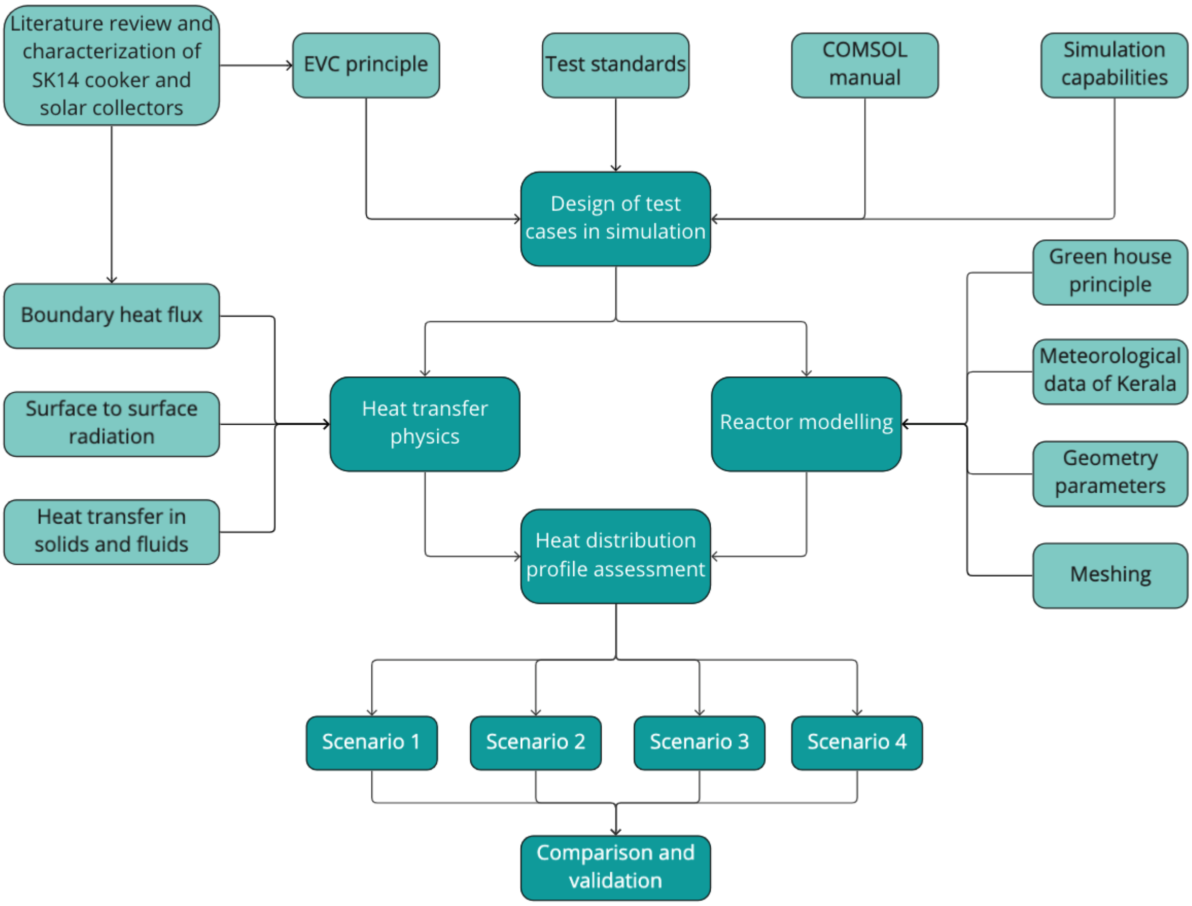

Figure 38: Flowchart portraying methodology followed for COMSOL simulation.

3.3.1 Major Governing Equations

Only the heat transfer module was applicable in the model, and hence the equations governing conduction, convection, and radiation were involved. The following partial differential equation governs heat transfer:

$$\frac{d}{dx}\left(k\frac{dT}{dx}\right)+\frac{d}{dy}\left(k\frac{dT}{dy}\right)+\frac{d}{dz}\left(k\frac{dT}{dz}\right)+Q=\rho C_p\frac{dT}{dt}+\rho C_p u.\nabla T \tag{14}$$

or:

$$\rho C_p\frac{\partial T}{\partial t}+\rho C_p u.\nabla T+\nabla.q=Q\ ;\ q=-k\nabla T \tag{15}$$

Where C_p is the specific heat capacity at constant pressure, u is the velocity vector, q is the heat flux, k (W/m.K) is the fluid or solid thermal conductivity and Q (W/m^3) is the volumetric rate of thermal energy. The Cartesian heat diffusion equation is used to analyze heat conduction analysis. The solution determines the model's temperature distribution along the T (x, y, z) axis where at each point in the medium, the net rate of conduction-related energy transfer plus the volumetric rate of thermal energy creation must match the volume's thermal energy change rate.

Fourier's law is a vector formula saying that heat movement is normal to an isotherm and in the direction of decreasing temperature (Allegrini et al., 2016). Solving the heat equation determines temperature distribution. Since the issue is time-dependent on the beginning medium conditions, the heat equation takes temperature and heat flux boundary conditions. From this, the PDE for heat transfer in solids and liquids, as shown in Equations 16 and 17 respectively (COMSOL Multiphysics, 2015):

$$\rho C_p \frac{\partial T}{\partial t} + \rho C_p u_{trans} . \nabla T + \nabla . (q + q_r) = Q + Q_{ted} \tag{16}$$

$$\rho C_p \frac{\partial T}{\partial t} + \rho C_p u . \nabla T + \nabla . q = Q + Q_p + Q_{vd} \tag{17}$$

Where for Equation 16, Q_{ted} is the thermoelastic damping which accounts for thermoelastic effects in solids. Q contains additional heat sources (W/m^3); q is the heat flux by conduction and q_r is the heat flux by radiation (W/m^2); u_{trans} is the velocity vector of translational motion (m/s).

For Equation 17, Q denotes the heat sources other than viscous dissipation (W/m^3), Q_p denotes the work done by pressure changes in the fluid due to heating under adiabatic compression as well as some thermoacoustic effects, Q_{vd} represents viscous dissipation in the fluid and u denotes the velocity vector in a Fluid Flow interface (m/s).

The boundary heat flux can be specified using the following equation, where Q_b is the boundary heat source specified in W/m^2 (COMSOL Multiphysics, 2015):

$$-n . q = Q_b \tag{18}$$

The radiation involved in the model was co-related to the conductive and convective heat transfer and was included using two boundary conditions: "*Surface-to-Surface Radiation*" and "*External Radiation Source*". The total irradiation 'G (W/m^2)' at any point can be defined as the sum of radiation from other boundaries (G_m), external radiation sources (G_{ext}), and the ambient radiation (G_{amb}). This can be represented by the following equation (Comsol Multiphysics Manual, 2012; Heat Transfer Module User's Guide, 1998):

$$G = G_m + G_{ext} + G_{amb} \tag{19}$$

G_{ext} is the sum of the products, of the external heat source's view factor F_{ext} by the corresponding source radiosity, where the first part represents the sum of radiation sources on a point and the second part denotes directional radiative sources. F_{amb} ($0 \leq F_{amb} \leq 1$) is an ambient view factor representing the fraction of field of vision that is not covered by other (Comsol Multiphysics Manual, 2012; Heat Transfer Module User's Guide, 1998). P_s is the source power of an external radiation source represented in and its faraway temperature is the value of T_{amb}:

$$G_{ext} = \Sigma F_{ext} P_s + \Sigma \mathrm{F}_{\mathrm{ext}} q_{0,s} \tag{20}$$

$$G_{amb} = F_{amb} e_b(T_{amb}) \tag{21}$$

Consider a point source 'x' as shown in Figure 39, with a surface emissivity ε (0<ε<1), reflectivity ρ_r, absorptivity α at temperature T. Assuming an opaque solid body, the total arriving radiative flux is the total irradiation, G and 'J' is the radiosity and represents the total outgoing radiative flux. The total radiosity is the sum of emitted and reflected radiation for a diffuse gray surface (Comsol Multiphysics Manual, 2012):

$$J = \varepsilon e_b(T) + \rho_r G \tag{22}$$

$$e_b(T) = n^2 \sigma T^4 \tag{23}$$

Here 'e_b(T)' is the blackbody hemispherical total emissive power (W/m^2) and σ is the Stefan-Boltzmann constant. According to the Stefan-Boltzmann law, e_b(T) is the power radiated across all wavelengths and depends on the fourth power of the temperature (Comsol Multiphysics Manual, 2012; Heat Transfer Module User's Guide, 1998).

Thus, the total inward radiative heat flux, q, is given by the difference between the total irradiation and radiosity using equations 22 and 23:

$$q = G - J = (1 - \rho_r)G - \varepsilon n^2 \sigma T^4 \tag{24}$$

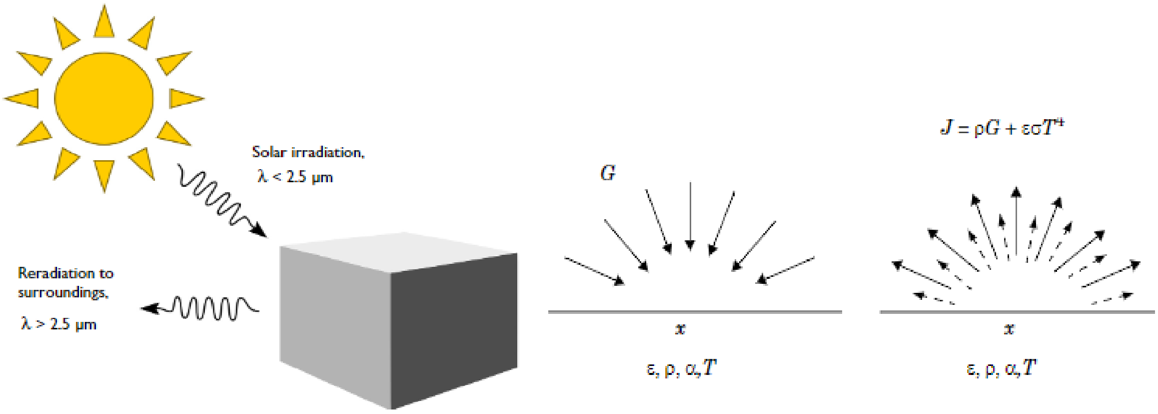

Figure 39: Absorption and emission of solar radiation theory in COMSOL resulting to total inward heat flux (Comsol Multiphysics Manual, 2012; Heat Transfer Module User's Guide, *1998).*

3.3.2 Double Layered Evacuated Solar Vacuum Tube

This model's geometry was created using simple multilayered structures in a "time-dependent" heat transfer physics. The prototype differs from a typical EVC since both the sides of the reactor are closed, and just the principle of the heat transfer through the tube was observed. The outer and inner glass tubes were made from borosilicate glass material, and they were assumed to be continuous by using the *"Join"* operator. These layers were separated by a perfect vacuum layer. The inner absorber tube had the properties of a selective coating to duplicate the geometry of an EVC. A thin layer of air separated the aluminum tube from the absorber tube as suggested by (X. Chen & Yang, 2022) in Section 2.4.2, as shown in Figure 40. This represented **Scenario 1**.

Another scenario *without the air layer* is modelled to analyse the change in temperature profile when there was no heat loss through the air domain, shown as **Scenario 2**. To make the geometry more realistic, two more scenarios were considered. In **Scenario 3**, *one of the covers* of the tube was also borosilicate glass and had a small vacuum domain to duplicate the U-Tube property as shown in Figure 21. In **Scenario 4**, *both the covers were borosilicate glass* coupled with a vacuum domain. An ellipse shaped boundary heat flux was added to the air and aluminium boundaries for the respective scenarios to simulate the concentrated solar energy based on the values obtained from Section 3.2. Table 5 shows the model's technical specifications for all the scenarios.

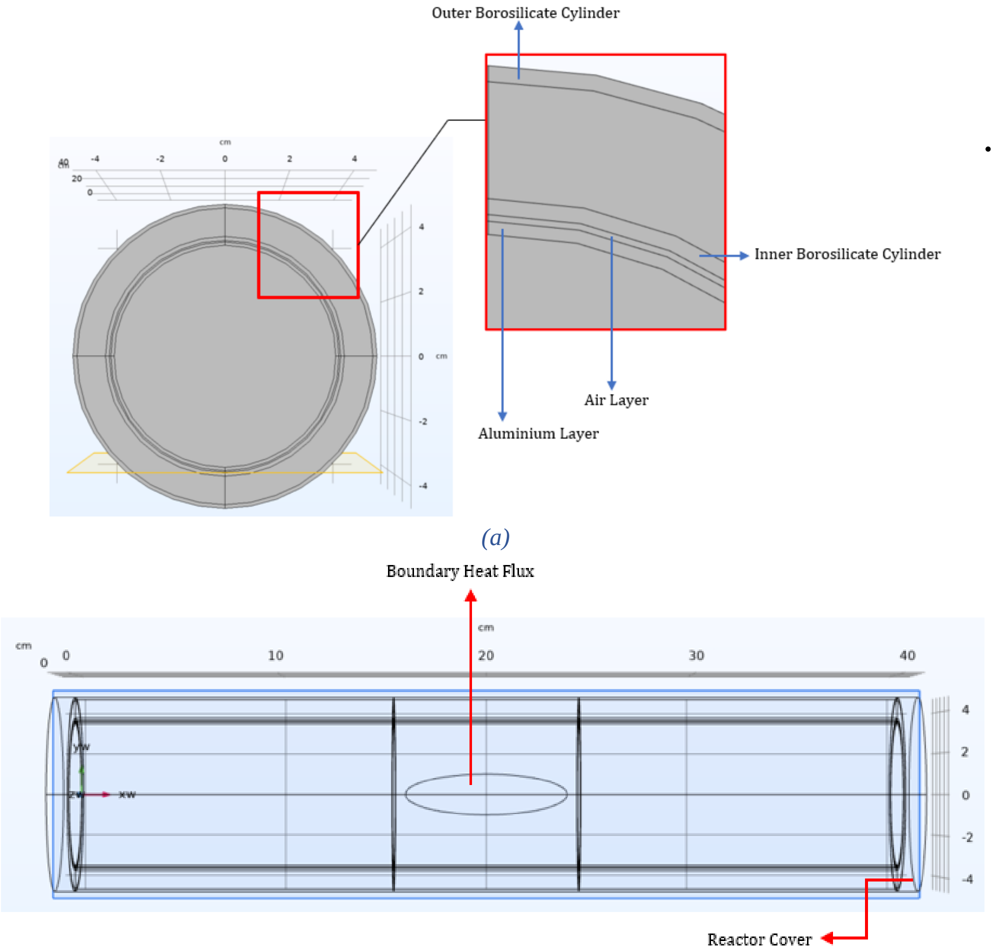

(a)

(b)

Figure 40: Cross Sectional and XY plane view of the conceptual Solar Vacuum Tube reactor modelled in COMSOL.

Assumptions:

1. The cross-sectional view of the reactor shows the piece volume of a real-world evacuated tube collector, and their geometrical properties are mentioned in Table 5. These were approximated from the values obtained from literature as mentioned in Table 6.
2. The selective coating was independent of the angle of solar radiation. A critical angle between the air and the glass medium sets the shape of the outer glass.

3. All the solar rays reflected from the Solar Cooker were incident on the boundary heat source i.e., efficiency of the reflecting plates η_{Al}=100 %.
4. Two reflecting wall layers with an emissivity (ε) of 0.1 were utilized on the glass fibre domain to increase the efficiency of the simulation in Scenario 1 and 2. Only one wall was used for Scenario 3 and none for Scenario 4.
5. The vacuum's thermal properties could not be entered as zero or infinite. So, the values for thermal conductivity and density were set to zero, and the value for heat capacity was set to infinity. The values of air, nitrogen and BCR glass fibre changed with respect to temperature and hence, a non-steady state condition was applied.
6. The boundary heat flux varied only with irradiation and did not follow the change in time step. Hence, the temperature of the model usually starts from a much higher temperature and not from the ambient temperature.

Table 5:The geometry parameters considered for building the reactor for two variants.

Domains	**Values (cm) (Scenario 1,3 and 4) With Air**	**Values (cm) (Scenario 2) Without Air**
Outer Glass Cylinder	Radius = 4.7 Height = 40 Thickness = 0.12	Radius = 4.7 Height = 40 Thickness = 0.12
Vacuum Layer	Radius = 4.58 Thickness = 0.88	Radius = 4.58 Thickness = 0.88
Inner Glass Cylinder	Radius = 3.7 Thickness = 0.12	Radius = 3.7 Thickness = 0.12
Air Layer	Radius = 3.58 Thickness = 0.05	Not Present
Aluminum Fin	Radius = 3.53 Thickness = 0.1	Radius = 3.58 Thickness = 0.1
Nitrogen	Radius = 3.43	Radius = 3.48
Covers	Radius = 4.7	Radius = 4.7
Focal Plane	Dimension: a=4, b=1 Position = (20,0)	Dimension: a=4, b=1 Position = (20,0)

Table 6:The computational parameters for the glass evacuated tube solar collector with air as the heating media (Badar et al., 2011; Chen & Yang, 2022; Kim et al., 2007; Ma et al., 2010).

Components	**Parameter**	**Value**
Outer glass tube	Outer Diameter	47 mm
	Transmittance	0.92
	Emissivity of glass	0.9
Absorber tube	Outer Diameter	37 mm
	Absorptivity	0.85
	Emissivity of selective coating (Inward)	0.9
	Emissivity of selective coating (Outward)	0.07
Air gap layer	Thickness	1 mm
	Conductivity	0.0267 W/ (m.K)
Aluminum fin	Thickness	0.5 mm
	Conductivity	202 W/ (m.K)

	Emissivity	0.1
	Emissivity of paint coating	0.9
Vacuum	Vacuum Pressure	<0.1 Pa

Table 7:Thermal properties of the materials in the model.

Domains	**Thermal Conductivity (k) [W/(m*K)]**	**Density (ρ) [kg/m^3]**	**Heat Capacity at constant pressure (C_p) [J/(kg*K)]**
Borosilicate Glass	1.13	2230	754
Vacuum Layer	0.001	0.01	9999
Aluminum	237	2700	904
Air	k(T)	rho(pA,T)	Cp(T)
Nitrogen	k(T)	rho(pA,T)	Cp(T)
Glass Fiber BCR 64	k(T[1/K])	rho(T[1/K])	C(T[1/K])

To make the simulation even more realistic, meteorological data for Kozhikode (Kerala) was taken on the 15th of May 2022, such that the ambient temperature, wind speed, precipitation, and irradiation data could be simulated. The geometry was split into three sections, with the centre one holding the boundary heat flux condition (focal point). This was done to mesh the geometry easily and reduce the computation time. As covers for the sides of the tube, a resin-bonded glass fibre board, BCR 64, was selected to provide a good insulation material. The innermost layer was made of nitrogen to simulate the torrefaction conditions of maintaining an inert environment and heat transfer in a gaseous medium.

Two kinds of physics were involved in the simulation. *'Heat Transfer in Solids and Fluids'* and *'Surface-to-Surface Radiation'*. Nitrogen was the only domain included in the fluid domain with a *'Convectively Enhanced Conductivity'* property to enact heating of the innermost layer through convection. An *'External natural convection'* property was given for the outer glass cylinder layer to simulate the effect of wind and ambient temperature on the glass tube and covers. A general heat source was given for the *'Boundary Heat Source'* with:

$$Q_b = ampr1.Is_{amb} * 21.7 * 0.8 * 0.32 \tag{25}$$

Where *ampr1.Isamb* was the irradiance value for every time step, 0.8 was the fraction of sunlight reaching the inner domain after optical losses of the EVC as deduced from Figure 25, the concentration factor of the EG SK14 cooker was 21.7, and the approximate efficiency of the solar cooker was taken as 32 %, calculated in Section 4.2. The *'Selective Coating-Opaque Surface'* for the Aluminium layer and the *'Outer Borosilicate Glass-Semi-transparent'* values were given from the values shown in Table 6. To model the effect of a Greenhouse, the Vacuum domain and Outer Glass were made transparent for short wavelength waves [0-2.5[µm]] for 'Study 2', i.e., when the irradiation enters the tube but were made *'Opaque'* for long wavelength waves [2.5[µm], +∞] when emitted back out of the tube in 'Study 1', as shown in Figure 39. An *'External Radiation Source'* with the selected Ambient conditions was added to this physics. These physics models make up the boundary conditions for the simulation. A Multiphysics was applied to merge both the physics at work in the model namely, *'Heat Transfer with Surface-to-Surface radiation'*. For Scenario 3, the only difference was to include one of the covers to act as a vacuum and outer borosilicate domain and the boundary entries, respectively *'Opaque'* and *'Outer Borosilicate Glass-Semi-transparent'* commands. Similarly, for Scenario 4, both the covers were included as vacuum and borosilicate domains and boundaries to simulate the *surface-to-surface radiation.*

The refractive index of the borosilicate glass is 1.5168 [17] and thus the critical angle of the incident light travelling from air to glass on the *'Outer Borosilicate Glass-Semi-transparent'* was calculated by using:

(26)

$$\theta_{crit} = \sin^{-1}\frac{n2}{n1} = \sin^{-1}\frac{1}{1.5168} \approx 42^{0} = 0.73308\,rad$$

Meshing of the model is done as efficiently as possible. Since the physics-controlled meshing had too many boundary elements and nodes involving free tetrahedral mesh, a user-based mesh was applied. This involved meshing the work planes first with a *"free tetrahedral mesh"* and then sweeping it over the remaining area using boundary conditions. It consisted of 32193 domain elements with an average element quality of 0.4749 and a minimum element quality of 0.0287 for Scenario 1. The mesh quality was satisfactory, and the simulation was smooth and not cumbersome. Figure 41 shows the meshed model used for the simulation. The meshing varied very little with the other scenarios.

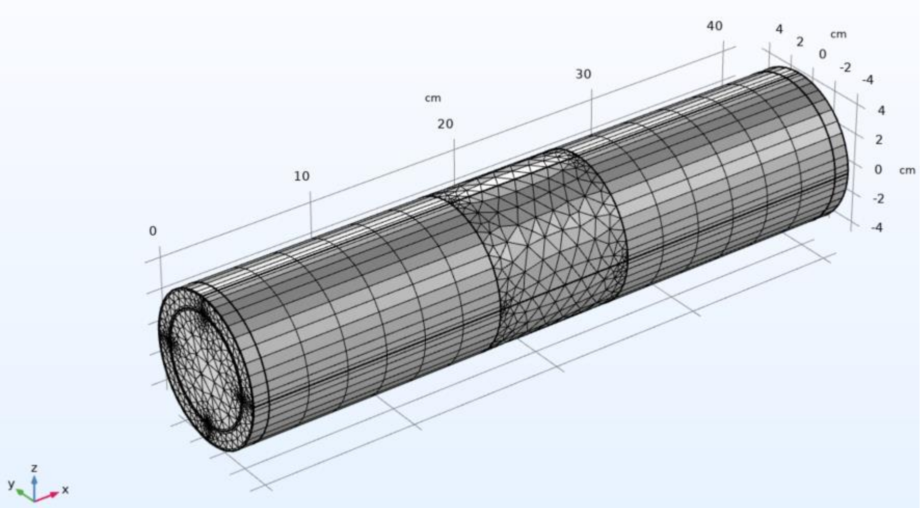

Figure 41: Meshing the model optimally.

Two-time dependent studies were considered for the simulation, and the output times were set for 2 hours from 10:00 hrs to 12:00 hrs for every 15-minute time interval. *Study 1* illustrated the non-transparent model and *Study 2* the transparent model, as mentioned earlier. Another *Study 3* was used to club the two studies, so that a coupled overall value was obtained in the simulation. This was done to apply the principle of *"greenhouse effect"* in compliance with Figure 39. The model was simulated, and the values obtained were tabulated. Some of the operations that were used to look at the simulation results were *Temperature, Isothermal Contours, Streamline*, and *Arrow Volumes*.

3.4 Solar-Biomass Torrefier Model

Experiments were conducted in two designed solar collectors to validate the most significant research question of **testing the viability of an SK14 solar cooker (coupled with a solar collector) featuring a solar torrefier**. The simulation results were used to study the primary function of an EVC and to assess the torrefier's ability to reach the specific temperature range. The experiments performed would not only torrefy the unprocessed SCG but also correlate to the simulation.

To closely regulate the originality of the experiment, the experiment was conducted in Hyderabad, India, which receives ample sunlight throughout the year. A SK14 solar cooker was ordered from 'Rudra Solar' and assembled to the closest perfection as shown in Figure 43. The specifications of the cooker are shown in Table 8. A Flir One thermal camera was used to gain a better understanding of heat dissipation as well as the temperature profile of the reactor as it was heated and to validate the COMSOL simulation. The average temperature was between 37 and 40 °C. The experimental data were collected on average between 10:00 and 15:00 hours, and the irradiance ranged from 316 to 989 W/m^2.hr, according to [18]. This set of studies were performed between May 10th and 19th, and Figure 42 shows the irradiance over time for those days. The specific observations are listed in Appendix 8.1.

The focal length, concentration ratio, surface area, and aperture area were calculated using equations specified in Section 2.4.5. Firstly, to calculate the efficiency of the reactor, 2 litres of water were placed in a pot and the time required to reach the boiling point (Δt) was calculated. The ambient temperature was noted from the beginning of the experiment to calculate ΔT. These values were used to calculate the efficiency of this SK14 cooker using Equation (9). The average irradiance (G_{av}) for this specific run was calculated based on the irradiance data obtained from [18] conducted on the 15th of May.

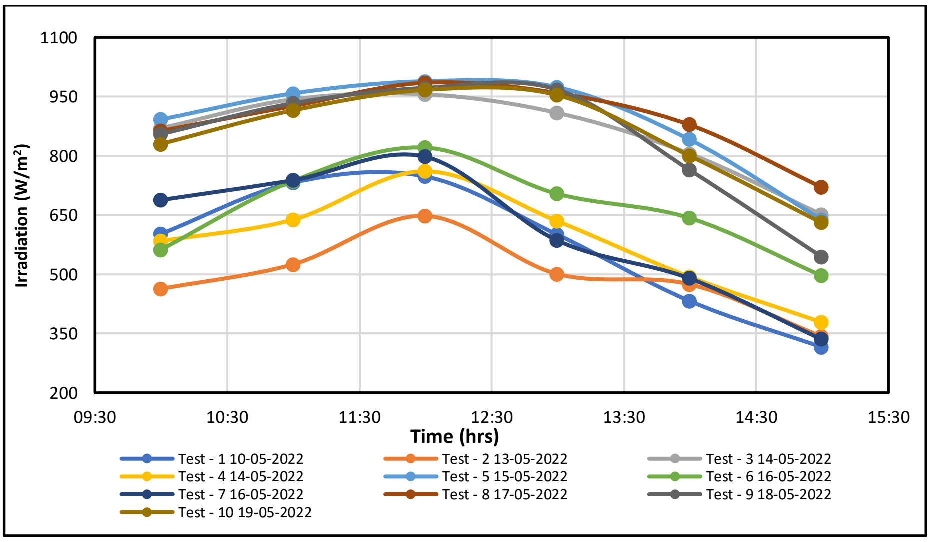

Figure 42:Time vs Irradiation graph for the respective experimentation dates.

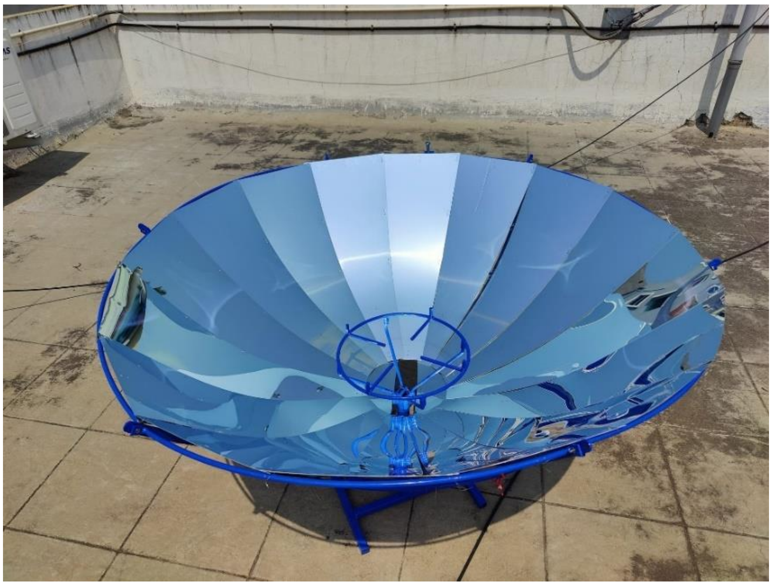

Figure 43: SK 14 solar cooker ordered from Rudra Solar.

Table 8:The specifications of the assembled Rudra SK14 solar cooker.

	Content	**Specification**
1	Aperture Diameter (D_{ap})	1.2 m
2	Average Focal Length (f)	0.2 m
3	Aperture Area (A_{ap})	1.13 m^2
4	Depth of Parabola (h)	0.43 m
5	Surface Area (A_s)	1.63 m^2
6	Pot stand Diameter	0.3 m
7	Receiver Area (A_r)	0.07 m^2
8	Concentration Ratio (C_A)	16
9	Aluminum sheet reflectivity (η_{Al})	0.9

3.4.1 Reactor Design

A single-layered glass pseudo heating chamber was designed to be placed at the focal point of the cooker. An *aluminum tube* was used as the inner heating chamber, coated with an enamel jet black paint. A 2 mm thick *transparent* borosilicate glass was used as the outer single glass layer to also act as a heat retention medium. An $10 \times 2 \times 1.5$ cm *aluminum crucible* was made to hold the SCG during the experiment. A rubber cork was used to seal the reactor as well as to act as an *insulator*. A *k-type multi-stem digital thermometer* was used to continuously measure the temperature of the reactor during the experiment. Table 9 lists the specs of the reactor, and Appendix 8.1 shows how the reactor is usually set up as a stand-alone system.

Table 9:Reactor parts and its specifications.

	Reactor parts	**Specifications**
1	Aluminum Tube	Outer Diameter: 40mm Thickness: 2 mm Reactor 1 length: 330mm Reactor 2 length: 300mm
2	Rubber Cork	PVC Thermal Type
3	Borosilicate Glass Tube	Inner Diameter: 50mm Length: 450 mm Thickness: 2.5mm
4	K-type thermometer	Range: -50 ℃ to 300 ℃
5	Pressure release glass pipe	Thickness: 2.5 mm

To find out the optimum experimental design and the aimed torrefaction temperature of 240 ℃, three different designs of the reactor were used. To do so, the reactor was placed on the focal point of the SK14 solar cooker, and its direction was changed every 15 minutes to align with the sun's position using the manual sun-tracker. The temperature of the reactor was noted every 5 minutes, and the reactor was allowed to heat till it reached its peak.

The initial temperature was always measured, which referred to the ambient temperature with respect to the reactor being used. As the reactor was heated, the thermal camera was used to obtain the temperature profile of the reactor (outer glass). This was done to not only provide further verification of the insulation of the Borosilicate glass but also to show the heat dissipation along the reactor since most of the concentrated sunlight was concentrated on the center of the reactor. This also provided a comparison between the inner metallic tube and the outer glass tube temperature.

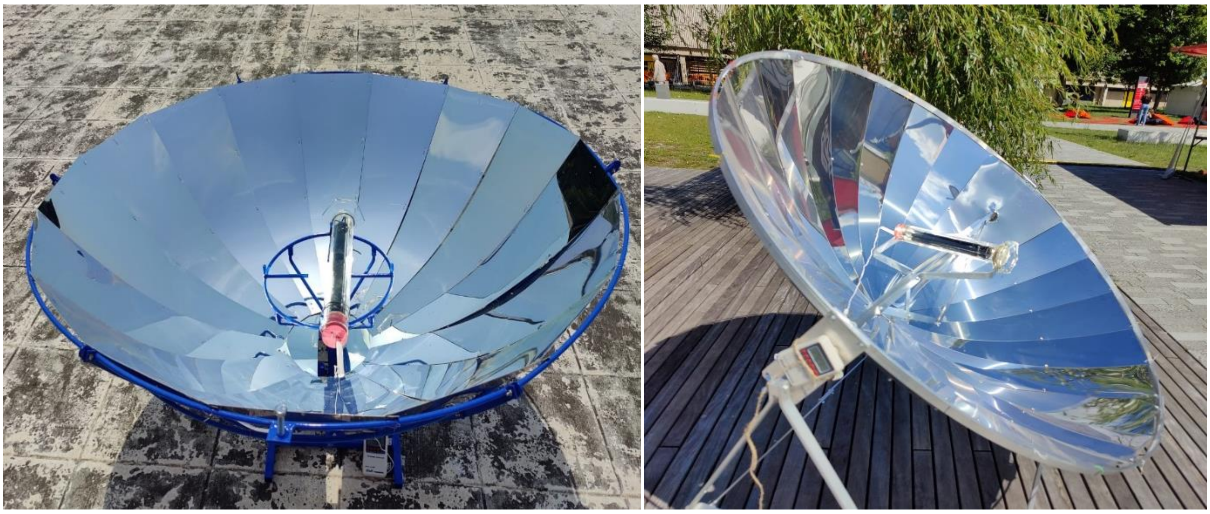

(a) Rudra Solar SK14 (b) EG Solar SK14

Figure 44:Basic Biomass SK14 torrefier design under irradiation.

Multiple experiments were conducted, and two reactors were employed for the considered results. At a later stage, the naturally dried SCG was charged in the reactor in an aluminum crucible to notice the effect of temperature on a variable residence time. A similar setup was later carried out on a sunny day at TU Delft, Netherlands, as shown in Figure 44(b). In this case, the only criteria that was taken into consideration was duplicating the procedure under the solar irradiation (significantly less than that of India) of the Netherlands. This SK14 cooker was ordered from 'EG Solar' and had similar characteristics as the one used in India. The only difference was the concentration factor (C_A), which was calculated and used in the COMSOL simulation. Since the laser experiments in Section 3.2 were done with this cooker, it was easier to set the focal point and adjust the reactor to match.

3.4.1.1 *Case 1: Reactor 1*

Reactor 1 was built with the intention of retaining heat for a longer period of time, so both the mouth of the aluminium reactor tube and the small gap with the glass shell were completely sealed with a rubber cork and a thermos seal, respectively. Two orifices were built for the release of pressure as well as hot air released in the heating process. The design of the reactor is shown in Figure 45.

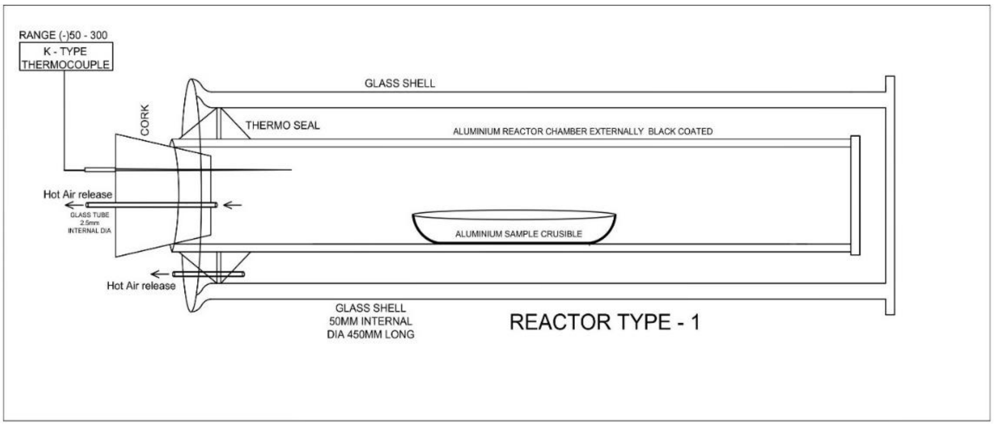

Figure 45:Design of the Reactor type 1.

Three experiments were conducted with this reactor, and a conclusion was made based on the peak temperature achieved as well as the incidents that occurred during the experiments. The SCG feedstock was charged during the beginning of the experiment to not only dry the product but observe the pattern when it is heated to a higher temperature. In due course, this reactor design was discarded due to incompetency even with good irradiation and weather conditions. If the pressure build-up could be released without considerable heat loss in the process, there would be very good potential for this reactor.

3.4.1.2 *Case 2: Reactor 2*

This reactor was designed taking into consideration the convective air heating of the whole reactor. Hence, both the ends of the metallic tube were kept open, and it was fixed at the centre of the glass tube. The aluminium crucible was placed in the middle of the chamber and fixed in that position. The mouth of the glass tube was sealed with a larger rubber cork with an outing for flue gases and pressure release and another orifice for the temperature sensing probe. This has been shown in Figure 46. Seven experiments were conducted in this reactor not only at the desirable torrefaction temperature but also at a smooth transition in the reactor at good ambient conditions. Reactor 2 was considered for the assessment of the values and the results obtained from most of the valid experiments. The whole reactor was fixed onto the potholder with a wire to prevent it from slipping out or moving out of position.

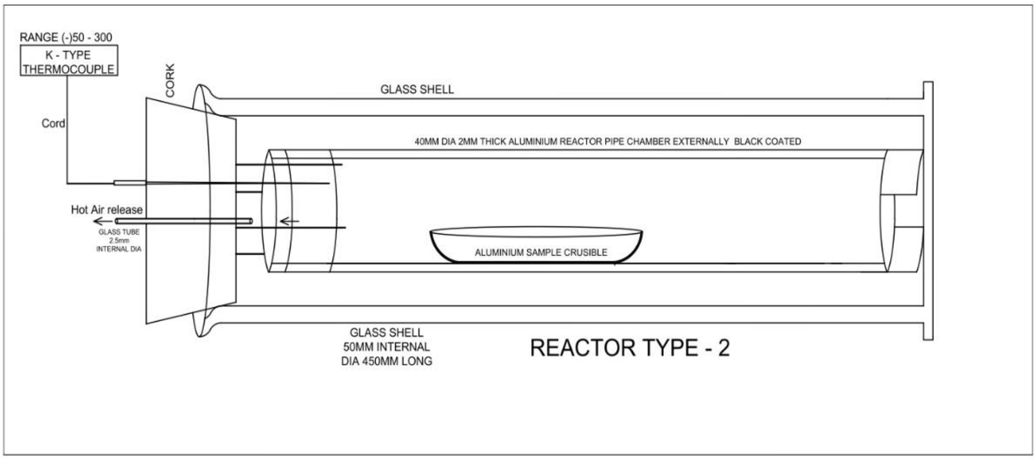

Figure 46:Design of the Reactor type 2.

3.4.2 Assumptions and viewpoints

1. Minor deformities while building the cooker were ignored. This may or may not have caused a minor shift in the focal point.
2. It was always ensured that the reactor did not come into contact with the outer borosilicate glass.
3. Since the temperature of the reactor was increasing rapidly, the first reading was not always accurate.
4. The volatile content released during the experiment was not collected or considered.
5. The overall area of the cooking pot, i.e., the effective concentration ratio, was considered as the receiver area and not just the focal point.
6. The heating was not homogeneous.
7. Inert environment is not considered for the torrefaction process.

4 Results

The present chapter concerns the results of the experiments conducted; the modelling and functionality of the Solar-Biomass reactor; and the simulation of the processes using COMSOL Multiphysics. The results are validated when combined and proposed as a working prototype.

4.1 Laser Experimentation

Multiple experiments were conducted to determine the pattern and location of the focal plane and point on the cooker's pot stand. In each experiment, the distance between the laser pointers was altered to determine if the concentrated rays were incident on the graph sheet without obstruction. **First and foremost, the most significant conclusion was that the SK14 solar cooker can either have multiple focal points or the pot receiver is not placed at the exact focal point of the cooker.** When the position of the laser pointers was altered, the reflected rays frequently shifted because they did not intersect in the receiver plane. The minor flaws in the cooker's construction or the design structure of the cooker could be a contributing factor.

Secondly, there was no stable focal plane when the graph paper was placed horizontally on the plane of the holding pot because the focal point averaged between 3 and 4 cm. Table 10 shows the change in focal point diameter as the graph sheet plane was relocated six steps. When the plane was shifted vertically downward by 6 centimeters, the diameter of the focal point increased from 4 to 14.5 cm. This shows the pattern of decreasing heat flux and concentration ratio as the focal plane was shifted. Figure 47 shows the focal point for the first step of the experiment as laser rays focusing on graph paper.

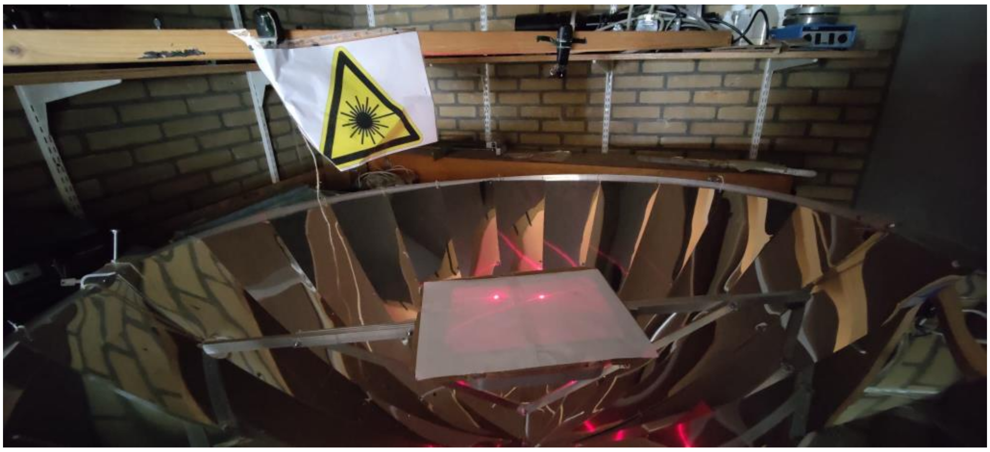

Figure 47:Reflection of laser rays captured on the graph sheet.

Thus, it was inferred that the cooker's focal point was designed to evenly heat the entire receiver rather than just the focal point. Furthermore, if concentrated to a point focus, the theoretical concentration factor was calculated to be greater than 80,000, which is undesirable for the functioning of a solar cooker. This deduction was used to build the prototype for future experiments. Furthermore, as shown in Figure 44, the trials in Hyderabad and TU Delft confirm the fact that both SK14 solar cookers lack a fixed-point focus. Table 10 displays the focal point concentration factor of the 'EG Solar' cooker derived from this experiment.

Finally, only the ‘Point 1’ diameter (4 cm) from this experiment was used to define the boundary heat diameter for simulations in COMSOL as shown in Figure 40. The effective concentration factor (C_A)

of EG SK14 cooker was calculated by considering its aperture area (1.54 m^2) and potholder area as the receiver area (0.07 m^2) to be 21.7 using equation (8). This value was also used to determine the boundary heat flux value as shown earlier to determine equation (25).

Table 10:Approximate focal point concentration factor achieved from the laser experiments.

Focal Plane Location	**Focal Point Diameter**	**Concentration Ratio**
Point 1 (0 cm)	4 cm	1225
Point 2 (1 cm)	3.4 cm	1695
Point 3 (2 cm)	5.3 cm	698
Point 4 (3 cm)	8.1cm	298
Point 5 (4 cm)	9.5 cm	217
Point 6 (5 cm)	12 cm	136
Point 7 (6 cm)	14.5 cm	93

4.2 COMSOL Simulation Results

Figure 48 shows the outcomes of the non-steady-state, time-dependent simulation for Scenario 1 in terms of temperature on the model's overall domains. Figure 48 presents the average temperature profile vs time throughout the domains for Scenario 1. Similar to the study described in Section 2.4.2, the evacuated vacuum tube model highlighted the key functions performed by the selective coating inner glass layer and the aluminum tube, which were responsible for heating the inner nitrogen domain. The results demonstrated that EVC combined with continuous irradiation can achieve pyrolytic temperatures (<350 °C) in just two hours. Even though heat loss through a probable pressure release was ignored, these simulations showed ample evidence to use its principle in designing the prototype reactor.

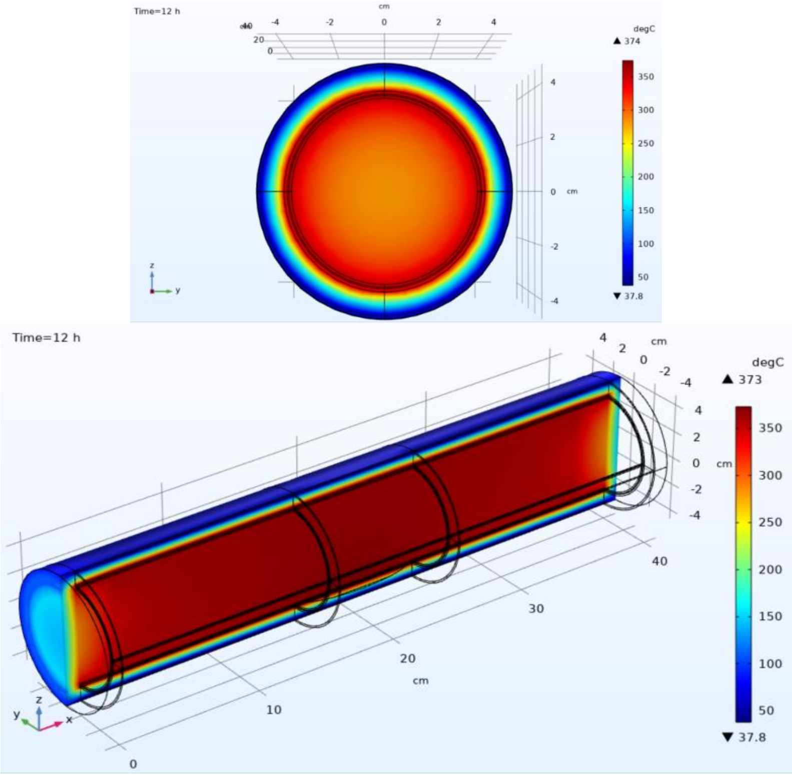

Figure 48: Volume cross sectional temperature profile of overall domain from Scenario 1.

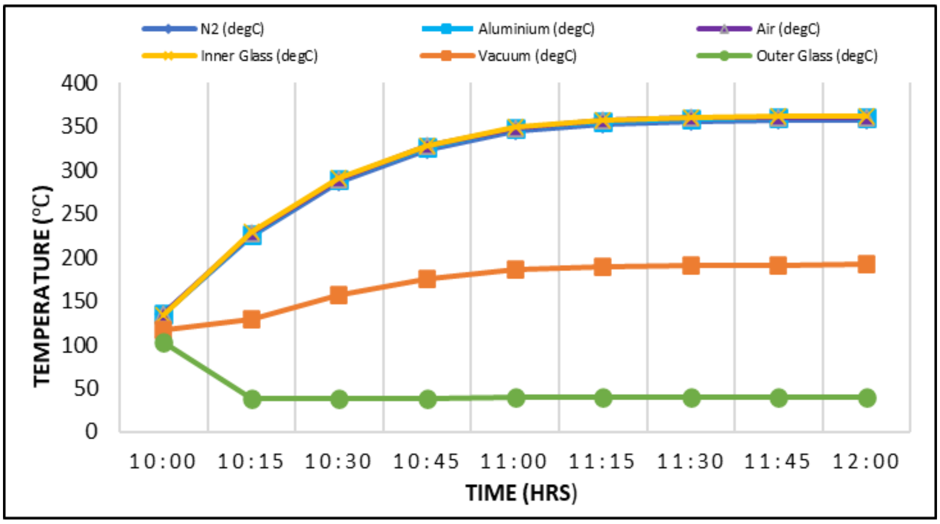

Figure 49:Time vs temperature graph of the domains involved in Scenario 1.

Assuming that the nitrogen layer holds the SCG, the heat distribution along this layer for the four scenarios was analysed. As is evident from Figure 48 and Figure 49, the outer-glass and vacuum layer operated as a perfect greenhouse element by trapping long wavelength waves, resulting in an average inner domain temperature of around 350 °C. The exterior glass layer was at a remarkably low temperature of around 50°C (accessible with bare hands), making the heat retention rather impressive. As seen in Appendix 8.2, there were just a few degrees of decrement from the selective coating to the nitrogen domain for all three cases.

4.2.1 Scenarios Correlation and Comparison

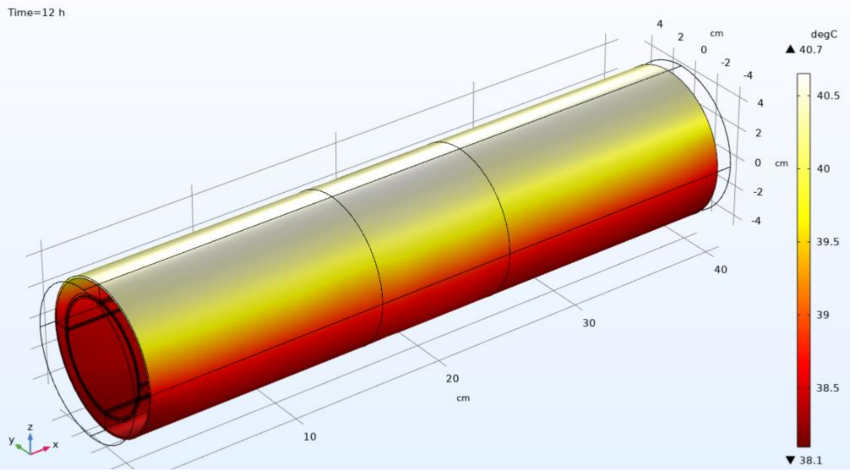

Figure 50:DNI heating the outer borosilicate layer in Scenario 4.

Isothermal contours and arrow plots were used to understand heat distribution along the reactor inside the selective coating domain. Figure 51 and Figure 52 compare heat retention at noon between two-sided covered glass fibre (Scenario 1) and one-sided clear tube (Scenario 3) inside the inner glass domain. The contour profiles illustrate the dominant sources of heating from selective solar absorption and by the boundary heat. This can be inferred by observing higher contour plots at the constantly irradiated upper surface of the tube and around the boundary heat flux, which signifies a concentrated heat flux from the solar cooker. This is further supported by observing the significantly lower surface temperature of the outer borosilicate layer as shown in Figure 50. Away from the heat flux, the bottom corners of the tube show a considerably lower temperature profile, indicating less DNI and heat flux heating. The *'Arrow surface'* and *'arrow line'* features illustrate heat dispersion and heat loss through the covers. The glass-vacuum cover domain end of Scenario 3 showed fewer heat transitions and low temperature contours compared to Scenario 1. For further clarification, Appendix 8.2 shows the values for average volume temperature and maximum volume temperature for different domains.

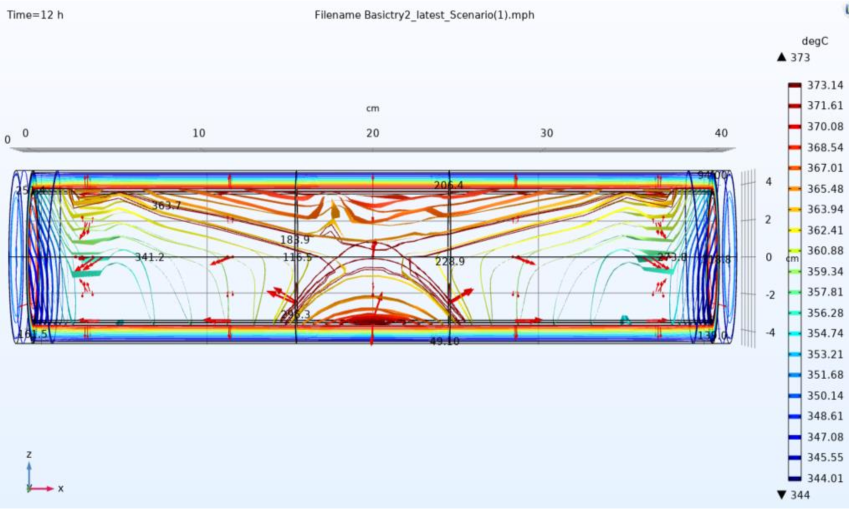

Figure 51: Temperature contours with arrow surface inside the selective coating domain in Scenario 1.

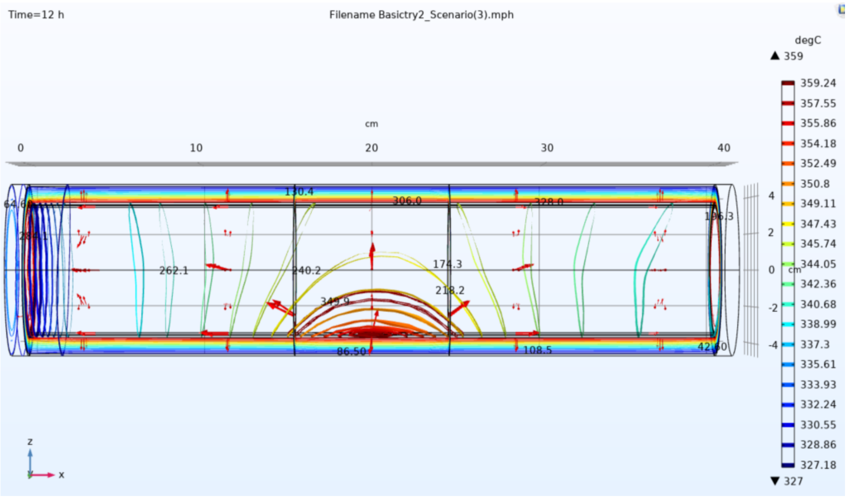

Figure 52:Temperature contours with arrow surface inside the selective coating domain in Scenario 3.

Another temperature contour comparison is shown between all the scenarios using the ‘arrow volume’ and ‘Isosurface’ features inside the nitrogen domain in Figures 52, 53, 54 and 55. Although there was a similar heat distribution profile as discussed earlier for Scenarios 1 and 3, the arrow volume and isosurface heat profile showed a clear difference between the scenarios. Along with the obvious minimal heat losses through the walls of the reactor, Scenarios 1, 2 and 3 showed additional heat losses through the BCR glass fibre cover, as seen by the red arrows and blue contour lines (along the covers). Viewing the scenarios, however, reveals an important inference about the uniformity of heat distribution across domains. Although the temperature contours show different heating profiles across all the domains, the overall temperature profile remains similar to the one shown in Figure 48. This is a property that must be further researched.

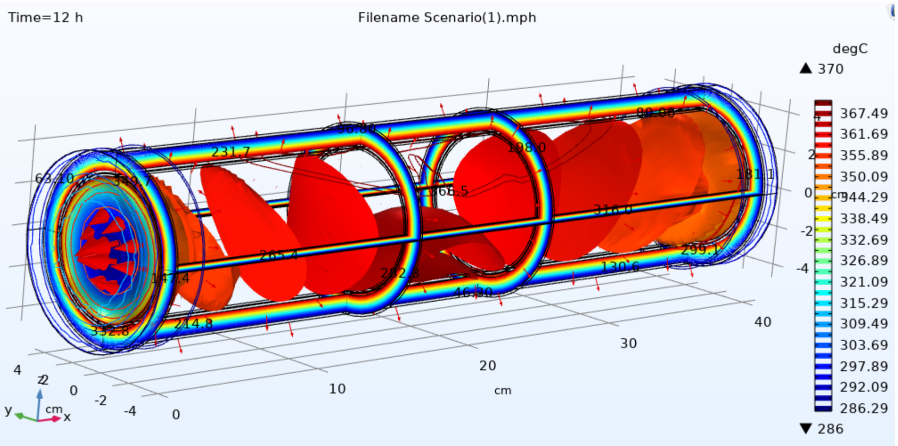

Figure 53: Temperature contour with arrow volume along the nitrogen domain in Scenario 1.

To compare the heat distribution profiles of the different Scenarios in detail, the difference in temperature between the focal point (boundary heat flux) and the edges of the tube was measured. The difference in temperatures between Scenarios 1, 2, 3, and 4 was about 12, 15, 15, and 16 °C, respectively. No matter how different the temperatures were across the whole area, the temperature profile between the two sliced work planes was always the same, especially in Scenarios 1 and 3

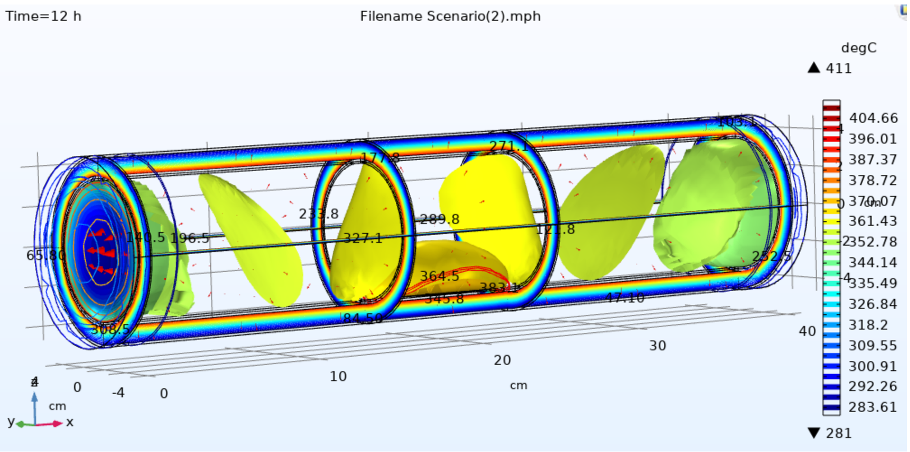

Figure 54: Temperature contour with arrow volume along the nitrogen domain in Scenario 2.

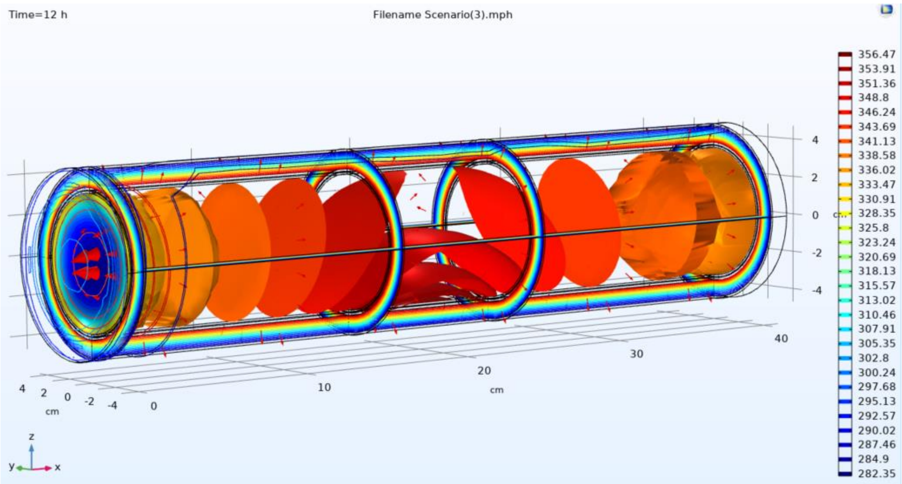

Figure 55: Temperature contour with arrow volume along the nitrogen domain for Scenario 3.

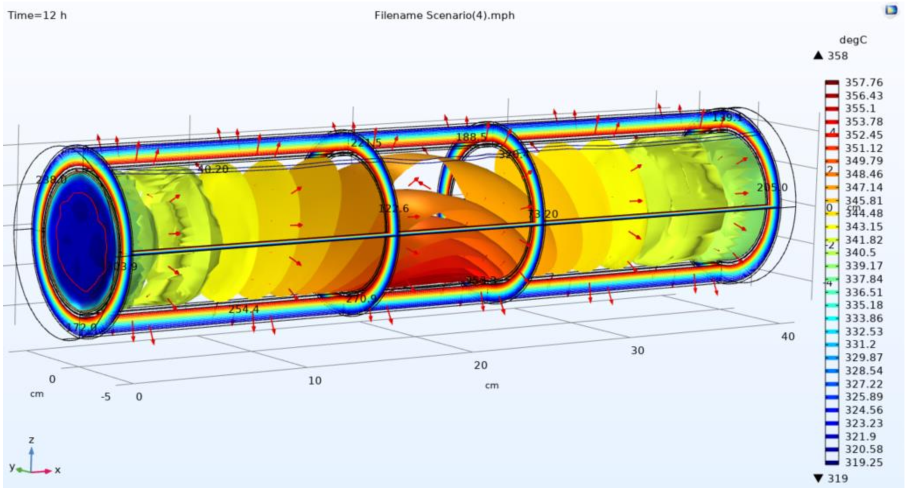

Figure 56: Temperature contour with arrow volume along the nitrogen domain in Scenario 4.

4.2.2 Nitrogen domain Temperature Profile

Figure 57(a) depicts the average temperature of the nitrogen domain for the four different situations. Scenarios 1 and 2 showed an exponential increase, and Scenarios 3 and 4 exhibited a somewhat linear increase, with Scenario 4 being slightly more linear than Scenario 3. By 12:00 hrs., the average temperatures for all four scenarios were almost the same, with temperatures in Scenario 1 and 2 being rather stable, but this was not the case for the other two scenarios. However, the profile shifts significantly when the highest temperature measured in the nitrogen domain is taken into account. As can be observed in Figure 57(b), Scenario 2 showed the maximum temperature, with a peak of 400 °C.

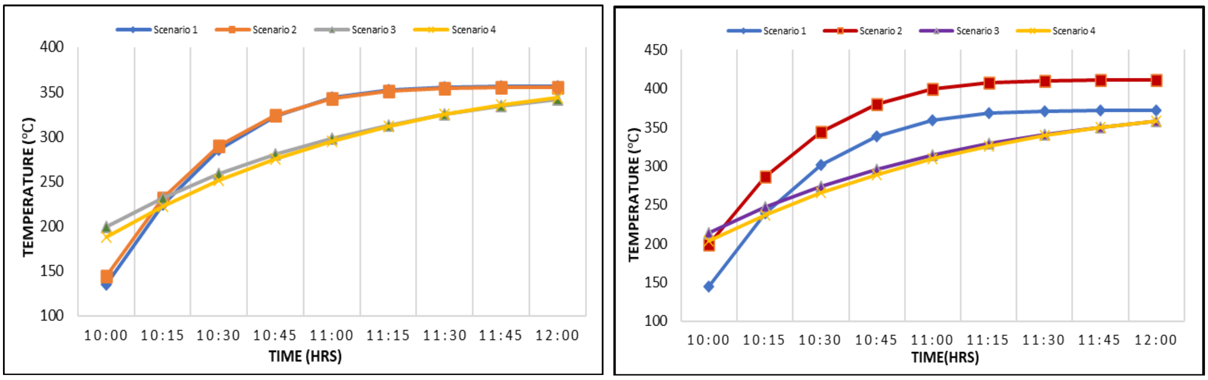

(a) *(b)*

Figure 57:Average Temperature and maximum temperature vs time graph of the Nitrogen Domain.

4.2.3 Boundary Heat Flux Temperature analysis

The boundary heat flow was modified into an ellipse to represent the model precisely. However, the modification of the temperature that could be achieved was dependent on the boundary material to which it was applied, i.e., an aluminium boundary for Scenario 2 and air for the rest. Figure 58 demonstrates that the focal point temperature in Scenario 2 is significantly greater than in Scenario 3. This was because the boundary heat flux in Scenario 2 was directed on the aluminium surface, but in Scenario 3, the air gap between the inner glass tube and the aluminium layer causes additional heat loss. Figure 59 shows the average increase in boundary flux temperature with time for the simulated scenarios. It follows a similar trend as Scenario 2 having a greater temperature, even though the only variable was the irradiation at that time step, which did not vary considerably between simulation times and averaged 932 W/m^2. The FP temperature for Scenarios 1 and 4 is shown in Appendix 8.2, following a similar pattern as Scenario 3.

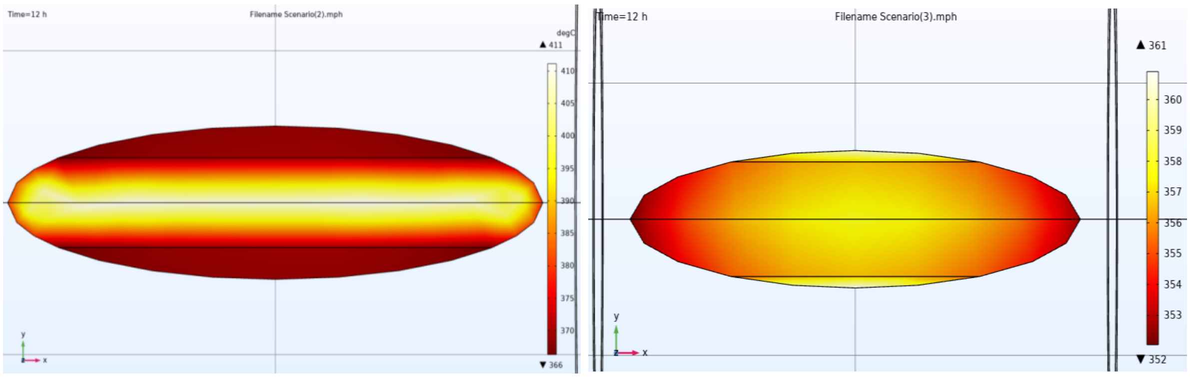

Figure 58: Focal point temperature profile of Scenario 2 and 3 respectively.

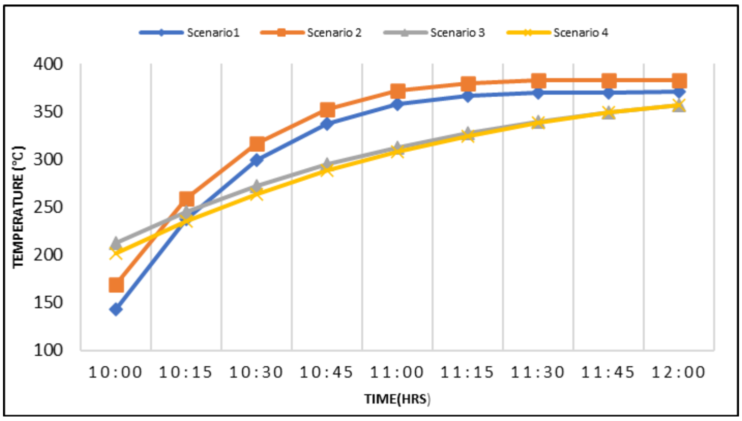

Figure 59: Average surface temperature graphs of the FP for the 4 scenarios.

The simulations were a valuable tool in further designing the prototype reactor because they allowed modifying geometrical and physical features. This enabled the estimation of the aimed temperature, system functioning, component interactions, and upgrading of the prototype based on simulation results. However, it was obvious that there would be additional heat losses while practically modelling a prototype, and hence a close to perfect scenario was modelled further, as shown in Appendix 8.2.1. The operating parameters obtained from the experiments conducted in Section 3.4 Using the same ambient circumstances, it could be possible to estimate a system's energy delivery and design variable modifications.

4.3 Prototype Reactor Torrefaction Experimentation

Most of the experiment's evaluations and assumptions were attributed to Reactor 2. It was quite clear from the COMSOL simulation that the principle of an solar Evacuated Vacuum tube Collector (EVC) can be applied to make a reactor that reaches pyrolysis temperatures. However, it was ambiguous if a single glass tube reactor without a vacuum domain could achieve a similar heating profile. Since the heat and pressure loss through an outlet was not considered in COMSOL, the experiments conducted in Hyderabad would also support the heat retention possibility and help verify the research question.

4.3.1 ‘Rudra’ SK14 Characterization

The primary objective of the experiment's design and execution was to verify the torrefaction temperature in the reactor. The efficiency of the Rudra SK14 cooker was found to be 31.4 % by using Equation (9) to solve from the values mentioned in Section 2.4.5. The specific heat of water (*Cp*) was taken as 4.182 kJ/kg. ΔT was calculated to be 61 K when water boiled at 97 °C and initial temperature of water was 36 °C. 1 litre of water in the pot took around 12.5 minutes to reach the boiling temperature (Δt). The experiment was started at 11:00 on the 15th of May. The values are mentioned in Table 11, inspired by equations mentioned in Section 2.4.5. Hence, the efficiency was calculated as:

$$\eta_{av} = \frac{mC_p\Delta T}{G_{av}A_{ap}\Delta t} = \left. 1\,kg \times 4.184\frac{kJ}{kg.K} \times 61\,K \middle/ 958\frac{W}{m^2} \times 1.13\,m^2 \times 12.5\,mins \right. = 31.43\ \% \tag{27}$$

The density of the solar radiation at the focal point (Q_f) can be calculated by:

$$Q_f = C_A \times G_{av} \times \eta_{Al} \ = \ 16 \times 958\frac{W}{m^2} \times 0.9 = 13795.2\ \frac{W}{m^2} \tag{28}$$

Further, the actual solar radiation power at the receiver area (pot area) and actual wattage available at the focal point are shown in Equations 29 and 30 respectively:

$$P_b = Q_f \times A_r = 13795.2\frac{W}{m^2} \times 0.07\,m^2 = 965.7\,W \tag{29}$$

$$P_{bf} = P_b\ \times \eta_{av} = 0.314 \times 965.7\,W = 303\,W \tag{30}$$

The approximate cooking power (P_c) can be calculated by finding out the useful energy obtained during the temperature rise from 60 to 97 °C. This took an instantaneous time interval of approximately 4.5 min to reach the boiling temperature calculated in Equation 32.

$$P = mC_p\left[\frac{T_{w2} - T_{w1}}{\Delta t}\right] = 1\,kg \times 4.184\ \frac{kJ}{kg.K}\ \times\ \frac{97 - 36}{12.5\,min} =\ 392\,W \tag{31}$$

$$P_c = mC_p\left[\frac{T_{w2} - T_{w1}}{\tau}\right] = 1\,kg \times 4.184\ \frac{kJ}{kg.K}\ \times\ \frac{97 - 60}{4.5\,min} =\ 573\,W \tag{32}$$

Table 11: Test load of system to calculate the efficiency and power of the SK14 cooker.

Parameter	**Designation**	**Rudra Solar Cooker**	**(Mekonnen et al., 2020)**
Mass of Water (kg)	m	1	5
Ambient temperature (°C)	T_a	40	27
Average irradiation (W/m^2)	G_{avg}	958	891
Starting temperature of water (°C)	T1	36	27.8
Ending temperature of water (°C)	T2	97	95
Time interval (min)	Δt	12	40
Instantaneous time (min)	τ	4.5	20

4.3.2 Observations

Only the values from Reactor 2 and Reactor 1 were considered, and the temperatures achieved from the experiments are shown in Table 12. The difference in the duration of the test was due to the intermittency of solar energy, wind, and location of the sun. The cooker often moved out of the focal point on the reactor due to the sun's position or errors, which sometimes resulted in a drop in temperature or a narrow uneven increase. Detailed values and graphs obtained from the experiments are presented in Appendix 8.1.

When adjusting the focal point of the RUDRA and EG SK14 cookers, the first major observation was that it **did not focus into a point**. Rather, a larger focus of approximately 5 or 6 cm was observed on the glass reactor at the focal plane**.** Experiments 2 and 3 were conducted in Reactor 1 and were valuable feedback in designing the reactor. In Experiments 2 and 3, the aluminium pipe (reactor) and the rubber cork popped out of the shell at 110.7°C and 177.1°C, respectively. This was caused by excessive pressure build-up due to gaseous expansion and water vapour inside the reactor. A pressure release method (by increasing the diameter of the gap at the thermal seal) or a 2 mm orifice in the rubber cork for releasing hot air, gases, and pressure was proposed. The idea of using reactor 1 was discarded after these experiments, and a much simpler system was implemented in reactor 2 for the rest. The biochar obtained from Experiment 3 looked incompletely charred, as can be seen in Figure 63.

Table 12:Summary of experimental values conducted in Hyderabad.

Experiment. No	Date	Duration of Experiment	Ambient Temp (°C)	Peak Temperature (°C)
1 (Reactor 1)	10/05/2022	3 hours	36	70
2 (Reactor 1)	13/05/2022	1 hour	37.6	111.2
3 (Reactor 1)	14/05/2022	1.35 hours	42.2	184.1
4 (Reactor 2)	14/05/2022	1.45 hours	41.6	121.2
5 (Reactor 2)	15/05/2022	38 minutes	41.3	239.9
6 (Reactor 2)	16/05/2022	1 hour	36	196.2
7 (Reactor 2)	16/05/2022	50 mins	46	184.3
8 (Reactor 2)	17/02/2022	1 hour	44.2	233.1
9 (Reactor 2)	18/02/2022	55 minutes	42.7	262.3
10(Reactor 2)	19/02/2022	1.10 hours	41.3	259.8

The results of experiments 5, 8, 9, and 10 showed that the developed prototype can achieve torrefaction temperatures of 240 and 260 °C, as can be seen in Figure 60. Figure 62 displays the temperatures that were observed while conducting the experiments in Hyderabad and Delft, respectively. The entire residence time was roughly the same, averaging 1 hour, even though these trials weren't started at the same time. It took an average of 40 minutes to reach the respective peak temperatures in the reactor. At 170 °C, water vapor condensation was observed, and by the end of the experiment, the inside walls of the tube had been tarnished by condensed gaseous feedstock products. In Experiment 5, the poly vinyl cushion (PVC) at the bottom and the HDPE rope fastened to the pedestal and aluminium tube were burned at 230 °C. Hence, a metallic platform and stainless-steel (SS) ropes were employed to triple the trial results. As observed in Figure 60, ignoring the minor kinks, a uniform pattern of temperature increase can be seen with increasing experiment time. Moreover, experiments 9 and 10 showed a peak of 262.3 °C and 259.8 °C as seen from Table 12, which implies different achievable torrefaction temperatures for future studies. It can be seen from Figure 63 that the spent coffee grounds underwent complete torrefaction, as shown by the darkish tint.

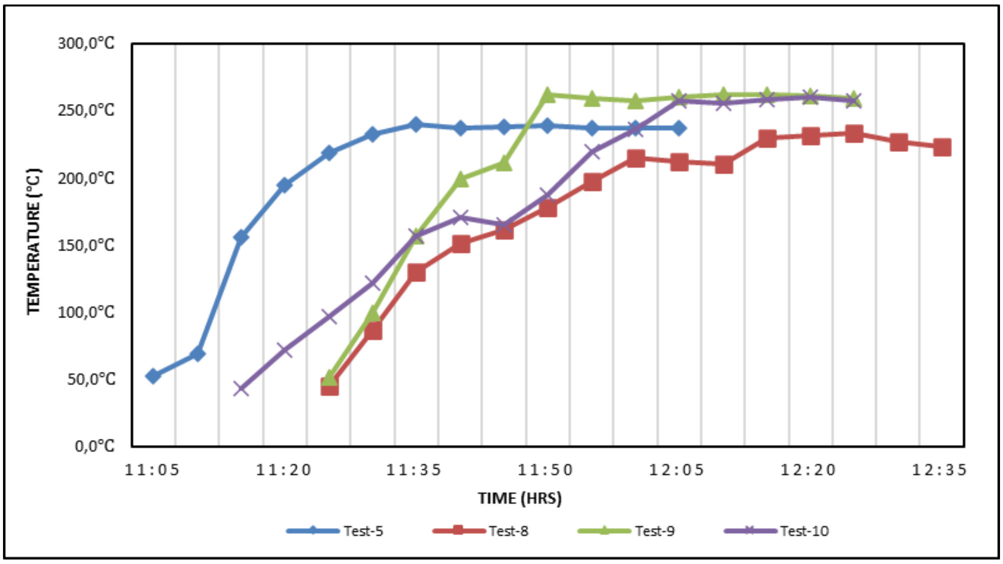

Figure 60:Time vs Temperature graph of achieved torrefaction experiments.

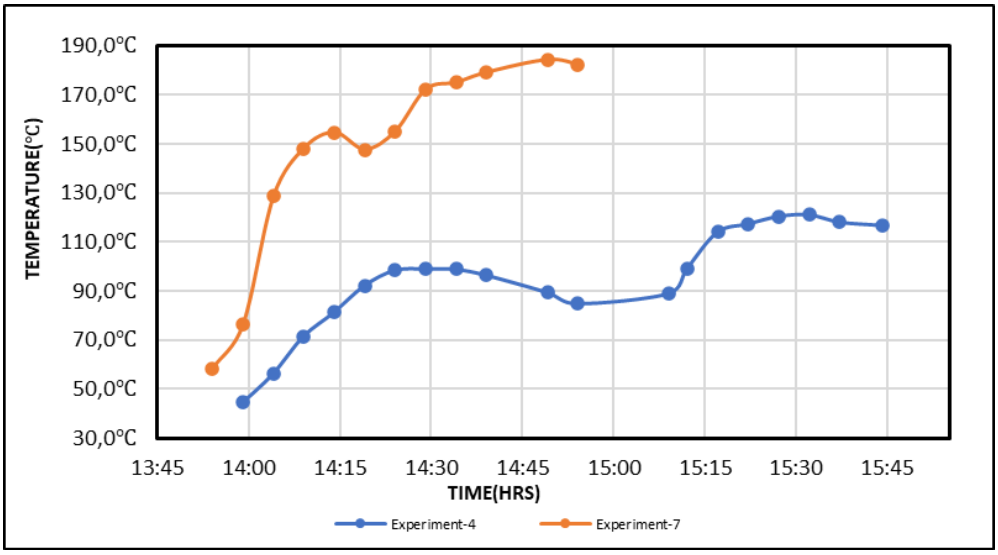

Figure 61:Time vs Temperature graph of experiments conducted beyond 14:00 hrs.

Experiments 4 and 7 continued after 14:00, and a shift in the reactor temperature pattern was noted. The irradiation was comparatively less. Hence, not only was the peak temperature less than expected, but it was also difficult to control the orientation of the reactor with respect to the sun's inclination. As can be seen in Figure 61, at 14:20 hours in Experiment 7 and beyond 15:00 hours in Experiment 4, either the temperature decreased or stayed constant despite re-aligning the cooker with the sun. The SCG charged in the reactor was partially dried, but there was hardly any charring or partial torrefaction occurring during this process. This was implied by the light brown tint of the products, as shown in Figure 63. Therefore, for the uniformity and efficiency of the experiments, the rest of them were conducted between 10:00 and 13:00 hours.


(a) (b)

Figure 62:Reactor readings of experiments conducted in (a)Delft and (b)Hyderabad.

4.3.3 Appearance of Partially charred SCG

Figure 63 shows the products obtained from Experiment 3 to Experiment 10. The SCG was placed inside the aluminium crucible and charged inside the metallic tube at the beginning of the experiment. Evidently, the obtained products as seen were either dried coffee grounds, partially or completely charred.

Experiments 4 and 7 produced comparatively less dark product because of the limited working conditions involving the reactor. However, the product obtained was dry and amorphous, which indicated either partial or complete drying of the feedstock as the temperature in the reactor. Around 190 °C, there was a strong stench of charred coffee through the glass pressure outlet. This outlet worked as a perfect medium for the release of flue gases generated from the reaction as well as the unnecessary additional gases released from design imperfection.

Figure 63:Partially or completely torrefied SCG from the designed solar torrefied.

4.3.4 Heat Distribution along the Reactor

Thermal imaging was used to analyse the outer temperature of the reactor (the borosilicate glass tube). This was done to find out the temperature distribution along the reactor. The centre of the reactor had a higher temperature compared to either side of it. This was because most of the concentrated sunlight was focused on the centre of the reactor. Moreover, the outer glass temperature was much lower compared to the inner aluminium and reactor temperatures as recorded by the thermometer. During experiments when the inner reactor temperaturee displayed 240 °C and 262.3 °C, the camera recorded an outer glass temperature of 113.1 and 114.2 °C respectively, as shown in Figure 64.

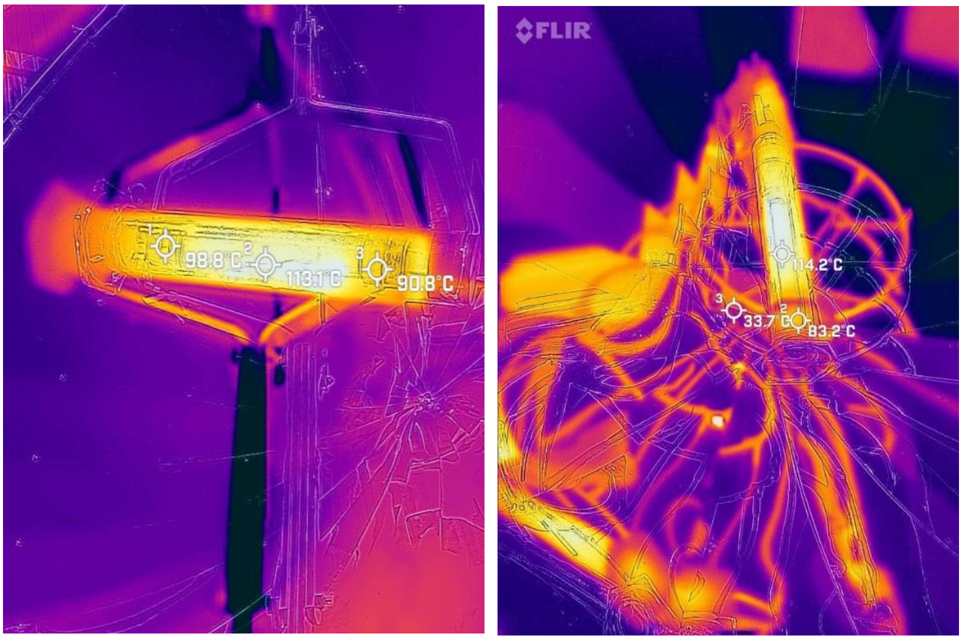

Figure 64:Temperature profile of the outer glass cylinder as captured by the FLIR thermal camera.

4.4 Characterization of raw and torrefied SCG

Table 13:Characteristics of Raw SCG.

Analysis	**Equipment**	**Standard**	**Content (Raw SCG)**
Moisture Content (wt %)	Nabertherm Heating Oven	NREL/TP-510-426221	59 ±7 %
Ash Content (wt%)	Nabertherm Heating Oven	NREL/TP-510-42622	0.37 ± 0.06 %
Ultimate Analysis (Dry Basis)	CHNS Analyzer	Standard from Groningen University	H_2= 6.56 % C = 51.88% S = 0.6 % O_2= 38.3 % N_2= 2.665 %
HHV (MJ/kg)	Parr 6772 Calorimetric Thermometer	UNI EN ISO 16948:2015/ EN 15104:2011	21.5

Table 14:Calorific Values, Mass and Energy yield of biochar obtained at different temperatures.

Experiment No.	Temperature (°C)	Initial Feedstock (g)	Biochar Product (g)	Mass Yield (%)	HHV (MJ/kg)	Energy Yield (%)
3	184	1.6	1.1308	70.67	-	-
4	122	1.6	1.457	91.06	21.3324	-
5	239.9	3	1.2129	40.43	26.0103	49
6	196.2	8.5	3.9342	46.28	25.4038	54
7	184.3	2.2	1.5332	69.69	21.6718	-
8	233.1	2.5	0.99	39.6	-	-
9	262.3	6.5	1.9846	30.53	26.3042	37.39
10	259.8	6.5	2.0769	32	26.2421	39.10

4.4.1 Mass Yield of Torrefied SCG

Figure 65 shows the influence of torrefaction temperature on mass yield on a wet basis. The mass yield decreased with increasing temperatures. Beyond 200 °C, the yield percentage decreased significantly. The mass yield decreased by almost 24 % between experiments 7 (184 °C) and 6 (196 °C) and 6% between experiments 6 (196 °C) and 5 (240 °C) as seen in the graph. There was also a significant deviation of 8 % in biochar yield when the temperature was increased from 240 °C. According to Table 13, the mass yield percentages for torrefaction temperatures of 200, 240, and 260 °C were 46%, 40%, and 32%, respectively.

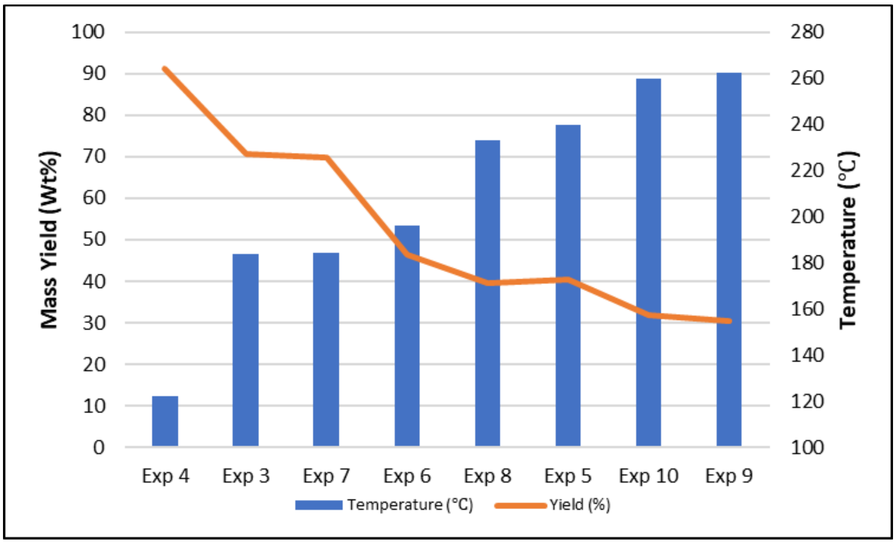

Figure 65: Effect of torrefaction temperature on solid mass yield.

4.4.2 Calorific Value (HHV) and Energy Yield

Initially, the HHV of the raw SCG was calculated to be 21.48 MJ/kg. The HHV for the calculated solid torrefied biochar is given in Table 14. The results revealed that the HHV of the biochar increased with increasing temperature. This can be linked to the reduced number of C-O bonds and increased C-C bonds during the torrefaction process (Cellatoglu & Ilkan, 2016).

The HHV of the torrefied products obtained at 240 °C and 260 °C had a 21% and 22.50% increase in calorific value compared to the HHV of the raw sample. Experiment 6 (18.24% increase) at 196 °C resulted in an unusually high HHV of 25.4 MJ/kg. This could be due to the non-homogeneous heating and chemical composition of SCG, much like some of the work presented by Celatoglu & Ilkan (2016) for the torrefaction of olive mill residue. Only Experiments 5, 6, 9, and 10 were chosen for this analysis to not only show a variation in HHV at 196 °C, 240 °C, and 260 °C, but also to compare with similar results obtained from the literature. The biochar obtained from Experiments 4 and 7 were hardly torrefied, proven by their low HHV values, and hence wasn't taken into consideration. Experiment 8 produced a promising biochar visually but was limited by the availability of the product required to analyze it in the bomb calorimeter.

The energy yield was calculated using Equation (3) on wet weighted percentage. They are calculated for temperature regimes of 196°C, 240°C, 262°C, and 260°C, with residence times of 1 hour, 40 minutes, 55 minutes, and 1.167 hours, respectively. The values are displayed in Table 14 and Figure 66 shows the yield percentage trend with increasing temperature. For the four considered experiments, the energy yield decreased with increasing torrefaction temperature, ranging from 49% to 37.4%.

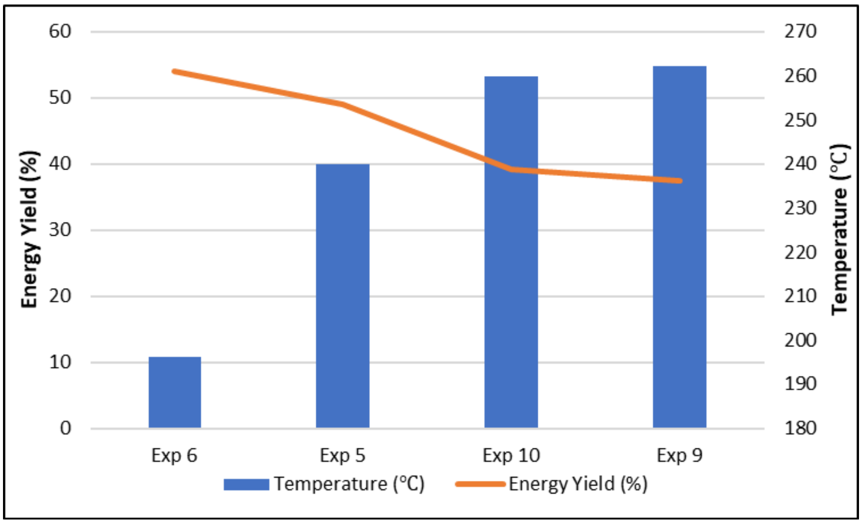

Figure 66: Energy yield % of the torrefied Biochar for Experiments 5,6,9 and 10.

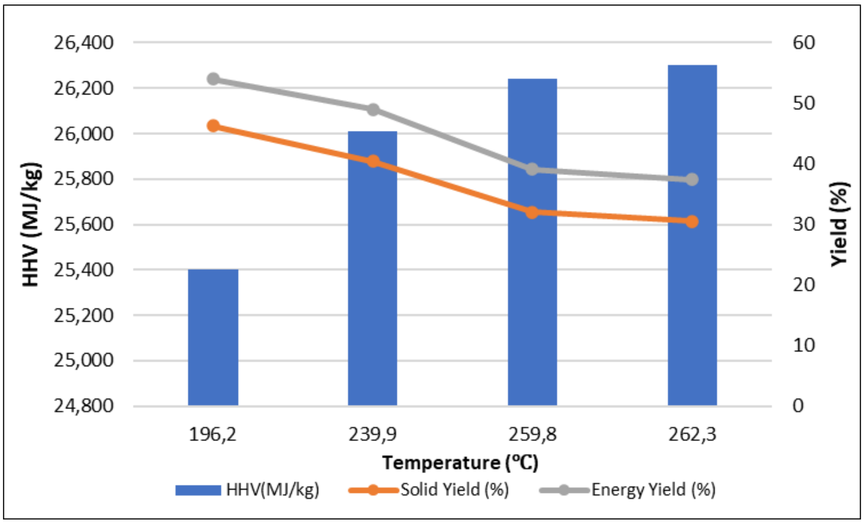

Figure 67: Temperature vs HHV vs Yield % for Experiments 6,5,10 and 9 respectively.

A co-relation between the HHV, mass and solid yield percent is shown in Figure 67. With increasing torrefaction temperature, the HHV of the biochar increase but the solid and energy yield decreased. According to the literature, a trade-off can be made between these properties to make a rough estimate about the optimum torrefaction temperature.

5 Discussion and Conclusion

This chapter discusses the conclusions of the results reported in the previous chapter and reflects on the research approach and on the literature findings. The main objective is to converge the results to try to answer the research questions and come to a conclusion. Finally, the limitations of this research are discussed.

5.1 Tackling research questions

The main research question was to check if it was possible to attain the torrefaction temperature using a SK14 Cooker coupled with a Solar Collector unit? If that was successful, was it possible to torrefy raw SCG to produce biochar? Throughout the research, solutions were tackled frugally. For example, using lasers to get an idea about the SK14's focal point. The results from the research need to be combined to co-relate and answer the sub-research questions.

Sub RQ 1: How is the heat distribution and retention along the simulated Solar Collector?

Sub RQ 2: Is it feasible to convert a SK14 solar cooker into a functioning solar torrefier? What function does the modified collector serve in the design of the torrefier?

Sub RQ 3: What are the test conditions required to effectively characterize the raw SCG and produced biochar? Can the biochar be used as a fuel**?**

- ***Characterization of the SK14 solar cookers***

As deducted from the characterization of the two SK14 cookers in Sections 4.1 and 4.3, it was evident that they had **more than one focal point** and **did not have a point focus** on the pot stand receiver. The observations from the laser experimentation, its derived focal point concentration factor values displayed in Table 10, as well as observing the pattern of the focal point while conducting experiments on the prototype in Hyderabad and Delft, validated this. This also helped in determining the concentration factor of the *EG Solar* and *RUDRA Solar* cookers to be **21.7** and **16** respectively. The difference in effective concentration factor was due to the difference in aperture diameters of the two cookers, which were 1.4 and 1.2 m, respectively. The concentration value for EG Solar was used as an input parameter for the COMSOL simulation and that of the Rudra Solar was used to calculate the efficiency and power of the SK14 cooker. This provided a basis for answering **Sub RQ 2**.

Even though PDCs can reach extremely high temperatures at their focal point, as discussed in Section 2.4.3, it was evident that the **SK14 cooker required an additional solar collecting mechanism to attain the torrefaction temperature**. However, an inference was drawn based on an ideal situation in which the reactor's position in the receiver zone may be determined based on the desired concentration factor. If only the torrefaction temperature (200-300 °C) is required, the reactor must be moved away from the actual focal plane. A modest alteration in the design of the receiver pot would be required to allow for easy adjustment of the reactor location. But it was suggested that changing the cooker's concentration ratio was a little hard to understand and would need more research.

- ***Linking COMSOL simulation findings and validation***

Analysing the literature also helped in eradicating the idea of direct concentration heating of SCG in a single glass, which is why the introduction of an aluminium tube with a black coating was a crucial addition to the prototype. A basic run of the model in COMSOL showed that **while the inner domain of the tube reached 350 °C, the vacuum and outer borosilicate layer maintained very low temperatures around 50 °C** as seen from Figure 48: Volume cross sectional temperature profile of overall domain from Scenario 1.Figure 48 and Figure 49. This was further supported by comparing the contour plots from the scenarios, the distribution along the nitrogen domain, and the temperature profile of the boundary heat flux. The EVC was clearly getting heated as a stand-alone system with DNI supported by the temperature profile in Figure 50 and the temperature contours on the upper surface of the inner domains as illustrated in Figure 51. Moreover, due to the vacuum-borosilicate glass cover domain, Scenario 3 showed better heat retention, as indicated by the scarcity of blue contour lines (lower temperature) and less concentrated arrows on one end of the tube. This was enabled by entrapping long wavelength waves and preventing them from escaping the glass cover.

The comparison between the four scenarios provided a better understanding of the temperature profile along the modelled reactor. The comparison between the scenarios for the nitrogen domain revealed **how the SCG feedstock would be heated inside the reactor**. The contour profiles revealed that the maximum temperature was at the focal point (represented by the boundary heat flux), but the temperature did not vary considerably across the tube. For example, for Scenario 3 in Figure 55, the temperature between the boundary heat flux and the two edges of the tube had a difference of approximately 15 °C, yet the temperature profile between the sliced work planes was nearly uniform for all scenarios. It was concluded that **the SCG feedstock positioned between the work planes would be uniformly heated.** However, if the reactor was charged with feedstock that was distributed over the tube, the torrefied biochar may not be uniform.

Based on the temperature vs time graphs for the scenarios in the nitrogen domain, an inference was made regarding the solar heating of the tube across all domains. Since one or both sides of Scenarios 3 and 4 were covered with a transparent borosilicate-vacuum domain, the heating of the tube through DNI was more homogeneous compared to the other scenarios. This was also due to fewer irregularities as well as non-uniform heat loss through the BCR fibre covers. Given that Scenario 3 is the most geometrically realistic approximation of a real-world EVC, a substantially higher peak is expected if the simulation is conducted for a longer period of time. The 'maximum temperature' peak as shown in Figure 57(b) for Scenario 2 signified the absence of the 1 mm air layer, which caused a considerable increase in temperature, aided by diminished heat loss between the inner borosilicate layer and the aluminium fin. This corresponds to the study described in Section 2.4.2 (Liang et al., 2012). This analysis was further supported by comparing the temperature profile of the boundary heat flux (focal point). **This partially verifies the literature research conducted in Section 2.4.4 on SK14 cookers and successfully simulates the condition of obtaining a focal point temperature of 350-400 °C.** As seen in Figure 58, because the boundary heat flux is flat, the edges extend into adjacent domains along the focal plane. This results in an uneven temperature profile. However, this is not practical and shows a limitation of the geometry of this model, particularly for Scenario 2.

The simulations validated the functionality of a modified EVC adopting the *green house* principle, with nitrogen serving as the heat transfer environment. Furthermore, by providing the possibility of obtaining torrefaction temperatures using this concept to design the prototype reactor, this contributes to answering **Sub RQ2** and **Sub RQ 1**. Based on the temperatures obtained in all scenarios, it was concluded that, provided an inert atmosphere is maintained, **the principle of an EVC can be used to construct a solar biomass torrefier or pyrolyzer.** Scenario 3 was the closest to duplicating the existing EVCs, which also showed better heat retention and uniform heating compared to Scenarios 1 and 2. The trade-off between Scenarios 3 and 4 had to be further studied to draw a conclusion. For simplicity, **Scenario 3 was chosen as the basis to build the prototype reactor for the experiments.**

- ***Prototype Torrefaction Experiment***

Despite having a lower aperture diameter of 1.2 m, **the thermal efficiency of the Rudra SK14 was within the range of the literature** reported in Section 2.4.5. Equations (32) and (33) indicated that there was a difference in cooking power when an instantaneous time range was compared to the actual time required to reach the boiling temperature of water. This can be attributed to the additional power used up between the starting and the stagnation temperature, which can be further explored by finding the standardized cooking power and adjusted cooking power as suggested by Funk & Larson, (1998); Mekonnen et al. (2020) and Purohit, (2010). However, the concentrator's cooking power was comparatively lower than the typical SK14 cooker's power of 700 W and 635 W reported by [13] and Mekonnen et al. (2020) respectively. The difference was caused by the fact that the Rudra SK14 cooker had a smaller aperture diameter, which led to a lower concentration factor.

The experimental observations of the focal point not only verify the laser experiment claims of the SK14 not having a point focus but also the shape of the boundary heat flux in COMSOL as an ellipse with a 4 cm axis. Clearly, the results of experiments 5, 8, 9, and 10 reached torrefaction temperatures rapidly due to higher irradiation and precise redirection of the focal point. The minor kinks in Figure 60 and Figure 61 can be oriented towards clouds and wind, stagnation or temperature slumps, resulting in exponential and non-homogeneous graphs for these tests. The constant temperature retention after reaching the peak in Figure 60, on the other hand, demonstrated the possibility of including residence time as a parameter. **It was proposed that this challenge could be handled by introducing a double-layered vacuum tube reactor with similar properties to those simulated in COMSOL.** Experiments 4 and 7 demonstrated the restriction of the SK14 cooker (Rudra Solar) in operation, as the cooker could not align with the sun beyond 15:00 hours. This did not happen with the EG solar cooker because the angle of tilt was not limited.

Because of the high irradiation, the best time to conduct the experiment was decided to be at noon but torrefying till sunset is possible if the cooker design is compatible and the reactor retains heat better. **Torrefaction experiments revealed that when the torrefaction temperature rises, the torrefied SCG darkens.** Although no investigations into the grindability of torrefied products were undertaken, it was observed that **torrefied SCG became highly brittle and easily ground to a fine powder following torrefaction**. This technology shows that it may be used as a solar dryer to roast or dry coffee beans in low-irradiation conditions, in addition to a torrefier.

After producing torrefied biochar with air as the convective heating medium, the question of "**how did the coffee get charred in a non-inert environment**" arose. One probable reason was that as the temperature inside the reactor increased, so did the pressure, resulting in the expulsion of air and gaseous products from the tube (observed by a thin stream of gas flowing from the pressure pipe). Another possibility was that the oxygen content inside the reactor eventually depleted, preventing SCG combustion. Further studies could prove this notion.

The COMSOL modelling principle and the temperature profile across the reactor's cross-section were supported by thermal imaging data. This demonstrates the use of borosilicate glass as a transparent heat retention medium, as well as the use of a gaseous medium in between to distribute and retain heat. Furthermore, if the simulated reactor was used, the reactor could be handled with bare hands even at high torrefaction temperatures.

- ***Biochar Characterisation***

The moisture content of the raw SCG was calculated to be 59%. In comparison to previous research, the solid yield percent for all torrefied biochar products obtained was relatively low. **This is due to directly torrefying raw SCG on a wet basis with a feedstock containing almost 59 % moisture**. Torrefaction and removal of bound moisture in the SCG therefore began only after the excess moisture in the sample evaporated. However, as indicated in Section 2.3.3, the pattern of solid yield reduction with increasing temperature was comparable to that generated by (Barbanera & Muguerza, 2020; W. H. Chen et al., 2012; Vakalis et al., 2019). It is estimated that if the sample was used dry, the mass yield percentage would have increased significantly.

As reported previously, torrefying raw SCG improved its calorific value and the HHV improved with increasing torrefaction temperature. This was higher than the proposed percentage increase in HHV listed in Table 3 by Barbanera and Muguerza (2020), which was 7.9% and 16.6% at 235 °C and 260 °C, respectively. Although residence time can affect solid yield percent and HHV, which in turn affects energy yield percent, it was not considered due to a non-uniform residence time. The percentage of energy yield is proportional to the mass yield and HHV. However, as evidenced by the literature, the loss in mass yield was more influential than the increase in HHV, resulting in a decrease in energy yield % with increasing temperature, as shown in Figure 66. This yield was also significantly lower due to the feedstock's high moisture content.

Because the operating parameters were difficult to determine, a rough estimate was made to determine the optimum torrefaction temperature. A trade-off between biochar generated at 240 and 260 °C for experiments 5 and 9, respectively, was proposed to maximize biochar production while maintaining a high HHV value. The HHV for the experiments was nearly comparable (i.e., ~26 MJ/kg), but the mass yield at 260 °C was 10% lower than the charcoal yield at 240 °C, resulting in a lower energy yield, as shown in Figure 67. **The optimal temperature for this research was determined to be 240 °C**, which produced not only a high calorific value for biochar but also a relatively high solid mass yield. Furthermore, while making pellets for the bomb calorimeter, it was discovered that all biochar products could be easily ground into a fine powder and pelletised without the need for binders. Thus, with an HHV in the range of **industrial coal** and a very low ash percentage of **0.37,** it was concluded that this **biochar had a high potential for usage as a small-scale alternative fuel**. These findings provide a solution to **Sub RQ-3.**

Having the sub-research questions answered, it is now possible to answer the main research question:

Is it possible to attain the torrefaction temperature using a SK14 Cooker coupled with a Solar Collector unit? If so, can raw SCG be torrefied in the reactor?

The implementation of the proposed framework indicated in Figure 68 used in this investigation, while keeping jugaad innovation in the background, provides an answer to the main research question of this study.

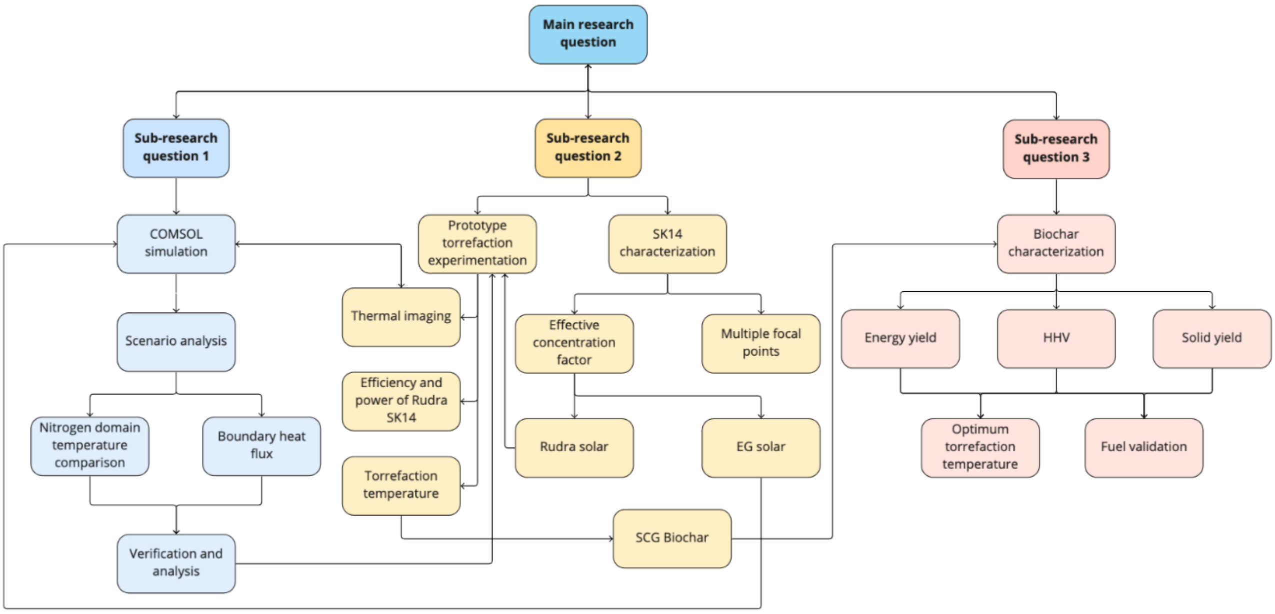

Figure 68: Flowchart connecting results to sub and main research questions.

5.2 Conclusion and Final Remarks

The following final conclusions were able to point out after answering the research questions involved in addressing the main objective of the research:

- Although the SK14 cooker has **multiple focal points** that do not concentrate to a **point**, it can be coupled with the concept of an EVC to develop a low-cost biomass-solar induced torrefaction unit. Their concentration factor was determined using the total pot-holder area as the receiver area, and the results were realistic. The Rudra and EG SK14 cookers' effective concentration factors were calculated to be **16** and **21.7**, respectively. Furthermore, the SK14 arrangement was straightforward to use as a dual cooker-torrefier system.

- The cooking power and efficiency of the 'Rudra Solar' were calculated as **575 W** and **31.4 %** respectively. Even with a smaller aperture area, the values were comparable to the standardized 'EG Solar' cooker.

- It is possible to attain torrefaction temperature even at lower irradiance than that in Hyderabad, as supported by the experiment conducted in Delft.

- The biochar solid and energy yield percent is low due to the high moisture content in the SCG feedstock. On the other hand, the calorific value (HHV) of the torrefied SCGs was significantly high and increased with increasing torrefaction temperature.

- The estimated optimum torrefaction temperature was **240 °C**, resulting in a high calorific value (**26 MJ/kg**) and comparatively greater solid biochar production (**40%**). Without the use of a **binding reagent**, the produced biochar was easy to **grind** and **pelletize**. Furthermore, because of their low ash content (**0.3%**) and similar calorific value to **industrial coal**, these pellets can be used as an alternative to conventional fuel, such as fuel storage for cooking and heating during sun-deprived hours.

- As verified in COMSOL, torrefaction temperatures can be obtained using a functionally modified EVC design. The modelled reactor's heat distribution analysis validates the green house principle of an evacuated vacuum tube collector. It also confirms that a gaseous environment can be used as a heat transfer medium. Even though the concept of duplicating the heat flux from the EG Solar cooker was successfully integrated into the simulation model, the heat transfer phenomenon across the boundary heat flux (focal point) was inaccurate due to geometrical limitations. Scenario 3 was selected as the trademark for the experiments' prototype. The simulation hypothesis was supported by thermal imaging during the experiments in Hyderabad.

5.3 Research limitations

Because the research needed various settings to achieve the main goal, there were constraints that hampered the precision of the results and limited the implementation of the desired methodology, scenarios, and analysis. The following are the research's theoretical and practical limitations:

- Because of time and biochar availability constraints, many characterizations of raw and torrefied SCG could not be performed. Some of the tests suggested to understand various parameters of the biochar and raw sample, such as: crystalline structure, carbon content increase, O/C and H/C atomic ratio, etc., would not only provide a better understanding of the type of coffee used, but would also provide more clarity on the torrefaction parameters and fuel characteristics of the produced biochar. For example, linking the proximate and ultimate analysis values to temperature increase could provide a better estimate for the optimum torrefaction temperature; making a Van-Krevelen diagram to compare the biochar with conventional fuel.

- Although the arrangements to replicate solar irradiation on the cooker were jugaad creative and efficient, there was no stable support, causing heavy deviation while moving the graph sheet along the focal plane during the laser experiments for the focal point analysis. As a result, there were irregularities and minor inaccuracies in obtaining the exact diameter of the point focus on the graph sheet.

- Due to the intermittency of solar energy in the Netherlands, the prototype experiments were relocated to Hyderabad (India). Despite the more realistic ambient conditions, the results (such as concentration factor) for the two types of the SK14 solar cooker were not uniform and so could not be co-associated. Furthermore, the Rudra Solar SK14 cooker could not be tilted beyond a certain angle, limiting the time available for the experiment.

- To model physics-related problems, COMSOL Multiphysics® 5.6 employs complex PDEs and operating parameters. As a result, the mathematical calculations required to combine heat transport phenomena with the current design were difficult to understand. Furthermore, running simulations on the practical EVC model and the prototype replica, as illustrated in Figure 72 and Figure 92, was time-consuming. Another challenge was simulating the boundary heat flux on a curved surface since the flat boundary exceeded its domain area, leading in an irregular and unclear temperature distribution along the simulated focus point.

- Despite the plan to incorporate the simulated working principles of a double borosilicate layer vacuum collector into the prototype reactor, only a single-layered glass tube reactor could be constructed. As a result, the reactor's heat retention properties could not be practically studied. This resulted in non-homogeneous reactor heating, unexpected temperature drops during cloudy weather, and irregular biochar production.

- Because raw biomass could not be torrefied on a dry basis, solid and energy yields were significantly reduced. Furthermore, during torrefaction, gaseous products and water vapor condensed on the edges of the glass tube, lowering reactor efficiency.

- Although transparent and having a good heat retention capacity, borosilicate glass is extremely fragile, raising concerns about the reactor's handling and durability.

- The inability to provide an inert environment to realistically carry out the torrefaction experiments was the most significant limitation for the investigation. This would require a continuous supply of nitrogen, which appears to be extremely challenging for a small-scale operation.

6 Recommendations

Despite the research's limitations, the results demonstrated a high potential for use as a small-scale solar- assisted biomass torrefier. However, there are numerous techniques and thought trains to improve the compound system's utility, efficiency, and viability. Furthermore, the feasibility, potential, and challenges of implementing such a system in small communities, such as for a single coffee farmer in Kerala, must be discussed. This section examines the probable next steps to not only improve the technological components of the idea but also to implement it in the real world.

6.1 Socio Economic Implementations

According to research, the Coffee Board of India has played an important role in supporting coffee cultivation among farmers through subsidizing and financing for coffee plantations throughout the country (Karunakaran, 2017). This research has already demonstrated that the torrefier can easily achieve temperatures of above 200 °C. As a result, not only can local farmers manufacture torrefied fuel from waste SCG, silver skins, and pulp, but they also have their own in-situ solar drying system for coffee beans. This can reduce time, human work, and contamination by, for example, eliminating the need for tarpaulin coverings on concrete floors, as seen in Figure 69.

Figure 69: Usage of tarpaulin covers to dry coffee beans (Bunn et al., 2015).

As demonstrated in Figure 70, small-scale biochar production has already been adopted among farmers to promote circular economic growth by managing and reusing waste to generate clean, decentralized energy. Farmers in Kerala can thus produce biochar from local biomass waste produced by local industries, small shops, agricultural sites, and their own abundant produce. This biochar can thus be utilized as a local compost and soil quality enrichment product, for disease management in crops by regulating pH, and, most importantly, as a fuel for cooking and heating. This would not only promote local circular economic growth, but it would also reduce pollution by transforming the coffee and waste management systems into a more sustainable industry. Furthermore, solar cookers are simple to install and significantly less expensive in India. With the central government and non-governmental organizations subsidizing installation and training on how to use solar cookers, the proposed addition of a solar-biomass torrefier to make in-situ biochar can be a success if supported. Furthermore, this allows small-scale coffee production units to be self-sufficient without the involvement of third parties, providing new jobs and revenue. Most crucially, any source of extra cash can be appealing to a low-wage farmer, making implementation of the system in rural communities quite simple.

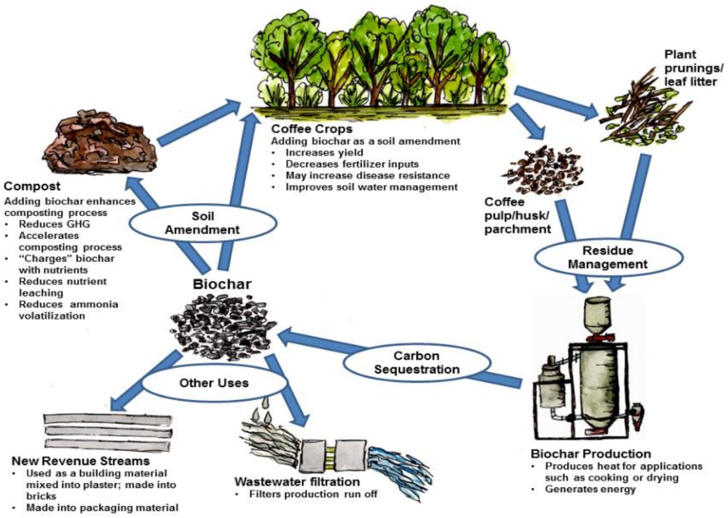

Figure 70:Biochar integration into a circular coffee production system (Draper, 2018).

Figure 71 shows a large-scale reactor proposal for producing large quantities of biochar in a relatively shorter time and with greater efficiency. In this study, the construction adheres to the simulated principle of an EVC and the created prototype. The charging trollery with a rail, spring, and accessible hindge door, the nitrogen inflow and outflow pipe, and the ceramic door lining for efficient insulation are a few important design changes. According to the findings of this study, the proposed large-scale model could easily achieve torrefaction as well as high pyrolysis temperatures, indicating the potential for producing bio-oil and bio-gas. The product output rate is the most essential factor for larger scale production, which is determined by the charging trolley, which can hold a comparably much larger volume of biomass feedstock.

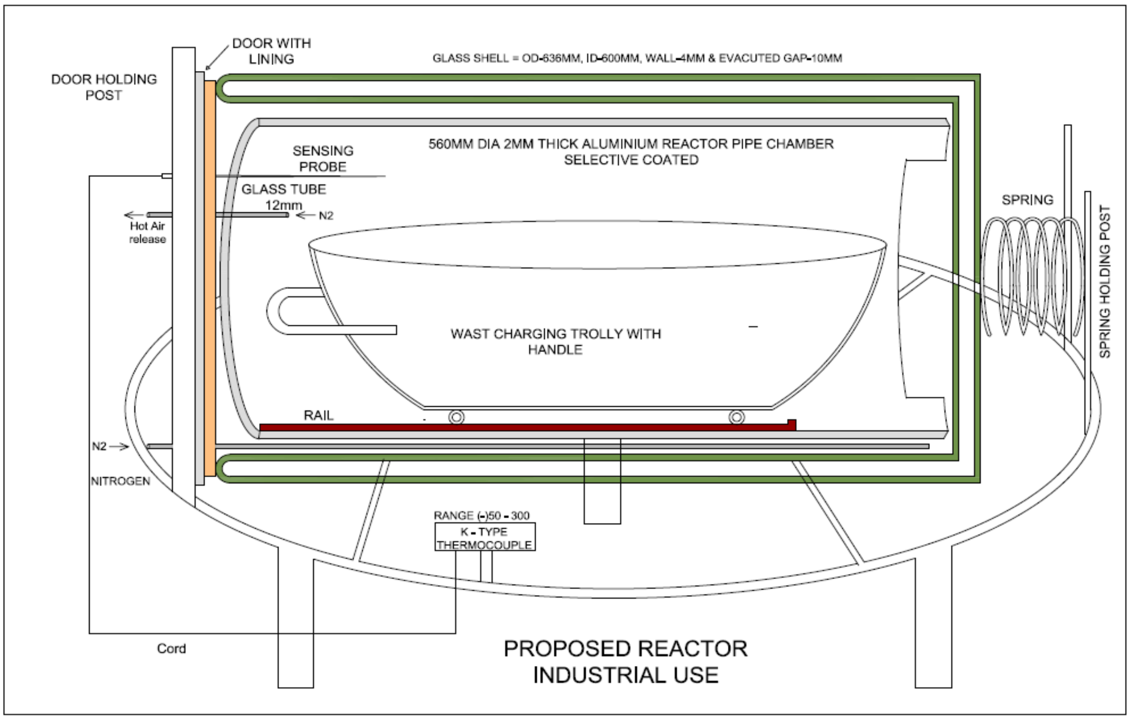

Figure 71: Large scale proposed solar assisted biomass torrefaction and pyrolyzing unit.

A vision of combining large and small-scale production between coffee farmers and local coffee production enterprises is suggested in order to develop a circular integrated coffee production, biochar, and waste management system.

6.2 Methodical and Practical future work

Figure 72 shows the COMSOL model for a practical EVC model-based reactor. This research showed the importance of modelling the reactor and simulating with realistic parameters, which facilitated building a similar prototype design while validating one of the torrefaction parameters (temperature). It is recommended to improve the simulation parameters and complexity for future work. One of the suggestions is to use the "Ray Optics" physics in COMSOL to duplicate and run the scenario of concentrated light from the cooker. This will provide a better understanding of the heat transfer and radiation phenomena, leading to better simulation results. Another suggestion to improve the efficiency of the reactor is to introduce a filled-type evacuated tube with a heat transmission component instead of air gaps inside the inner tube, as suggested by Liang et al. (2012) in Section 2.4.2. This could eradicate the additional heat losses as observed from the simulations conducted in this research.

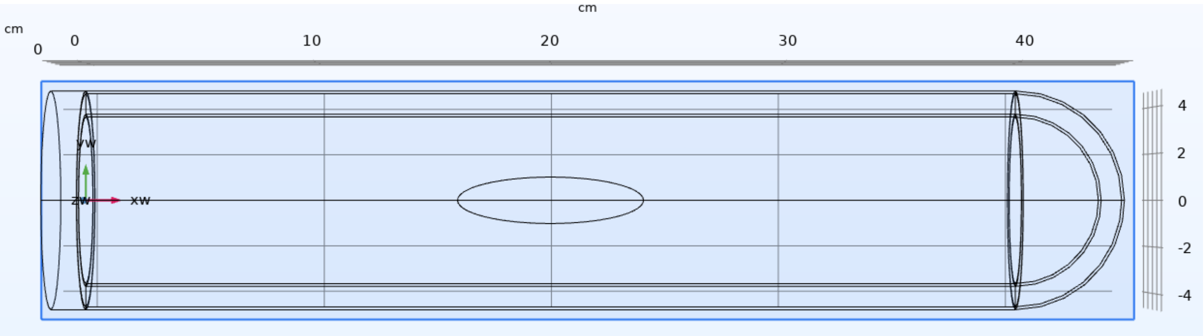

Figure 72: Practical EVC model.

The simulation of heat transfer in the biomass particle could be the next stage in this research. [19] conducted research on fast pyrolysis on woody biomass by modelling the heat transfer process in COMSOL, as shown in Figure 73. A similar method is proposed for future research to determine how long it would take for pelletized SCG of a specific size, shape, and structure to reach ideal decomposition temperatures. This, in association with a reactor design structure in COMSOL, will provide an accurate torrefier design structure, as well as comprehend the effect of torrefaction temperature on feedstock.

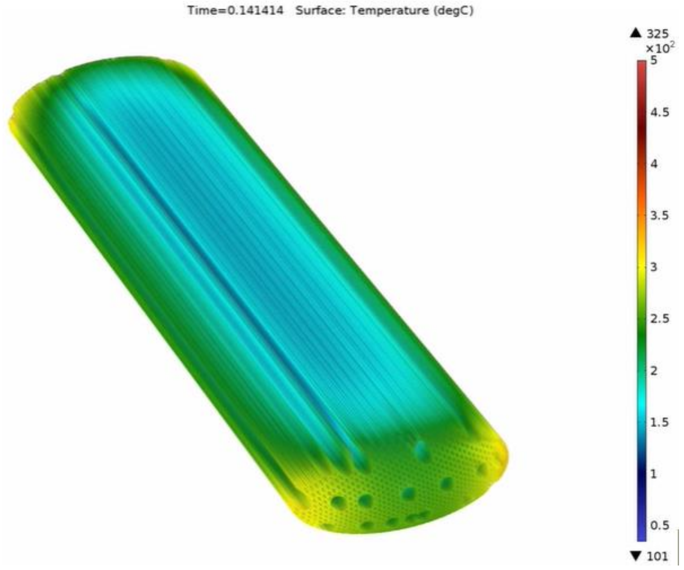

Figure 73: Simulating heat transfer in a biomass particle [19].

Although the prototype reactor could achieve torrefaction temperature, the process had many limitations. The following are some suggestions for improving the research functionality and design:

- Tempered glass, which is four times stronger than borosilicate glass, can be utilized to improve durability. This also eliminates the risk concern of installing the system in small-scale rural areas. However, the transmissivity and optical characteristics of tempered glass must be investigated further.

- Developing a double-layered glass vacuum reactor, for better heat retention and even heat distribution. This can enable conducting experiments at homogeneous and pre-determined operating parameters. An inert environment can be created by a constant flow of nitrogen gas. However, as demonstrated by this study, the coffee was torrefied even in the absence of a nitrogen source. Because the solution is ambiguous, it requires further investigation.

- As demonstrated in the experiment, condensation causes the bio-oil and condensed gases to stick to the reactor walls. This can be avoided by tilting the reactor while positioning it on the pot receiver surface. Gas Chromatography can be used to collect and analyze flue gases (GC).

- According to the research literature review, residence time can increase the calorific value of the feedstock (SCG). To further investigate the effect of solar torrefaction on coffee wastes or SCGs, residence time must be introduced as a parameter. This is highly dependent on the reactor's heat retention and temperature stability.

- Biochar characterization techniques such as CHNS analysis, volatile content, FC, TGA, ash content, SEM analysis (pore size distribution), and BET analysis (specific surface area) are proposed for future research to assess the potential of biochar not only as a fuel, but also as a soil enhancer. This would make the production of such biochar an even more appealing option for Kerala's coffee farmers. Since coffee wastes are already contaminating the environment, introducing biochar as a fuel and soil enrichment product is a particularly problematic scenario; thus, studies such as FTIR are suggested to determine whether this is a clean product.

- The water heating test performed by Mekonnen et al. (2020) is recommended to appropriately calculate the heating and cooking characteristics of the SK14 cooker by finding the standard cooking power and error estimation.

7 Bibliography

A. Ayala-Cortés, Camilo A Arancibia-Bulnes, H.I Villafán-Vidales, & Diego Ramón Lobato-Peralta. (2019). Solar Pyrolysis Of Agave And Tomato Pruning Wastes : Insights Of The effect Of Pyrolysis Operation Parameters On The Physicochemical Properties Of Biochar. *AIP Conference Proceedings 2126, 180001 (2019)*, 5–8. https://doi.org/https://doi.org/10.1063/1.5117681

Aggarwal RK. (2020). Institution Based Solar Steam Cooking Systems in India. *Current World Environment*, *15*, 204–210. https://doi.org/10.12944/cwe.15.2.07

Ahmed, S. M. M., Al-Amin, M. R., Ahammed, S., Ahmed, F., Saleque, A. M., & Abdur Rahman, M. (2020). Design, construction and testing of parabolic solar cooker for rural households and refugee camp. *Solar Energy*, *205*, 230–240. https://doi.org/10.1016/j.solener.2020.05.007

Aljabair, S., Habeeb, L. J., & Ali, A. mohammed. (2019). Study the Effect of Diameter and Depth of Parabolic Dish Collector on the Concentration Ratio and Temperature Amount of Solar Tower Receiver. *Journal of University of Babylon for Engineering Sciences*, *27*(1), 142–156. https://doi.org/10.29196/jubes.v27i1.1977

ALKE Heating Technology. (2005). *Heating technology*. 2005. https://www.alke.nl/download/1329756518_solar-collector-systems.pdf

Allegrini, Micangeli.A, & Michelangeli.E. (2016). Heat transfer simulation of evacuated tube collectors (ETC): An application to a prototype. *Contemporary Engineering Sciences*, *9*(23), 1125–1136. https://doi.org/10.12988/ces.2016.6429

Anil Kumar, N. P., Saleem Khan, A. I. K., & Balakrishnan, V. (2019). Coffee, Climate and Biodiversity: Understanding the Carbon Stocks of the Shade Coffee Production System of India. In *Climate Change Management* (pp. 113–134). Springer. https://doi.org/10.1007/978-3-319-98681-4_7

Arora, S., Chitkara, S., Udayakumar, R., & Ali, M. (2011). Thermal analysis of evacuated solar tube collectors. *Journal of Petroleum and Gas Engineering*, *2*(4), 74–82. http://www.academicjournals.org/JPGE

Badar, A. W., Buchholz, R., & Ziegler, F. (2011). Experimental and theoretical evaluation of the overall heat loss coefficient of vacuum tubes of a solar collector. *Solar Energy*, *85*(7), 1447–1456. https://doi.org/10.1016/j.solener.2011.04.001

Ballesteros, L. F., Teixeira, J. A., & Mussatto, S. I. (2014). Chemical, Functional, and Structural Properties of Spent Coffee Grounds and Coffee Silverskin. *Food and Bioprocess Technology*, *7*(12), 3493–3503. https://doi.org/10.1007/s11947-014-1349-z

Bangkha, N., Saechua, W., Nuamyakul, T., & Jongyingcharoen, J. S. (2020). Effect of torrefaction temperature on energy properties of spent coffee ground. *E3S Web of Conferences*, *187*, 3–10. https://doi.org/10.1051/e3sconf/202018703009

Barbanera, M., & Muguerza, I. F. (2020). Effect of the temperature on the spent coffee grounds torrefaction process in a continuous pilot-scale reactor. *Fuel*, *262*(June 2019), 116493. https://doi.org/10.1016/j.fuel.2019.116493

Barlev, D., Vidu, R., & Stroeve, P. (2011). Solar Energy Materials & Solar Cells Innovation in concentrated solar power. *Solar Energy Materials and Solar Cells*, *95*(10), 2703–2725. https://doi.org/10.1016/j.solmat.2011.05.020

Bedi, H. P. (2021). *Solar power for some ? Energy transition injustices in Kerala , India*. https://doi.org/10.1177/25148486211046963

Bhaskar, T., & Pandey, A. (2015). Advances in Thermochemical Conversion of Biomass-Introduction. In *Recent Advances in Thermochemical Conversion of Biomass* (pp. 3–30). Elsevier Inc. https://doi.org/10.1016/B978-0-444-63289-0.00001-6

Caputo, C., & Mašek, O. (2021). Spear (Solar pyrolysis energy access reactor): Theoretical design and evaluation of a small-scale low-cost pyrolysis unit for implementation in rural communities. *Energies*, *14*(8). https://doi.org/10.3390/en14082189

Cassidy, V. M. (1981). Solar Collectors. In *Specifying engineer* (Vol. 46, Issue 6). https://doi.org/10.1016/b978-0-12-811662-3.00003-7

Cellatoglu, N., & Ilkan, M. (2016). Effects of torrefaction on carbonization characteristics of solid olive mill residue. *BioResources*, *11*(3), 6286–6298. https://doi.org/10.15376/biores.11.3.6286-6298

Chandak, A., Somani, S. K., & Suryaji, P. M. (2011). Comparative analysis of SK-14 and PRINCE-15 solar concentrators. *Proceedings of the World Congress on Engineering 2011, WCE 2011*, *3*(July), 1949–1951.

Chen, D., Cen, K., Cao, X., Zhang, J., Chen, F., & Zhou, J. (2020). Upgrading of bio-oil via solar pyrolysis of the biomass pretreated with aqueous phase bio-oil washing, solar drying, and solar torrefaction. *Bioresource Technology*, *305*(January), 123130. https://doi.org/10.1016/j.biortech.2020.123130

Chen, W. H., & Kuo, P. C. (2011a). Isothermal torrefaction kinetics of hemicellulose, cellulose, lignin and xylan using thermogravimetric analysis. *Energy*, *36*(11), 6451–6460. https://doi.org/10.1016/j.energy.2011.09.022

Chen, W. H., & Kuo, P. C. (2011b). Torrefaction and co-torrefaction characterization of hemicellulose, cellulose and lignin as well as torrefaction of some basic constituents in biomass. *Energy*, *36*(2), 803–811. https://doi.org/10.1016/j.energy.2010.12.036

Chen, W. H., Lu, K. M., & Tsai, C. M. (2012). An experimental analysis on property and structure variations of agricultural wastes undergoing torrefaction. *Applied Energy*, *100*, 318–325. https://doi.org/10.1016/j.apenergy.2012.05.056

Chen, X., & Yang, X. (2022). Heat transfer enhancement for U-pipe evacuated tube solar absorber by high-emissivity coating on metal fin. *Journal of Building Engineering*, *50*. https://doi.org/10.1016/j.jobe.2022.104213

Chen, Y. C., & Jhou, S. Y. (2020). Integrating spent coffee grounds and silver skin as biofuels using torrefaction. *Renewable Energy*, *148*, 275–283. https://doi.org/10.1016/j.renene.2019.12.005

Chiari, L., & Zecca, A. (2011). Constraints of fossil fuels depletion on global warming projections. *Energy Policy*, *39*(9), 5026–5034. https://doi.org/10.1016/j.enpol.2011.06.011

Chintala, V., Kumar, S., Pandey, J. K., Sharma, A. K., & Kumar, S. (2017). Solar thermal pyrolysis of non-edible seeds to biofuels and their feasibility assessment. *Energy Conversion and Management*, *153*(August), 482–492. https://doi.org/10.1016/j.enconman.2017.10.029

Coccia, G., di Nicola, G., Pierantozzi, M., Tomassetti, S., & Aquilanti, A. (2017). Design, manufacturing, and test of a high concentration ratio solar box cooker with multiple reflectors. *Solar Energy*, *155*, 781–792. https://doi.org/10.1016/j.solener.2017.07.020

Colantoni, A., Paris, E., Bianchini, L., Ferri, S., Marcantonio, V., Carnevale, M., Palma, A., Civitarese, V., & Gallucci, F. (2021). Spent coffee ground characterization, pelletization test and emissions assessment in the combustion process. *Scientific Reports*, *11*(1), 1–14. https://doi.org/10.1038/s41598-021-84772-y

COMSOL Multiphysics. (2015). The COMSOL Multiphysics Reference Manual. *Manual*, 1–1336. www.comsol.com/blogs

Comsol Multiphysics Manual. (2012). *Comsol Multiphysics*.

Cuce, E., & Cuce, P. M. (2013). A comprehensive review on solar cookers. *Applied Energy*, *102*, 1399–1421. https://doi.org/10.1016/j.apenergy.2012.09.002

Dhungana, A., Dutta, A., & Basu, P. (2012). Torrefaction of non-lignocellulose biomass waste. *Canadian Journal of Chemical Engineering*, *90*(1), 186–195. https://doi.org/10.1002/cjce.20527

Diwan, K., & S. Soni, M. (2015). Heat Transfer Enhancement in Absorber Tube of Parabolic Trough Concentrators Using Wire-Coils Inserts. *Universal Journal of Mechanical Engineering*, *3*(3), 107–112. https://doi.org/10.13189/ujme.2015.030305

Dr. Ambedkar Veedhi. (2021). *Market Research & Intelligence Unit Coffee Board; Database on Coffee*. https://www.indiacoffee.org/Database/DATABASE3_July2021.pdf

Draper, K. (2018). *The Potential for Biochar to Improve Sustainability in Coffee Cultivation and Processing: A White Paper*.

Du, M., Hao, L., Mi, J., Lv, F., Liu, X., Jiang, L., & Wang, S. (2011). Optimization design of Ti0.5Al0.5N/Ti 0.25Al0.75N/AlN coating used for solar selective applications. *Solar Energy Materials and Solar Cells*, *95*(4), 1193–1196. https://doi.org/10.1016/j.solmat.2011.01.006

Gao, Y., Fan, R., Zhang, X. Y., AN, Y. J., Wang, M. X., Gao, Y. K., & Yu, Y. (2014). Thermal performance and parameter analysis of a U-pipe evacuated solar tube collector. *Solar Energy*, *107*, 714–727. https://doi.org/10.1016/j.solener.2014.05.023

Giwa, A., Yusuf, A., Ajumobi, O., & Dzidzienyo, P. (2019). Pyrolysis of date palm waste to biochar using concentrated solar thermal energy: Economic and sustainability implications. *Waste Management*, *93*, 14–22. https://doi.org/10.1016/j.wasman.2019.05.022

Heat Transfer Module User's Guide. (1998). www.comsol.com/blogs

Hegde, G., & Ramachandra, T. V. (2012). Scope for Solar Energy in Kerala and Karnataka. *National Conference on Conservation and Management of Wetland Ecosystems*, *November*, 1–7. http://wgbis.ces.iisc.ernet.in/energy/paper/lake2012_solar_energy/solar_energy.pdf

Hlaing, S., & Soe, M. M. (2014). Design Calculation and Heat Transfer Analysis of Heat Pipe Evacuated Tube Solar Collector for Water Heating. *International Journal of Science, Engineering Research (IJSETR)*, *03*(12), 2606–2611.

Joardder, M. U. H., Halder, P. K., Rahim, A., & Paul, N. (2014). Solar Assisted Fast Pyrolysis: A Novel Approach of Renewable Energy Production. *Journal of Engineering (United Kingdom)*, *2014*. https://doi.org/10.1155/2014/252848

Joshi, Y. V. (2015). *Torrefaction of herbaceous Biomass - A study of Product, Process and Technology*.

Karunakaran, N. (2017). Coffee Cultivation in Kerala: Some Economic Aspects. *Artha - Journal of Social Sciences*, *16*(4), 97–108. https://doi.org/10.12724/ajss.43.6

Kataki, R., Chutia, R. S., Mishra, M., Bordoloi, N., Saikia, R., & Bhaskar, T. (2015). Feedstock Suitability for Thermochemical Processes. In *Recent Advances in Thermochemical Conversion of Biomass* (pp. 31–74). Elsevier Inc. https://doi.org/10.1016/B978-0-444-63289-0.00002-8

Kosov, V. F., Kuzmina, J. S., Sytchev, G. A., & Zaichenko, V. M. (2016). Challenges and opportunities of torrefaction technology. *Journal of Physics: Conference Series*, *774*(1). https://doi.org/10.1088/1742-6596/774/1/012139

Kumar, A., Said, Z., & Bellos, E. (2021). An up-to-date review on evacuated tube solar collectors. *Journal of Thermal Analysis and Calorimetry*, *145*(6), 2873–2889. https://doi.org/10.1007/s10973-020-09953-9

Kumar, D. (2020). Satellite-based solar energy potential analysis for southern states of. *Energy Reports*, *6*, 1487–1500. https://doi.org/10.1016/j.egyr.2020.05.028

Kuthanazhi, V., Kottantharayil, A., & Narayanan, N. C. (2014). *Planning for Integration of Solar Photovoltaics into the Energy Needs of Villages through Local Self Governments : An experience in the state of*. 1452–1457.

Lee, K.-T., Cheng, C.-L., Lee, D.-S., Chen, W.-H., Vo, D.-V. N., Ding, L., & Lam, S. S. (2021). Spent coffee grounds biochar from torrefaction as a potential adsorbent for spilled diesel oil recovery and as an alternative fuel. *Energy*, *xxxx*, 122467. https://doi.org/10.1016/j.energy.2021.122467

Liang, R., Ma, L., Zhang, J., & Zhao, D. (2012). Experimental study on thermal performance of filled-type evacuated tube with U-tube. *Heat and Mass Transfer/Waerme- Und Stoffuebertragung*, *48*(6), 989–997. https://doi.org/10.1007/s00231-011-0912-7

Mcdonald, G. (1980). A PRELIMINARY STUDY OF A SOLAR SELECTIVE COATING SYSTEM USING A BLACK COBALT OXIDE FOR HIGH TEMPERATURE SOLAR COLLECTORS *. In *Thin.Solid Films* (Vol. 72).

Mekonnen, B. A., Liyew, K. W., & Tigabu, M. T. (2020). Solar cooking in Ethiopia: Experimental testing and performance evaluation of SK14 solar cooker. *Case Studies in Thermal Engineering*, *22*(August), 100766. https://doi.org/10.1016/j.csite.2020.100766

Mon, M. M., Soe, M. M., & Htay, M. M. (2015). 3D Modeling of Temperature Distribution for Absorber Tube of Parabolic Trough Collector. *International Journal of Engineering and Applied Sciences*, *2*(6), 99–103.

Morales, S., Miranda, R., Bustos, D., Cazares, T., & Tran, H. (2014). Solar biomass pyrolysis for the production of bio-fuels and chemical commodities. *Journal of Analytical and Applied Pyrolysis*, *109*, 65–78. https://doi.org/10.1016/j.jaap.2014.07.012

Mukherjee, A., Okolie, J. A., Niu, C., & Dalai, A. K. (2022). Experimental and Modeling Studies of Torrefaction of Spent Coffee Grounds and Coffee Husk: Effects on Surface Chemistry and Carbon Dioxide Capture Performance. *ACS Omega*, *7*(1), 638–653. https://doi.org/10.1021/acsomega.1c05270

Mussard, M., Gueno, A., & Nydal, O. J. (2013). Experimental study of solar cooking using heat storage in comparison with direct heating. *Solar Energy*, *98*(PC), 375–383. https://doi.org/10.1016/j.solener.2013.09.015

Ndukwu, M. C., Horsfall, I. T., Ubouh, E. A., Orji, F. N., Ekop, I. E., & Ezejiofor, N. R. (2020). Journal of King Saud University – Engineering Sciences Review of solar-biomass pyrolysis systems : Focus on the configuration of thermal-solar systems and reactor orientation. *Journal of King Saud University - Engineering Sciences*, *xxxx*. https://doi.org/10.1016/j.jksues.2020.05.004

Nkwetta, D. N., Smyth, M., Zacharopoulos, A., & Hyde, T. (2012). Optical evaluation and analysis of an internal low-concentrated evacuated tube heat pipe solar collector for powering solar air-conditioning systems. *Renewable Energy*, *39*(1), 65–70. https://doi.org/10.1016/j.renene.2011.06.043

Nosek, R., & Tun, M. M. (2020). *Energy Utilization of Spent Co ff ee Grounds in the*. 1–8.

Padmapriya, R., Tharian, J. A., & Thirunalasundari, T. (2019). *Coffee waste management-An overview Coffee waste management-An overview*. *February*.

Paradis, P. L., Rousse, D. R., Hallé, S., Lamarche, L., & Quesada, G. (2015). Thermal modeling of evacuated tube solar air collectors. *Solar Energy*, *115*, 708–721. https://doi.org/10.1016/j.solener.2015.03.040

Parameshwaran, M. P., Anantha, L., G Menon, R. v, Damodaran, V. K., Rao, J., Issac, T., Thomas, K. v, Kharul, R., Kumar, S., Pimperkhedkar, S., Chakraborty, S., Dhakate, N., Gupta, D., John, R., Bhide, R., Joglekar, S., Worah, S., Panwar, T. S., Mathew Varghese, R., & Joy Disclaimer, J. (2013). *THE ENERGY REPORT– KERALA The Energy Report – Kerala: 100% Renewable Energy by 2050*.

Purohit, I. (2010). Testing of solar cookers and evaluation of instrumentation error. *Renewable Energy, 35*(9), 2053–2064. https://doi.org/10.1016/j.renene.2010.02.006

Rafiq, M. K., Bachmann, R. T., Rafiq, M. T., Shang, Z., Joseph, S., & Long, R. L. (2016). Influence of pyrolysis temperature on physico-chemical properties of corn stover (zea mays l.) biochar and feasibility for carbon capture and energy balance. *PLoS ONE, 11*(6), 1–17. https://doi.org/10.1371/journal.pone.0156894

Ronsse, F., Nachenius, R. W., & Prins, W. (2015). Carbonization of Biomass. In *Recent Advances in Thermochemical Conversion of Biomass* (pp. 293–324). Elsevier Inc. https://doi.org/10.1016/B978-0-444-63289-0.00011-9

Sermyagina, E., Mendoza Martinez, C. L., Nikku, M., & Vakkilainen, E. (2021). Spent coffee grounds and tea leaf residues: Characterization, evaluation of thermal reactivity and recovery of high-value compounds. *Biomass and Bioenergy*, *150*(May), 106141. https://doi.org/10.1016/j.biombioe.2021.106141

Sharma, A., Gakare, A., & Saxena, G. (2018). Performance Investigation of Evacuated Tube Solar Heating System : A Review. *Journal of Alternate Energy Sources and Technologies*, *9*(3), 15–26.

Siva Kumar, S., Kumar, K. M., & Kumar, S. R. S. (2017). Design of Evacuated Tube Solar Collector with Heat Pipe. *Materials Today: Proceedings*, *4*(14), 12641–12646. https://doi.org/10.1016/j.matpr.2017.10.075

Sluiter, A., Hames, B., Hyman, D., Payne, C., Ruiz, R., Scarlata, C., Sluiter, J., Templeton, D., & Nrel, J. W. (2008). Determination of total solids in biomass and total dissolved solids in liquid process samples. *National Renewable Energy Laboratory (NREL), March*, 3–5.

Sluiter, A., Hames, B., Ruiz, R., Scarlata, C., Sluiter, J., & Templeton, D. (2008). *Determination of Ash in Biomass: Laboratory Analytical Procedure (LAP); Issue Date: 7/17/2005*. www.nrel.gov

Suman, S. K., & Ahamad, J. (2019). *Solar Energy Potential and Future Energy of India : An Overview Solar Energy Potential and Future Energy of India : An Overview*. *November*, 6–11.

Swaminathan, R., & Nandjembo, F. N. P. (2016). Design and Testing of a Solar Torrefaction Unit to Produce Charcoal. *Journal of Sustainable Bioenergy Systems*, *06*(03), 66–71. https://doi.org/10.4236/jsbs.2016.63007

Tong, Y., & Cho, H. (2015). Comparative study on the thermal performance of evacuated solar collectors with U-Tubes and heat pipes. *International Journal of Air-Conditioning and Refrigeration*, *23*(3). https://doi.org/10.1142/S2010132515500194

Tsai, W. (2017). Chapter 10 - The potential of pyrolysing exhausted coffee residue for the production of biochar. In *Handbook of Coffee Processing By-Products*. Elsevier Inc. https://doi.org/10.1016/B978-0-12-811290-8/00010-4

Tsai, W. T., & Liu, S. C. (2013). Effect of temperature on thermochemical property and true density of torrefied coffee residue. *Journal of Analytical and Applied Pyrolysis, 102*, 47–52. https://doi.org/10.1016/j.jaap.2013.04.003

Tumuluru, J. S., Sokhansanj, S., Hess, J. R., Wright, C. T., & Boardman, R. D. (2011). A review on biomass torrefaction process and product properties for energy applications. In *Industrial Biotechnology* (Vol. 7, Issue 5, pp. 384–401). https://doi.org/10.1089/ind.2011.7.384

Vakalis, S., Moustakas, K., Benedetti, V., Cordioli, E., Patuzzi, F., Loizidou, M., & Baratieri, M. (2019). The “COFFEE BIN” concept: centralized collection and torrefaction of spent coffee grounds. *Environmental Science and Pollution Research*, *26*(35), 35473–35481. https://doi.org/10.1007/s11356-019-04919-3

Weldekidan, H., Strezov, V., Town, G., & Kan, T. (2018). Production and analysis of fuels and chemicals obtained from rice husk pyrolysis with concentrated solar radiation. *Fuel*, *233*(April), 396–403. https://doi.org/10.1016/j.fuel.2018.06.061

Zeng, K., Gauthier, D., Minh, D. P., Weiss-Hortala, E., Nzihou, A., & Flamant, G. (2017). Characterization of solar fuels obtained from beech wood solar pyrolysis. *Fuel*, *188*, 285–293. https://doi.org/10.1016/j.fuel.2016.10.036

Zeng, K., Gauthier, D., Soria, J., Mazza, G., & Flamant, G. (2017). Solar pyrolysis of carbonaceous feedstocks: A review. *Solar Energy*, *156*, 73–92. https://doi.org/10.1016/j.solener.2017.05.033

Zhang, C., Ho, S. H., Chen, W. H., Fu, Y., Chang, J. S., & Bi, X. (2019). Oxidative torrefaction of biomass nutshells: Evaluations of energy efficiency as well as biochar transportation and storage. *Applied Energy*, *235*(October 2018), 428–441. https://doi.org/10.1016/j.apenergy.2018.10.090

Zhang, H. L., Baeyens, J., Degrève, J., & Cacères, G. (2013). Concentrated solar power plants: Review and design methodology. *Renewable and Sustainable Energy Reviews*, *22*, 466–481. https://doi.org/10.1016/j.rser.2013.01.032

[1] https://www.theindianiris.com/solar-cooker-programme-government-of-india/

[2] https://moneymint.com/coffee-plantations-kerala-india/

[3] https://yourstory.com/2019/05/frugal-innovation-navi-radjou-jaideep-prabhu/amp

[4] https://www.brahmakumaris.org/hope/renewable-energy/india-one-solar-thermal-power-plant

[5] https://www.downtoearth.org.in/coverage/renewable-energy/bon-appetit-with-sun-40457

[6] https://www.onmanorama.com/food/features/2022/04/23/wayanad-coffee-set-to-be-introduced-in-netherlands.html

[7] https://www.indiacoffee.org/Publications/December%202019%20final.pdf

[8] https://www.indiacoffee.org/Publications/October%202019%20final.pdf

[9] https://english.mathrubhumi.com/news/kerala/haritha-karma-sena-s-waste-collection-across-kerala-fetches-rs-6-59-crore-in-2021-1.7454280

[10] http://sanitation.kerala.gov.in/wp-content/uploads/2019/03/sbm-coffee-table.pdf

[11] http://www.biochar-international.org/

[12] https://www.astm.org/

[13] https://eg-solar.de/

[14] https://www.e-education.psu.edu/eme812/node/8

[15] https://india.mongabay.com/2021/08/indias-biomass-power-sector-meets-target-but-stares-at-a-stagnant-future/

[16] https://www.keralaspicesonline.com/product/coffee-powder-kerala/

[17] https://www.filmetrics.com/refractive-index-database/BSG/Borosilicate-Glass-Microscope-Slide#:~:text=(BK7%20is%20a%20particular%20kind,refractive%20index%20and%20extinction%20coefficients.

[18] https://en.tutiempo.net/solar-radiation/india/hyderabad-airport.html

[19] https://www.comsol.com/blogs/nrel-enhances-biofuel-conversion-processes-with-simulation/

8 Appendix

8.1 Reactor Model Results

TESTING REPORT TEST - 1			
Date of experiment:10/05/2022		Reactor Type:1	
Sample: SCG		**Location: Hyderabad, Telangana, India**	
Atmospheric Temp - 36℃			
Time	**Temperature**	**Irradiance W/mm^2**	**Remarks**
11:07	37.5℃	732	
11:12	42.5℃	732	Bright sun light.
11:17	49.4℃	732	
11:22	55.6℃	732	
11:27	60.2℃	732	
11:32	62.2℃	748	
12:03	66.8℃	748	
12:15	70.0℃	748	Peak temperature.
12:32	64.1℃	748	
13:00	55.2℃	601	
13:34	55.8℃	601	
14:10	55.8℃	433	

Table 15: Experiment 1 data.

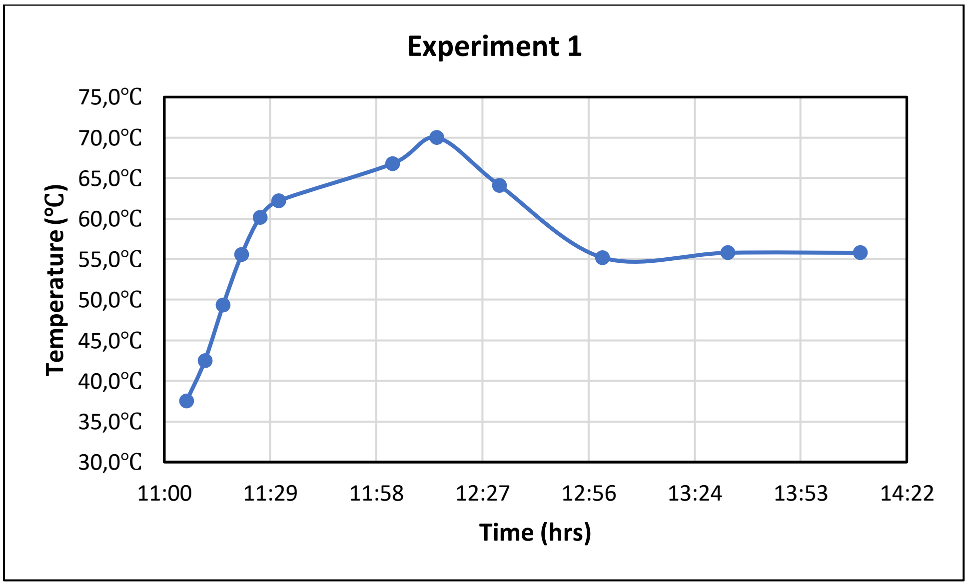

Figure 74: Time vs temperature graph for Experiment 1.

TESTING REPORT TEST - 2

Date of experiment: 13/05/2022	**Reactor type: 1**
Sample: No sample	**Location of test: Hyderabad, Telangana, India**

Time	**Temperature**	**Irradiance W/mm^2 Hr**	**Remarks**
12.20 Hrs	37.6°C	648 W/m^2 Hr	Temp under open sun = 36.40 °C
12.25 Hrs	49.0°C	648 W/m^2 Hr	
12.30 Hrs	61.0°C	648 W/m^2 Hr	
12.35 Hrs	79.9°C	648 W/m^2 Hr	
12.40 Hrs	80.2°C	648 W/m^2 Hr	
12.45 Hrs	75.9°C	648 W/m^2 Hr	Temporarily Cloudy.
12.50 Hrs	80.5°C	648 W/m^2 Hr	
12.55 Hrs	74.7°C	501 W/m^2 Hr	
13.00 Hrs	77.7°C	501 W/m^2 Hr	
13.05 Hrs	110.9°C	501 W/m^2 Hr	Bright sun.
13.10 Hrs	111.2°C	501 W/m^2 Hr	At 110.7°C, the outer cork burst out.
13.15 Hrs	109.5°C	501 W/m^2 Hr	Cloudy. Started decreasing gradually.

Observations:

1. At 110.7°C, the aluminium pipe (Reactor) and cork popped out of shell. This may be due to additional pressure due to gaseous expansion and water vapour. A pressure release method (by increasing the diameter of gap at the thermal seal) or a 2mm orifice in thermal seal for releasing hot air or smoke can be proposed.
2. Residence time was 55 minutes with an increasing temperature.
3. Initial ambient temperature was 37 degrees as recorded by the thermal camera and the sensor probe.
4. Focus point of the solar cooker is adjusted on the glass tube. A slow increase in temperature can point towards either disoriented focal plane or intermittency.
5. The amorphous residue is stored for future test. The finding seems like dried SCG.

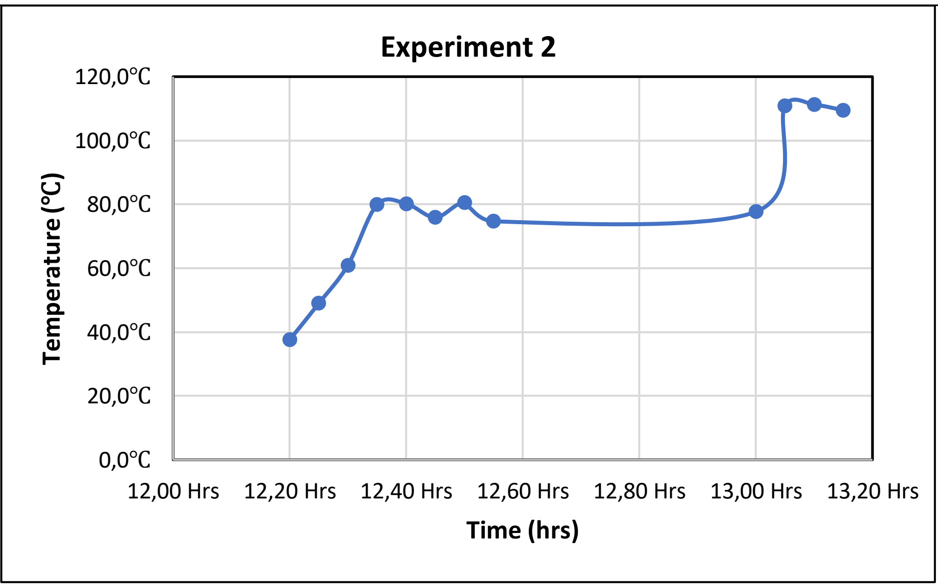

Figure 75: Time vs temperature graph for Experiment 2.

TESTING REPORT - TEST - 3

Date of experiment: 14/05/2022 **Reactor Type:1**

Sample: SCG **Location of test: Hyderabad, Telangana, India**

Time	**Temperature**	**Irradiance W/mm^2 Hr**	**Remarks**
10:55	42.2℃	870 W/mm^2 Hr	Atmospheric Temperature = 42.20 ℃
11:00	52.1℃	943 W/mm^2 Hr	
11:05	60.9℃	943 W/mm^2 Hr	
11:10	69.3℃	943 W/mm^2 Hr	
11:15	78.0℃	943 W/mm^2 Hr	
11:20	88.9℃	943 W/mm^2 Hr	
11:25	112.0℃	943 W/mm^2 Hr	
11:30	130.3℃	943 W/mm^2 Hr	
11:35	146.3℃	956 W/mm^2 Hr	
11:40	162.0℃	956 W/mm^2 Hr	At 177.7℃, the aluminium pipe popped out 20mm from glass shell.
11:45	175.0℃	956 W/mm^2 Hr	
11:50	178.9℃	956 W/mm^2 Hr	
11:55	183.8℃	956 W/mm^2 Hr	
12:00	184.1℃	956 W/mm^2 Hr	The bottom cork inside pipe part melted & popped out slightly at 184.1 ℃.
12:05	181.8℃	956 W/mm^2 Hr	
12:10	180.0℃	956 W/mm^2 Hr	Glass shell wall shaded with brown tint due to cork smoke.
12:15	174.3℃	956 W/mm^2 Hr	
12:20	172.1℃	956 W/mm^2 Hr	
12:26	166.2℃	956 W/mm^2 Hr	
12:30	160.4℃	956 W/mm^2 Hr	

Observations:

1. At 177.1℃, the aluminium pipe (Reactor) popped out of shell. This may be due to cork melting smoke or higher expansion of air in between reactor and shell wall. Proposed to provide 2mm orifice in thermal seal for releasing hot air or smoke from shell and aluminium pipe gap.
2. Bottom Cork melted at 184.1℃ resulting brown smoke tinting shell wall. Proposed for metal sealing of bottom end of reactor instead of rubber. A 2mm diameter drilled hole will be provided for release of hot/generated gas from bottom end for better release of pressure and gases.
3. The coffee combustion smell emerged from reactor cork hole at 130 ℃. This could be the beginning of breaking of SCG components or burning in limited oxygen.
4. A 3mm hole was made in outer cork of aluminium pipe reactor for release of hot/effluent vapour. The reactor popped out from shell at 110 7℃ during experiment - 2. It was successful here during this test & no adverse reaction seen even up to the peak temperature.
5. The amorphous residue is stored for future test. The finding seems like burnt residue.

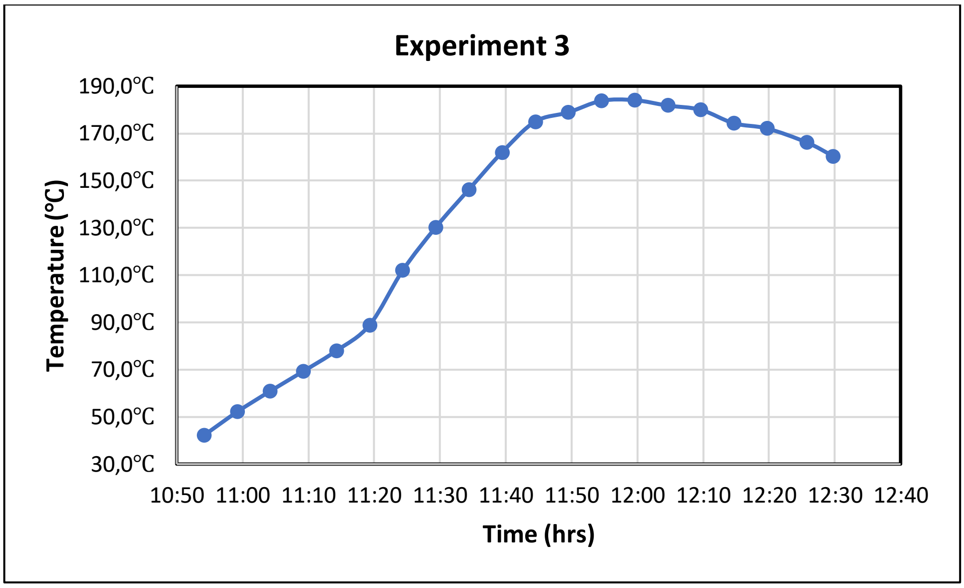

Figure 76: Time vs temperature graph for Experiment 3.

TESTING REPORT - TEST - 4

Date of experiment:14/05/22 Reactor Type :2

Sample: Cofee waste **Location: Hyderabad, Telangana, India**

Time	**Temperature**	**Irradiance W/mm² Hr**	**Remarks**
14:00:00	44.5°C	635 W/mm² Hr	
14:05:00	56.2°C	635 W/mm² Hr	
14:10:00	71.5°C	635 W/mm² Hr	
14:15:00	81.3°C	635 W/mm² Hr	
14:20:00	92.2°C	635 W/mm² Hr	
14:25:00	98.5°C	635 W/mm² Hr	
14:30:00	99.1°C	635 W/mm² Hr	Slight temporary shading.
14:35:00	98.9°C	494 W/mm² Hr	
14:40:00	96.5°C	494 W/mm² Hr	
14:50:00	89.5°C	494 W/mm² Hr	
14:55:00	84.9°C	494 W/mm² Hr	
15:10:00	89.1°C	494 W/mm² Hr	Bright sun restored.
15:13:00	99.2°C	494 W/mm² Hr	
15:18:00	114.1°C	494 W/mm² Hr	
15:23:00	117.4°C	494 W/mm² Hr	
15:28:00	120.5°C	494 W/mm² Hr	
15:33:00	121.2°C	494 W/mm² Hr	
15:38:00	118.2°C	379 W/mm² Hr	
15:45:00	116.8°C	379 W/mm² Hr	Sun ray inclined beyond Cooker provision.

Inference: The experiment was difficult to conduct beyond 15:00 Hrs due to the angle of the sun and the limitation of this particular SK-14 solar cooker inclination. This was further noted for the future experiments. Although there was sufficient irradiation, it was difficult to progress the experiment any further.

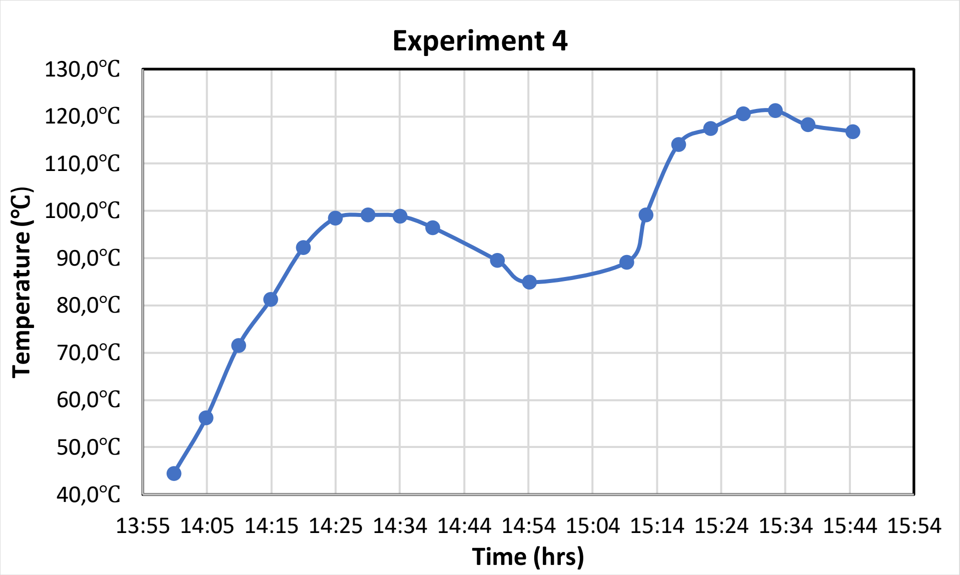

Figure 77: Time vs temperature graph for Experiment 4.

TESTING REPORT - TEST - 5

Date of experiment:15/05/2022		**Reactor Type: 2**	
Sample: SCG		**Location: Hyderabad, Telangana, India**	
Time	**Temperature**	**Irradiance**	**Remarks**
11:05	52.2°C	958 W/m²	Atmospheric Temp - 41.3°C
11:10	69.3°C	958 W/m²	
11:15	155.5°C	958 W/m²	Bright sun through out.
11:20	194.6°C	958 W/m²	
11:25	219.0°C	958 W/m²	
11:30	232.1°C	958 W/m²	
11:35	238.8°C	989 W/m²	
11:38	239.9°C	989 W/m²	
11:40	236.8°C	989 W/m²	
11:45	237.8°C	989 W/m²	
11:50	238.9°C	989 W/m²	
11:55	237.3°C	989 W/m²	
12:00	237.5°C	989 W/m²	
12:05	237.1°C	989 W/m²	
<u>Observation:</u>			

3. Glass shell ambient temp 110°C measured through thermal camera when reactor temp 150°C correspondingly. This glass temp remains similar throughout the experiment from this point.

4. Coffee burning smell at 230°C. The burning or limited burning could have started much earlier but the smell was significant at this point. This points out the difference between burning and torrefaction.

6. HDPE tie for pedestal to aluminium tube & poly vinyl cushion at bottom burnt at 230°C. Metallic pedestal proposed.

Inference: The coffee produced is burnt/partially torrefied if the expansion causes air to flow out. Maybe residence time can make a difference to the produced**.** Peak temperature denotes the possibility of production of a Solar Torrefier in a single layered glass reactor. Triplication is further aimed.

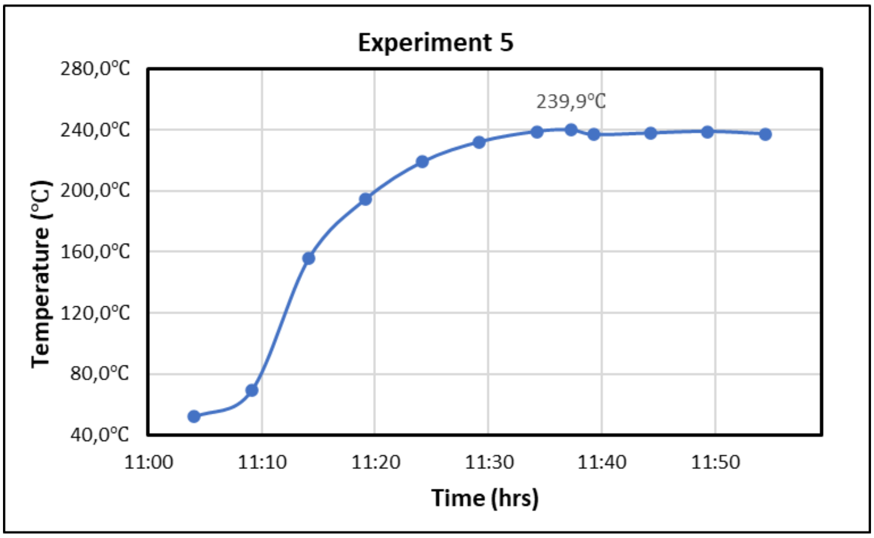

Figure 78: Time vs temperature graph for Experiment 5.

TESTING REPORT – TEST-6

Date: 16/05/2022, Reactor: 2

Sample: SCG **Location: Hyderabad, Telangana, India**

Time	Temperature	Remarks
11:27	52.0°C	Atmospheric Temp - 36°C
11:28	63.5°C	
11:31	101.3°C	Bright sun throughout.
11:35	128.8°C	
11:40	147.7°C	Higher wind.
11:45	153.7°C	
11:50	159.0°C	
11:55	162.8°C	
12:00	167.2°C	
12:05	168.0°C	
12:10	171.0°C	
12:15	186.3°C	
12:20	185.4°C	
12:25	187.5°C	
12:30	194.5°C	
12:35	194.5°C	
12:40	196.2°C	Peak temperature
12:45	194.7°C	
12:50	195.5°C	
12:55	188.2°C	Reactor removed from Cooker.
13:00	171.1°C	

Inference: This experiment was a perfect example of intermittency causing decrease in temperature in the experiments. The same experiment will be duplicated in better weather conditions, since there is projection for 240 C.

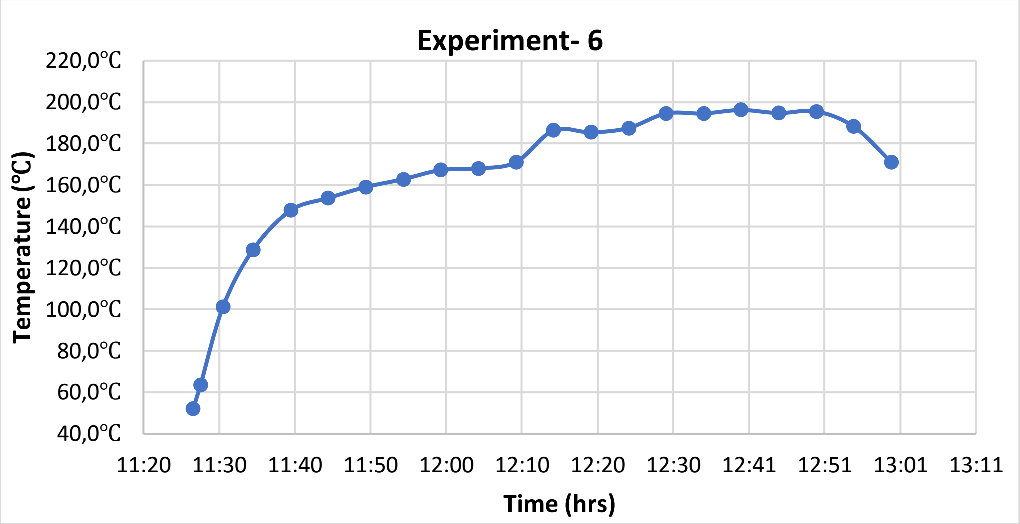

Figure 79: Time vs temperature graph for Experiment 6.

TESTING REPORT – TEST-7

Date of experiment:16/05/2022

Sample: SCG

Location: Hyderabad, Telangana, India

Time	**Temperature**	**Remarks**
01:55	58.4°C	Atmospheric Temp - 46°C
02:00	76.3°C	Bright sun throughout.
02:05	128.6°C	
02:10	148.2°C	
02:15	154.6°C	
02:20	147.7°C	Focus point changed.
02:25	155.1°C	Focus readjusted.
02:30	172.2°C	
02:35	175.0°C	
02:40	179.1°C	
02:42	184.3°C	Peak temperature.
02:45	182.2°C	Ray inclined below limit.

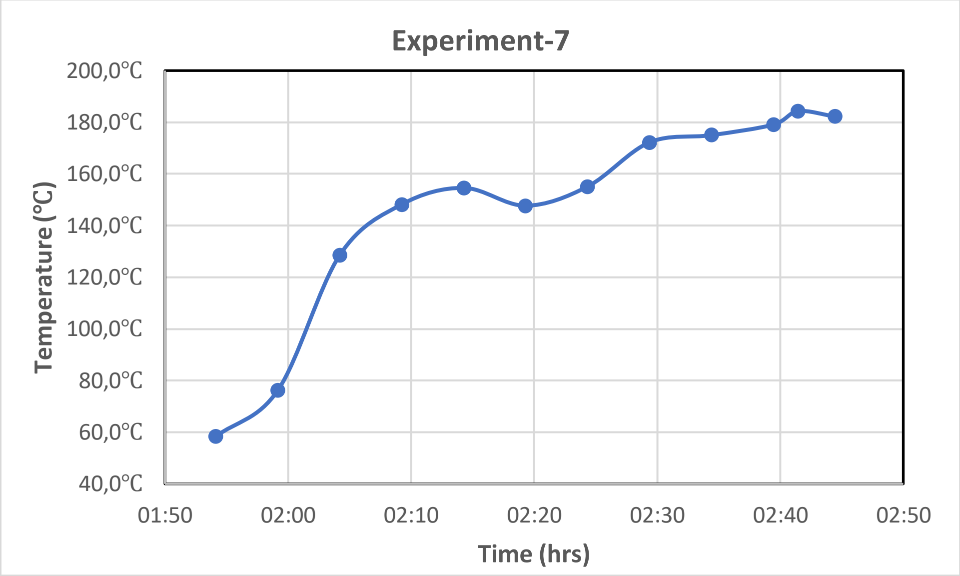

Figure 80: Time vs temperature graph for Experiment 7.

TESTING REPORT TEST - 8		
Date of experiment:17/05/2022		
Sample: SCG, Location: Hyderabad, Telangana, India		
Time	**Temperature**	**Remarks**
11:25	45.0°C	Atmospheric Temp - 44°C
11:30	87.1°C	Variable irradiation.
11:35	130.2°C	But strong sunlight high irradiation.
11:40	151.1°C	
11:45	161.4°C	
11:50	178.3°C	
11:55	197.4°C	
12:00	214.8°C	
12:05	211.9°C	Focal point changed.
12:07	204.4°C	
12:10	210.4°C	Focal point adjusted.
12:15	229.6°C	
12:17	231.3°C	
12:18	233.1°C	Peak temperature.
12:20	227.1°C	
12:25	223.4°C	Glass shell broke while opening.
12:35	217.8°C	

Inference: This experiment proved a strong insight on the function of the reactor/torrefier even in intermittent solar conditions. There was cloudy weather throughout the time of the experiment. It resulted in a stunted increase of temperature after 197.4 °C, but the adjustment of the SK14 cooker with respect to the alignment of the sun helped attaining a peak temperature of 233.1 °C. Uneven heating of the charged SCG resulted in visually complete combustion of the charged feedstock. Figure 29 explains the temperature profile with respect to time. This was considered a duplication of Experiment 5 which validates the theme of the experiment.

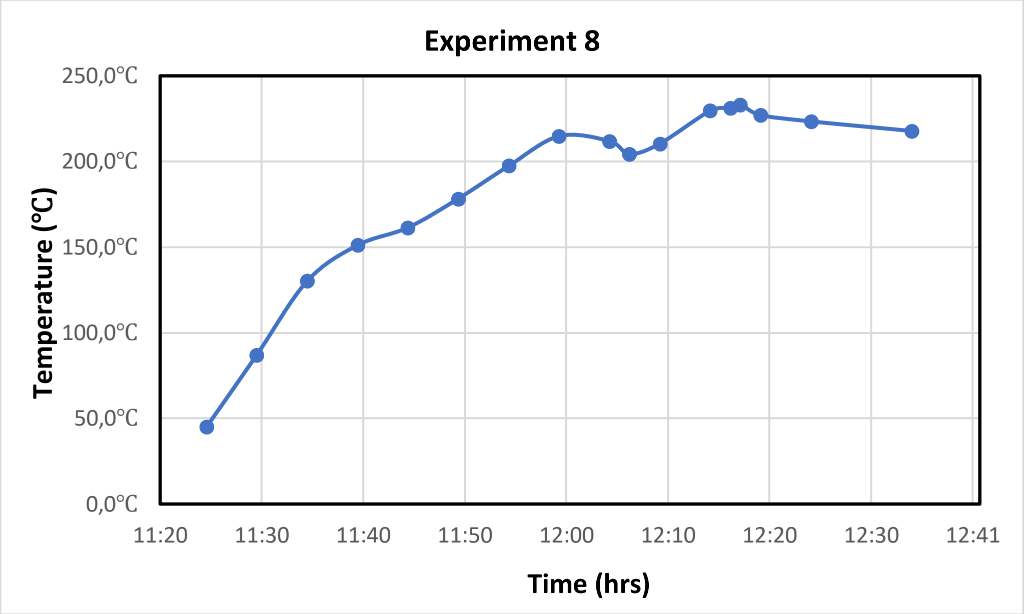

Figure 81: Time vs temperature graph for Experiment 8.

TESTING REPORT TEST - 9			
Date of experiment:18/05/2022			**Reactor type: 2**
Sample: Cofee waste		**Location: Hyderabad, Telangana, India**	
Date	**Time**	**Temperature**	**Remarks**
18-05-2022	11:25	51.2°C	Atmospheric Temp - 42.7°C
	11:30	99.3°C	
	11:35	156.8°C	
	11:40	199.2°C	
	11:45	210.9°C	
	11:50	262.2°C	
	11:55	259.3°C	
	12:00	257.8°C	
	12:05	260.4°C	
	12:10	262.3°C	Peak temperature
	12:15	261.7°C	
	12:20	261.2°C	
	12:25	259.5°C	

Inference: The reactor temperature reached a peak of 262.3 °C which triplicates the final temperature of the experiment. The focal point was fixated on the center of the reactor and high irradiation caused the temperature in the reactor to go beyond the desirable temperature of 240 °C. Coffee was combusted/partially burned at a much faster rate as the peak temperature was obtained in 35 minutes. Figure 30 shows the temperature profile of the reaction with respect to the time period of the experiment. There was further potential of the reactor under good conditions and hence this result was aimed to be duplicated. Figure 32 shows the triplicated attainable Torrefaction temperature in different experimental conditions with SCG as the feedstock.

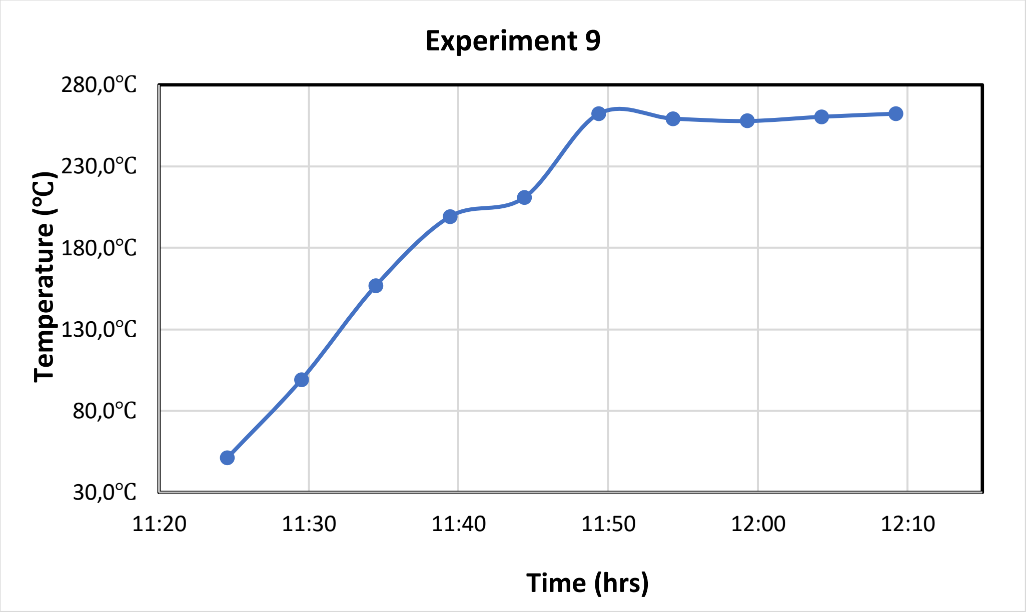

Figure 82: Time vs temperature graph for Experiment 9.

TESTING REPORT TEST - 10			
Date of experiment:19/05/2022			**Reactor type: 2**
Sample: Coffee waste		**Location: Hyderabad, Telangana, India**	
Date	**Time**	**Temperature**	**Remarks**
19-05-2022	11:15	43.0°C	Atmospheric Temp - 41.3°C
	11:20	72.2°C	
	11:25	96.4°C	
	11:30	121.5°C	
	11:35	157.1°C	
	11:40	170.4°C	
	11:45	165.2°C	
	11:50	187.6°C	
	11:55	219.7°C	
	12:00	235.8°C	
	12:05	257.9°C	
	12:10	255.2°C	
	12:15	258.4°C	
	12:20	259.8°C	
	12:25	257.7°C	

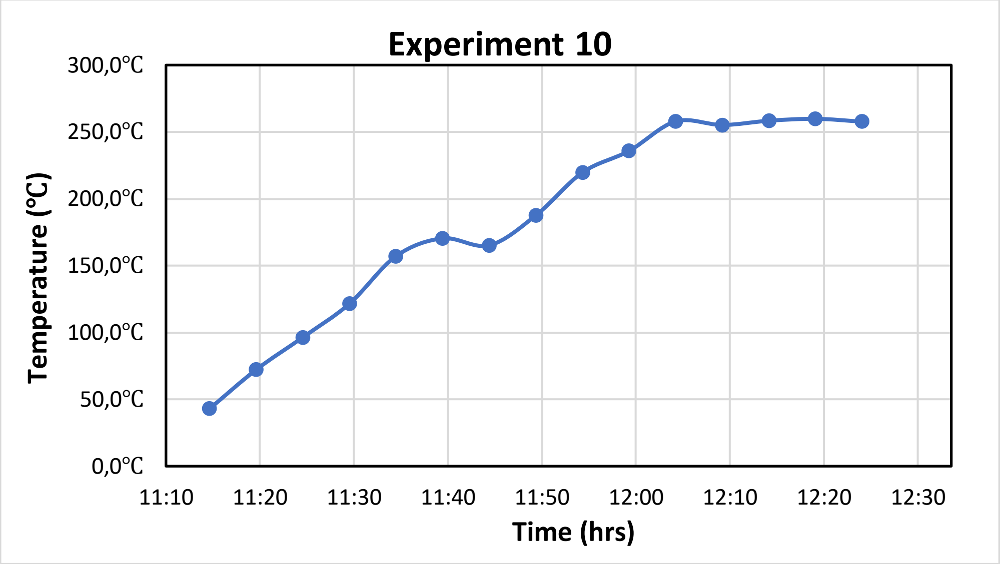

Figure 83: Time vs temperature graph for Experiment 10.

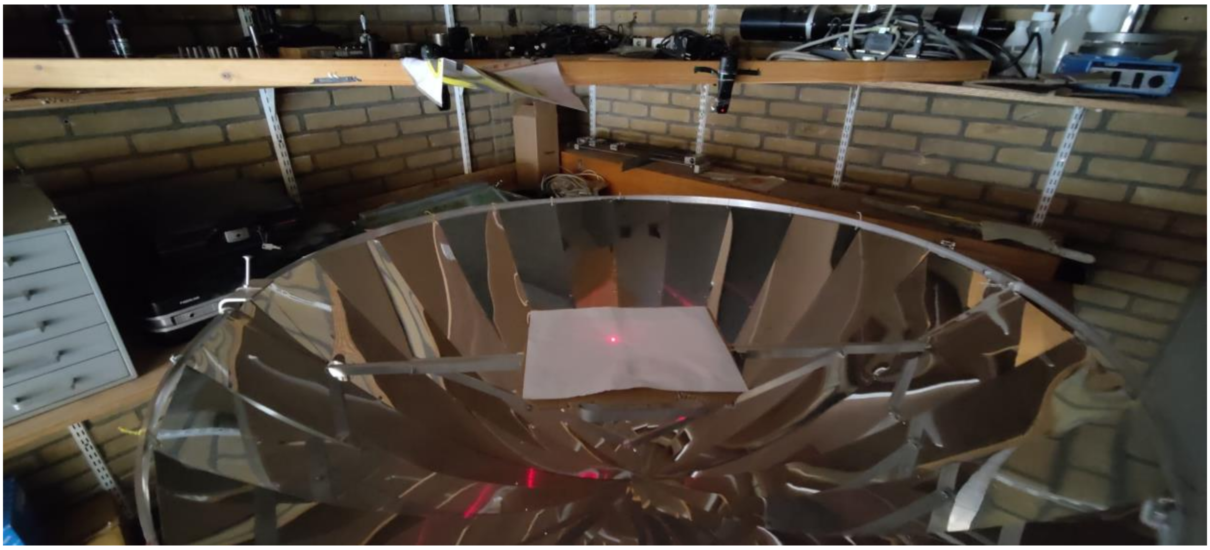

Figure 84: Laser experimentation when the lasers were interesting.

Figure 85: Reactor 2 design as a standalone system.

8.2 COMSOL Parameters and Results

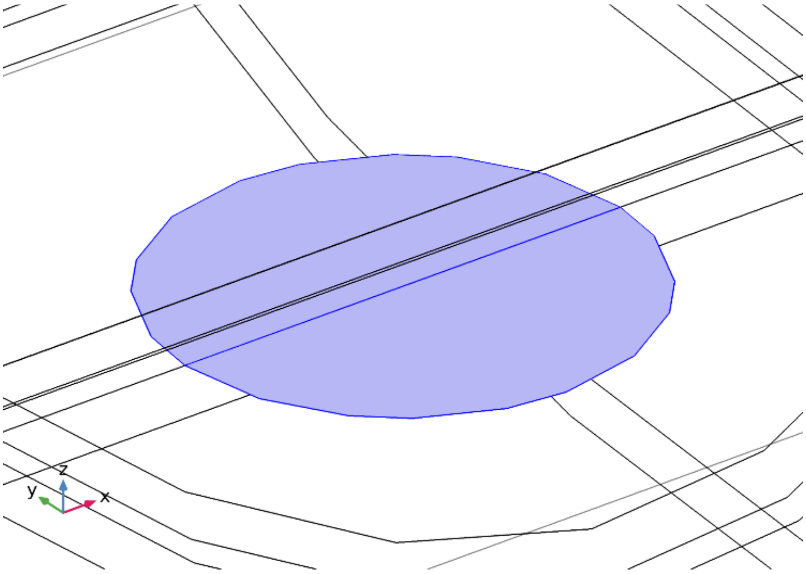

Figure 86: Boundary heat flux shown as a variating focal point.

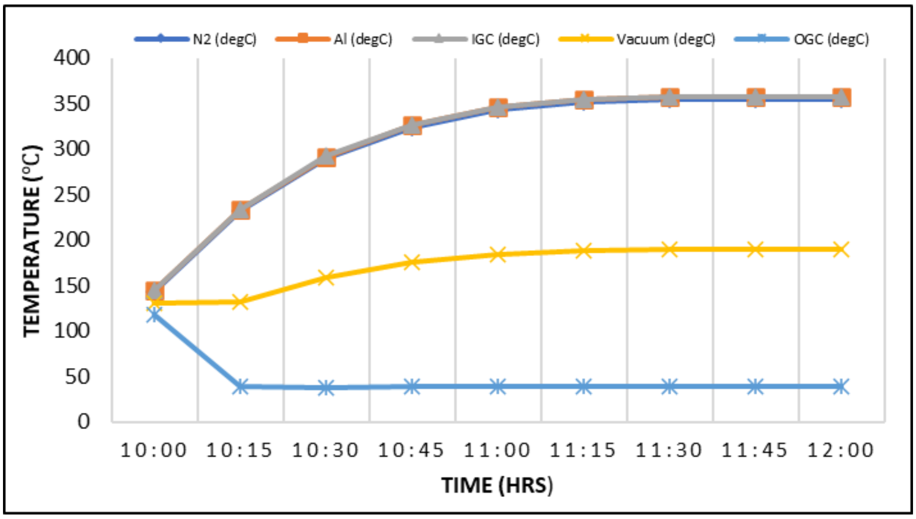

Figure 87:Time vs temperature average of Scenario 2.

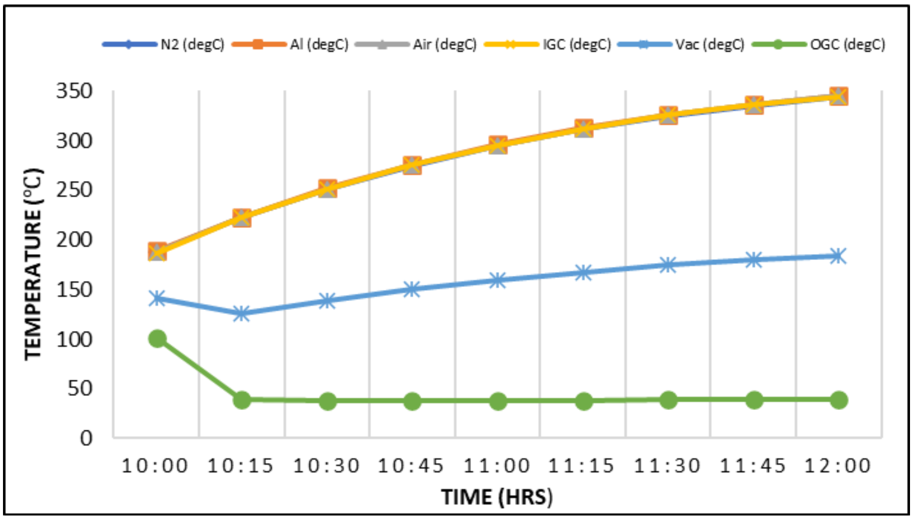

Figure 88:Time vs temperature average of Scenario 3.

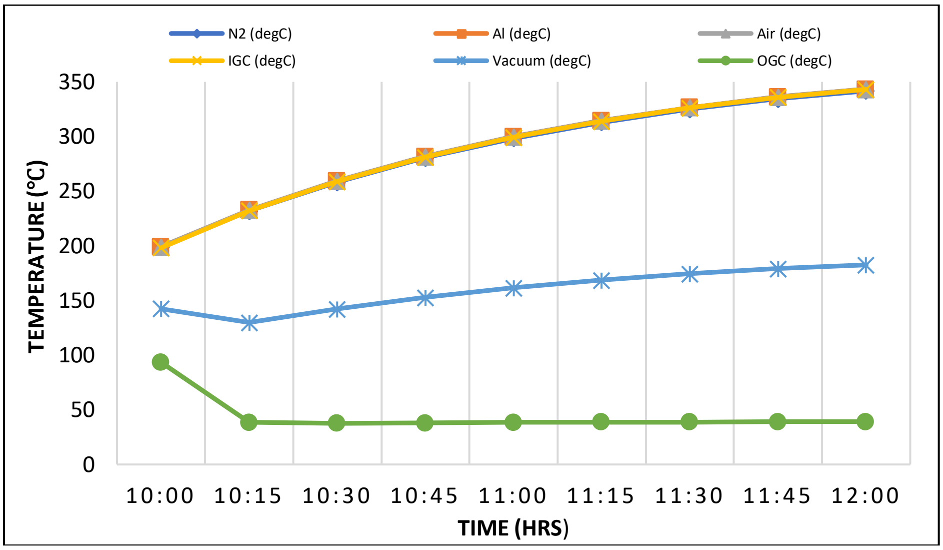

Figure 89:Average temperature vs time for Scenario 4.

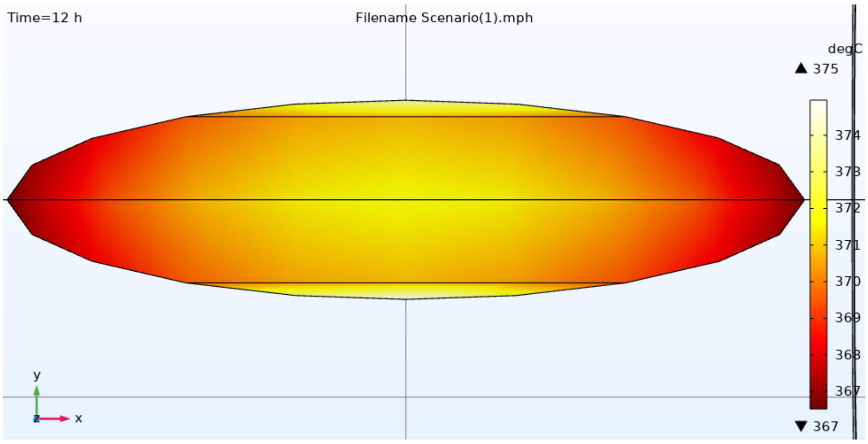

Figure 90: Focal plane temperature distribution in Scenario 1.

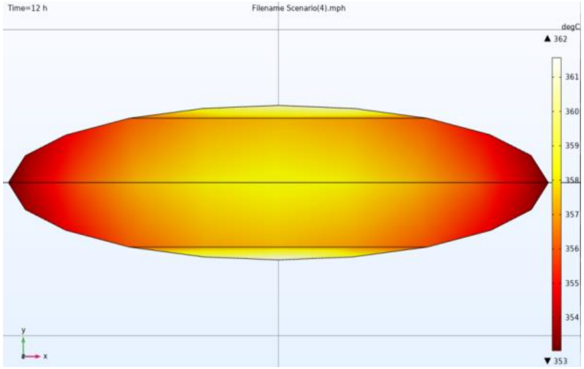

Figure 91: Focal plane temperature distribution in Scenario 4.

Table 16: Irradiation data

Time (h)	Ambient solar irradiance (W/m^2)	Clear sky noon beam normal irradiance (W/m^2)	Clear sky noon diffuse horizontal irradiance (W/m^2)
10:00	932.92	748.41	184.51
10:15	932.92	748.42	184.50
10:30	932.91	748.43	184.48
10:45	932.91	748.44	184.47
11:00	932.90	748.45	184.46
11:15	932.90	748.45	184.45
11:30	932.90	748.46	184.44
11:45	932.89	748.47	184.42
12:00	932.89	748.48	184.41

Table 17: Volume average temperature for Scenario 1.

Time (h)	N2 (℃)	Aluminium (℃)	Air (℃)	Inner Glass (℃)	Vacuum (℃)	Outer Glass (℃)
10:00	135.25	135.87	134.64	133.29	117.11	102.79
10:15	224.9	226.8	227.69	228.65	128.5	38.96
10:30	286.04	288.57	289.48	290.43	157.32	38.37
10:45	323.33	326.23	327.1	328.01	175.42	39.10
11:00	343.94	347.03	347.86	348.71	185.48	39.66
11:15	352.58	355.75	356.55	357.37	189.68	39.90
11:30	355.56	358.76	359.55	360.36	191.13	39.99
11:45	356.28	359.48	360.28	361.08	191.49	40.02
12:00	356.34	359.54	360.33	361.13	191.53	40.04

Table 18: Volume average temperature for Scenario 2.

Time (h)	N2 (℃)	Al (℃)	IGC (℃)	Vacuum (℃)	OGC (℃)
10:00	144	144.45	144.37	130.21	117.69
10:15	231.91	233.73	233.85	131.54	39.44
10:30	289.48	291.92	292.03	158.55	38.46
10:45	324.17	326.96	327.05	175.46	39.11
11:00	343.27	346.24	346.32	184.86	39.64
11:15	351.3	354.34	354.42	188.81	39.88
11:30	354.08	357.15	357.22	190.18	39.95
11:45	354.78	357.86	357.93	190.53	39.98
12:00	354.86	357.93	358.01	190.58	40.01

.

Table 19: Volume average temperature for Scenario 3.

Time (h)	N2 (℃)	Al (℃)	Air (℃)	IGC (℃)	Vacuum (℃)	OGC (℃)
10:00	199.05	199.19	199.19	198.15	142.65	93.48
10:15	231.95	232.73	232.73	232.24	129.92	38.42
10:30	258.37	259.37	259.37	258.93	142.08	37.61
10:45	280.44	281.62	281.62	281.22	152.79	37.98
11:00	298.45	299.78	299.78	299.41	161.59	38.39
11:15	312.97	314.41	314.41	314.07	168.64	38.65
11:30	325.07	326.61	326.61	326.29	174.52	38.84
11:45	334.55	336.16	336.16	335.86	179.11	38.99
12:00	341.73	343.4	343.4	343.12	182.6	39.11

Table 20: Volume average temperature for Scenario 4.

Time (h)	N2 (℃)	Al (℃)	Air (℃)	IGC (℃)	Vac (℃)	OGC (℃)
10:00	187.65	188.46	187.7	186.79	141.48	101.68
10:15	222.18	222.94	222.59	222.14	125.44	38.90
10:30	251.02	251.89	251.59	251.2	138.5	37.65
10:45	274.91	275.87	275.61	275.26	150.05	38.01
11:00	294.61	295.64	295.42	295.11	159.62	38.39
11:15	311.31	312.41	312.22	311.95	167.71	38.65
11:30	324.96	326.11	325.95	325.7	174.31	38.84
11:45	335.58	336.77	336.63	336.41	179.44	38.98
12:00	343.64	344.86	344.74	344.53	183.34	39.10

Table 21: Volume maximum temperature for Scenario 1.

Time (h)	N2 (degC)	Al (degC)	Air (degC)	Inner Glass (degC)	Vacuum (degC)	Outer Glass (degC)
10:00	144.95	144.95	144.89	144.93	148.05	143.85
10:15	239.45	239.45	243.43	242.15	242.02	50.992
10:30	301.26	301.26	304.99	303.82	303.69	54.329
10:45	338.8	338.80	342.30	341.19	341.03	57.237
11:00	359.48	359.48	362.79	361.71	361.53	58.955
11:15	368.12	368.12	371.33	370.27	370.06	59.654
11:30	371.09	371.09	374.25	373.20	372.99	59.911
11:45	371.8	371.80	374.93	373.88	373.67	59.987
12:00	371.84	371.84	374.96	373.91	373.70	60.017

Table 22: Volume maximum temperature for Scenario 2.

Time (h)	N2 (degC)	Al (degC)	IGC (degC)	Vac (degC)	OGC (degC)
10:00	199.32	155.13	155.12	154.61	145.75
10:15	286.11	246.05	246.11	246.11	51.371
10:30	344.61	304.26	304.31	304.31	54.518
10:45	379.93	339.20	339.22	339.22	57.312
11:00	399.38	358.37	358.37	358.36	58.965
11:15	407.54	366.41	366.40	366.39	59.656

11:30	410.37	369.19	369.18	369.16	59.901
11:45	411.07	369.87	369.87	369.84	59.975
12:00	411.14	369.94	369.93	369.91	60.009

Table 23: Volume maximum temperature for Scenario 3.

Time (h)	N2 (degC)	Al (degC)	Air (degC)	IGC (degC)	Vac (degC)	OGC (degC)
10:00	214.29	214.31	216.71	215.36	215.13	160.38
10:15	247.16	247.16	250.62	249.52	249.48	51.661
10:30	273.8	273.80	277.17	276.16	276.11	52.457
10:45	296.04	296.04	299.34	298.38	298.34	54.04
11:00	314.18	314.18	317.44	316.52	316.48	55.392
11:15	328.79	328.79	332.02	331.13	331.09	56.398
11:30	340.98	340.98	344.18	343.32	343.28	57.212
11:45	350.52	350.52	353.69	352.85	352.82	57.856
12:00	357.75	357.75	360.91	360.08	360.05	58.38

Table 24: Volume maximum temperature for Scenario 4.

Time (h)	N2 (degC)	Al (degC)	Air (degC)	IGC (degC)	Vac (degC)	OGC (degC)
10:00	203.33	203.33	206.26	205.03	204.86	157.37
10:15	236.61	236.61	240.11	239.00	238.95	41.32
10:30	265.54	265.54	268.92	267.88	267.83	39.28
10:45	289.49	289.49	292.80	291.81	291.77	39.58
11:00	309.25	309.25	312.50	311.55	311.51	39.94
11:15	326	326.00	329.21	328.29	328.25	40.22
11:30	339.69	339.69	342.86	341.97	341.93	40.41
11:45	350.34	350.34	353.50	352.63	352.59	40.55
12:00	358.42	358.42	361.57	360.71	360.67	40.65

Table 25: FP average temperature for scenarios.

Time (h)	FP AVG (degC)			
	Scenario 1	Scenario 2	Scenario 3	Scenario 4
10:00	143.35	169.34	212.61	201.65
10:15	237.82	258.75	245.51	234.96
10:30	299.63	317.06	272.15	263.89
10:45	337.18	352.14	294.39	287.85
11:00	357.86	371.42	312.53	307.61
11:15	366.5	379.5	327.15	324.36
11:30	369.48	382.3	339.34	338.05
11:45	370.18	382.99	348.87	348.71
12:00	370.23	383.06	356.1	356.79

8.2.1 Prototype Biomass- Torrefier reactor

Like the modelling of the ECV in the previous section the basic principle of heat transfer and surface-to-surface radiation was followed. However, according to the availability of the materials for a prototype, this model was developed trying to replicate Figure 46. The developed model has been shown in Figure 92 which followed the geometrical parameters mentioned in Table 26.

The ambient conditions were set for Hyderabad, India also on the 15th of May 2022 since the experiments with the prototype were to be conducted there. As can be seen from the reactor design, the outer cylinder was a 2.5 mm thick borosilicate glass enclosing a black painted aluminium fin inside an air domain. A poly iso-butyl material cork closed the mouth of the reactor which was extended with a 75mm glass pressure pipe to enact releasing pressure and flue gases during the simulation. A similar boundary heat flux was built on the aluminium tube but in this case, the concentration factor (C_A) of the solar cooker was calculated to be 16. Therefore, the boundary heat flux used was:

$$Q_b = ampr1.Is_{amb} * 16 * 0.6049 \tag{33}$$

Heat transfer and *Surface-to-surface radiation* coupled with a Multiphysics operation were taken as the physics involved in this model. Natural Air convection was simulated on the outer materials by adding a *'Heat Flux'* operation with respect to the ambient wind and ambient conditions. The air domain was selected as the *'Fluid'* boundary for the simulation with a convectively enhanced conductivity sub-division to enact convective heating in the reactor. The solid domains selected were responsible for conductive heat transfer in the model.

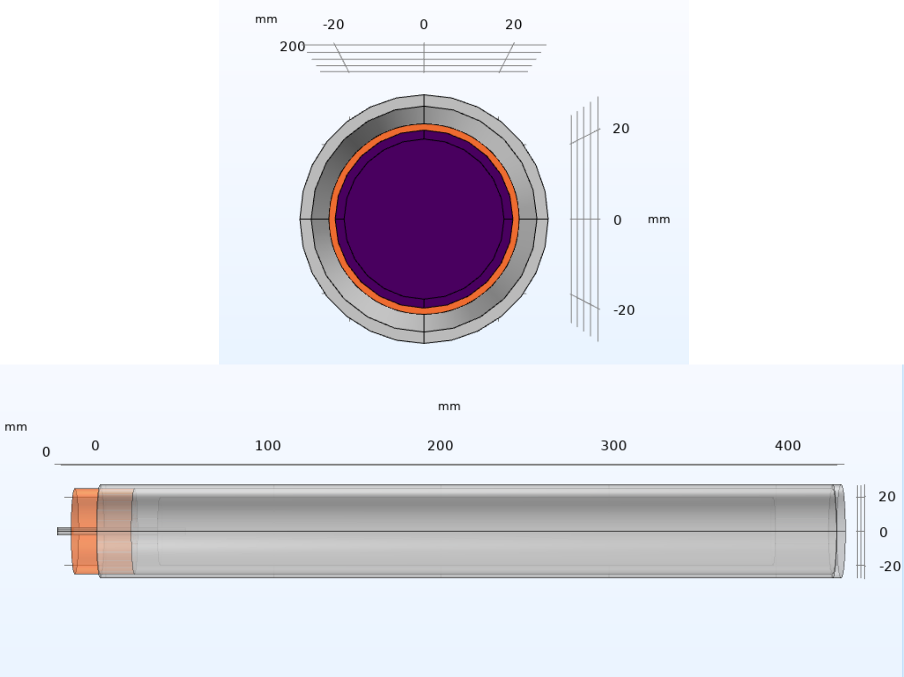

Figure 92:Single glass prototype model.

Domains	**Values (mm)**
Outer Borosilicate Cylinder	Radius = 27.5 Height = 430 Thickness = 2.5

Pressure Pipe	Radius = 2.25 Height = 75 Thickness = 1
Aluminum Fin	Radius = 20 Thickness = 2
Borosilicate Cover	Height=5 Radius = 27.5
PIB Cork	Length = 35 Radius = 25
Focal Plane	a-semiaxis= 30 b-semiaxis = 10 Position = (215,0)

Table 26:Geometrical parameters used for building the prototype reactor model.

To model the heating of the aluminium tube and the air inside the reactor through surface-to-surface radiation a transparent and non-transparent study was conducted involving the principle of a greenhouse. *Semi-Transparent boundary* was applied for the outer borosilicate glass with a surface emissivity (ε) of 0.9, diffuse reflectivity (ρ_d) of 0.075, surface transmissivity (τ) of 0.92 and an air-glass critical angle of 42° (0.73309 radians). An opaque surface with a high emissivity of 0.96 and diffuse reflectivity of 0.01 is assumed on the top layer of aluminium boundary to enact the matte black paint. The rest of the aluminium tube boundary receives the material properties of ε=0.65 and reflectivity ρ_d=0.9095. The Outer Glass was made transparent for light wavelengths below 2.5[μm] and 'Opaque' for long wavelength waves [2.5[μm], +∞] to replicate the greenhouse effect.

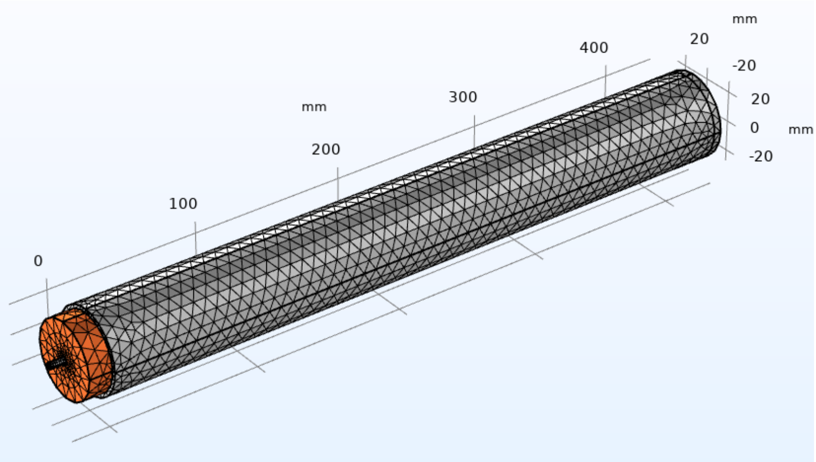

Figure 93:Physics controlled mesh of the model.

A physics-controlled mesh was applied to the model which consisted of 32816 domain elements, 11565 boundary and 1353 edges of free tetrahedral mesh. Two-time dependent studies were considered for the simulation and the output times were set for 1 hour from 11:00 hrs to 12:00 hrs for every 10 minutes time interval. *Study 1* was illustrating the non-transparent model and *Study 2* the transparent model as mentioned earlier. *Study 3* was used to club the two studies, so that a combined value is obtained in the simulation. The model was simulated, and the values obtained were tabulated for Study 3. Surface Radiosity, Temperature, Isothermal Contours, Slice etc. were some of the operations used in evaluating the simulation results. The temperature profiles, heating pattern and distribution were observed by using the Arrow Volume and Streamline operators.